NTNU

Norwegian University of
Science and Technology

Design and Automated Optimization of Mooring Systems for Shallow Water and Harsh Environments

Christine Krugerud

Marine Technology
Submission date: June 2016
Supervisor: Kjell Larsen, IMT

Norwegian University of Science and Technology
Department of Marine Technology

NTNU Trondheim
Norges teknisk-naturvitenskapelige universitet
Institutt for marin teknikk

MASTER THESIS SPRING 2016

for

Stud. tech. Christine Krugerud

Design and Automated Optimization of Mooring Systems for Shallow Water and Harsh Environments

Automatisert optimalisering av forankringssystemer for grunt vann og værharde områder

Background

The purpose of the mooring system is to keep a floating vessel safely at a required position. It normally consists of 8-16 mooring lines of heavy chain, steel wire ropes and/or synthetic polyester ropes connected to a seabed anchor.

During the past years, the requirements to the mooring and station keeping systems of mobile and permanent units have become more complex;
- The industry is moving into new frontiers (ultra-deep water down to 3000m depth and into arctic areas).
- There are more operations adjacent to other installations (floatel operations and tender support vessel operations).
- The new mobile units are becoming larger and many units are at the end of their lifetime.
- There are too many anchor line failures.

The overall objective of this thesis is to assess and perform automated optimization for ULS design of shallow water mooring systems. The rig Safe Scandinavia semisubmersible unit as studied during the project work in the autumn 2015 shall be used as the floating structure.

Analysis methods for estimating ultimate mooring line tension and vessel offset can be divided into frequency domain (FD) methods and time domain (TD) methods. When using TD methods, all non-linearities in the dynamic system (stiffness and damping) and in the excitation may be taken into account. The results of TD simulations are time series of selected responses that must be carefully analysed by relevant statistical methods in order to establish a reliable estimate of the characteristic load effect. Simulations in the time domain shall be used as the basic method for the automated optimization in this thesis.

Scope of Work

1) Review relevant literature for mooring systems. Describe the theory and methods related to coupled and separated analysis methodology; focus shall be on time domain methods, but frequency domain method shall be briefly described. Describe the relevant time domain simulation tools available in SIMA and how SIMA can effectively be utilized.

2) Establish an appropriate simulation model for SIMO/RIFLEX for the semisubmersible Safe Scandinavia.

3) Theory related to automated optimization shall be studied and described based on relevant literature and papers. A recipe on how automated optimization can be performed when using the SIMA workbench shall be described.

4) Mooring systems based on steel components like chain and steel wire rope as well as a system based on chain and synthetic ropes (polyester) shall be optimized and compared. Sensitivity studies shall be carried out as agreed with the supervisor.

5) Quantify and compare the load effects of the selected mooring systems by comparing results from quasi-static analysis using SIMO with results from dynamic analysis using RIFLEX. The time domain results shall also be compared with results from frequency domain using MIMOSA.

6) Conclusions and recommendations for further work.

General information

The work shall build on the project work report "Design and Optimization of Mooring Systems for Shallow Water and Harsh Environment".

The work scope may prove to be larger than initially anticipated. Subject to approval from the supervisor, topics may be reduced in extent.

In the project the candidate shall present her personal contribution to the resolution of problems within the scope of work.

Theories and conclusions should be based on mathematical derivations and/or logic reasoning identifying the various steps in the deduction.

The candidate should utilise the existing possibilities for obtaining relevant literature.

Thesis report

The thesis report should be organised in a rational manner to give a clear exposition of results, assessments, and conclusions. The text should be brief and to the point, with a clear language. Telegraphic language should be avoided.

The report shall be written in English and edited as a research report including literature survey, description of relevant mathematical models together with numerical simulation results, discussion, conclusions and proposal for further work. List of symbols and acronyms, references and (optional) appendices shall also be included. All figures, tables and equations shall be numerated.

The original contribution of the candidate and material taken from other sources shall be clearly defined. Work from other sources shall be properly referenced using an acknowledged referencing system.

The report shall be submitted in two copies:

- Signed by the candidate
- The text defining the scope included
- In bound volume(s)
- Drawings and/or computer prints which cannot be bound should be organised in a separate folder.

Ownership

NTNU has according to the present rules the ownership of the project results. Any use of the project results has to be approved by NTNU (or external partner when this applies). The department has the right to use the results as if the work was carried out by a NTNU employee, if nothing else has been agreed in advance.

Thesis supervisor**:**

Prof. II Kjell Larsen, NTNU/Statoil

Co-supervisor: Vegard Aksnes, Sintef Marintek

Deadline: June 10th, 2016

Trondheim, June 2016

Kjell Larsen (date and signature): June 8th 2016 Kjell Larsen

Christine Krugerud (date and signature): June 8th 2016 Christine Krugerud

Preface

The work executed in this master's thesis concludes the Master of Science degree in Marine Technology at the Norwegian University of Science and Technology (NTNU). The work was carried out during the spring of 2016.

The work is based on the project thesis "Design and Optimization of Mooring Systems in Shallow Water and Harsh Environment" developed during the autumn of 2015. The scope of the master's thesis was established based on discussions with supervisor combined with personal interest.

During the process, several obstacles have been encountered, especially when formulating and performing the automated optimization of two mooring systems in SIMA. A lot of time was spent on trial and error on this subject, as no work on this subject has been previously performed. Overall, I am satisfied with the thesis, and I have gained valuable knowledge of automated optimization and its usefulness in the design of a mooring system.

The reader of this report would benefit from having a basic understanding of marine hydrodynamics, marine structures and dynamic analysis.

Trondheim, 2016-06-10

Christine Krugerud

Acknowledgment

First and foremost many thanks to my dedicated and highly appreciated supervisor Kjell Larsen, for his enthusiastic guidance and help throughout the process. The theory behind mooring design appeared quite extensive and complex, and he offered invaluable explanation and insight on the subject. Weekly meetings, lecture notes and overall correspondence have been essential. Statoil is acknowledged through Kjell Larsen for providing the necessary information on the semi-submersible Safe Scandinavia.

Secondly, I would like to thank my co-supervisor Vegard Aksnes at MARINTEK for invaluable guidance during the process of formulating and performing an optimization of mooring systems in SIMA. He has been extremely helpful in discussing problems and observations throughout the entire process by email correspondence and scheduled meetings. Pål Levold at MARINTEK has also been very helpful answering questions related to the optimization in SIMA, and a warm thank is also given to him.

I would also like to thank Xiaopeng Wu for helping with the modeling in SIMO and Riflex. He was always available on email and scheduled meetings to troubleshoot issues related to the modeling of a mooring system in SIMO and Riflex. This was very much appreciated.

Lastly, I wish to thank my fellow students at office C1.076 for providing invaluable discussions and insight. A special thank goes to Kristine Klingan, whom is also writing a thesis on automated optimization of mooring systems, for highly appreciated discussions in the process of formulating an optimization problem and evaluating the results from the optimization procedure.

C.K.

Abstract

The present market places significant cost pressure on the design of a mooring system. It is therefore important to be able to produce a mooring system at the lowest possible cost, and at the same time, to ensure a safe design that meets the requirements set by standards. Various optimization procedures are available for this purpose, although limited work has been conducted regarding the automated cost optimization of mooring systems. This is the governing motivation for the work executed in this thesis.

A model of the semi-submersible Safe Scandinavia is established in SIMO, together with suitable mooring systems. One system with 12 lines of a chain-steel wire-chain configuration, termed the steel system, and one system with 12 lines comprised of a chain-polyester rope-chain configuration, which is referred to as the polyester system, are considered for the optimization. The main objective of this thesis is to optimize both the polyester and steel system with constraints that correspond to four different cases, and evaluate the results and investigate the sensitivity of the optimization formulation.

The optimization problem is formulated in the SIMA workbench developed by MARINTEK. The mooring systems are optimized with respect to hardware cost, whereby the cost of each material (chain, polyester rope and steel wire) depends on the respective length and diameter. Constraints in the various optimization cases involve maximum allowable tension in the mooring lines and maximum allowable offset in the horizontal plane. The time domain simulation within the optimization procedure is executed in SIMO, whereby the motions are separated into wave frequency and low frequency contributions, and a quasi-static method to calculate the mooring line tension is provided. The final or optimum mooring system configurations that result from each optimization case are verified through the run of several time domain realizations in order to obtain reliable statistics of the response, i.e. the most probable largest motions and line tension. A sensitivity study of the optimization formulation in SIMA is conducted in order to investigate the robustness of the formu-

lation.

The polyester system provides the most cost efficient configuration in comparison to the steel system. The optimization case with the softest constraints on maximum allowable mooring line tension and horizontal offset results in the cheapest system. In the comparison of the polyester system and the steel system, it is evident that a stricter constraint on safety factor results in the most expensive polyester system, whereas a reduced maximum allowable offset significantly increases the cost of the steel system.

The sensitivity study concludes that the optimization formulation appears overly sensitive to a minor change in the environmental conditions, whereby two optimization runs with a $10cm$ difference in significant wave height result in almost a 15% cost difference for the steel system. Additionally, the verification of the optimized systems highlights the importance of running several time domain simulations in order to obtain reliable statistics, for instance in terms of most probable largest tension and offset.

The heaviest loaded line from both the steel and polyester system is analyzed in Riflex, to investigate the influence of mooring line dynamics on the tension. A quasi-static approach proves to be adequate to compute the tension in the polyester line, whereas this approach results in an underestimate of the tension in the steel line, whereby the dynamics from drag and inertia in the line enhances the tension.

Sammendrag

Dagens marked setter betydelig press på kosteffektiviteten til et forankringssystem. Å designe et forankringssystem som tilfredsstiller gitte sikkerhetskrav spesifisert i standarder til lavest mulig kostnad er derfor viktig. Flere automatiske optimeringsalgoritmer er utviklet gjennom årene, men det er gjort lite forskning på automatisk kostnadsoptimering for forankringssystemer. Dette er derfor motivasjonen bak oppgaven.

En modell av den halvt nedsenkbare plattformen Safe Scandinavia er i denne oppgaven etablert i SIMO, med tilhørende forankringssystemer. To ulike systemer er evaluert. En løsning består av en kjetting og stål vaier sammensetning, og en består av sammensetning av kjetting og polyester. Disse er videre referert til som stålsystemet og polyestersystemet. Hovedformålet med denne oppgaven er å optimere både polyester- og stålsystemet. For hvert system defineres fire ulike caser, hvor hver case har sine respektive restriksjoner. I tillegg er robustheten til optimeringsformuleringen evaluert, og de optimerte forankringssystemene er verifisert.

Optimeringsproblemet er formulert i programmet SIMA utviklet av MARINTEK. Målet er å optimere materialkostnaden til ankerlinene, der kostnaden for hvert materiale (kjetting, stål vaier og polyester tau) avhenger av de respektive lengder og diametere. Restriksjoner til forankringssystemet definert i optimeringsproblemet tilsvarer maks tillatt linestrekk og horisontal forskyvning av det forankrede fartøyet. Disse parameterne beregnes ved tidsplananalyse i programmet SIMO, som resulterer i at linestrekket regnes kvasi-statisk og bevegelsen til plattformen er simulert i hvert tidssteg. Det optimerte stål- og polyester systemet er verifisert ved å kjøre flere tidsplananalyser tilsvarende ulike realisasjoner av sjøtilstanden. På denne måten blir realistiske statistiske parametere estimert fra de ulike tidsseriene, blant annet mest sannsynlig største linestrekk og forskyvning.

Ved sammenligning av de optimerte systemene fremkommer det tydelig at et polyestersystem er

mest kosteffektivt. Det er også tydelig, for både polyester- og stålsystemet, at den optimeringscasen med de ”snilleste” restriksjonene gir lavest kostnad. Det dyreste polyestersystemet er gitt fra optimeringscasen der det høyeste kravet er satt til maks tillatt linestrekk, mens det dyreste stål systemet oppstår ved å vesentlig begrense maks tillatt horisontal forskyvning.

Sensitivitetsstudiet indikerer at optimeringsformuleringen i SIMA er litt for sensitiv i forhold til små endringer i værbetingelsene. Dette vises ved at $10cm$ økning i bølgehøyde resulterer i omtrent 15% økning i kost for stålsystemet, som virker urealistisk. Det er i tillegg nødvendig å understreke viktigheten av å kjøre tidsplananalyser med flere realisasjoner av samme sjøtilstand. Dette er observert i verifiseringen av de optimerte systemene, hvorav det ene frøtallet brukt i tidsplananalysen i optimeringen indikerer en noe ”snill” sjøtilstand, og igjen underestimerer maksstrekket i linene og maks horisontal forskyvning.

Den mest belastede linen fra både stål- og polyestersystemet er analysert i programmet Riflex. Dette undersøker effekten av å beregne maksstrekket i linen dynamisk i stedet for kvasi-statisk. Sammenligningen mellom SIMO og Riflex indikerer at den kvasi-statiske metoden for beregning av linestrekk gir relativt korrekt linestrekk for polyesterlinen, mens den underestimer linestrekket i stållinen. De dynamiske effektene som influerer linestrekket resulterer fra drag og treghet i linen. Grunnet stållinens vekt og catenary utforming vil de dynamiske effektene i større grad påvirke strekket i stållinen i motsetning til polyesterlinen.

Contents

List of Figures

List of Tables

Nomenclature

General

- Parameters that appear in equations are explained after the equations are presented
- Abbreviations are given after first use of the terms

Abbreviations

ALS Accidental Limit State

API American Petroleum Institute

DAF Dynamic Amplification factor

DLF Dynamic Load Factor

DOF Degree Of Freedom

DNV Det Norske Veritas

FD Frequency Domain

FEM Finite Element Method

FFT Fast Fourier Transformation

FLS Fatigue Limit State

HF High Frequency

ISO International Standard Organization

LF Low Frequency

MBS/MBL Minimum Breaking Strength or Minimum Breaking Load

MPM Most Probable Maximum

NCS Norwegian Continental Shelf

RAO Response Amplitude Operator

sf safety factor

SQP Sequential Quadratic Programming

TD Time Domain

WAMIT Wave Analysis at MIT

WF Wave Frequency

wd wave drift

ULS Ultimate Limit State

Latin Characters

$\boldsymbol{A}$ Added mass matrix

A Area

$\boldsymbol{C}$ Potential damping matrix

C_{cu} Current force coefficient

C_D Drag force coefficient

C_{wd} Wave drift force coefficient

C_{wi} Wind force coefficient

d_1 Diameter segment 1

d_2 Diameter segment 2

d_3 Diameter segment 3

$\boldsymbol{D}$ Damping matrix

E Modulus of elasticity

F_H Horizontal top end tension

F_v Vertical top end tension

$F_y(y)$ Cumulative density function of response y

$f_y(y)$ Probability density function of response y

$f(x)$ Objective function

$g(x)$ Constraint function

$h(\tau)$ Retardation function

H_{LF} Transfer function for relation between LF force and LF response

H_S Significant wave height

H_{WF} Transfer function for relation between WF force and WF response

I Moment of inertia

$\boldsymbol{K}$ Restoring matrix

$k_{elastic}$ Elastic stiffness

$k_{geometric}$ Geometric stiffness

k_{tot} Total stiffness

l_1 Length segment 1

l_2 Length segment 2

l_3 Length segment 3

$\boldsymbol{M}$ Mass matrix

m Structural mass

p_{factor} Factor for calculation of pretension

$\boldsymbol{Q}$ Total excitation load matrix

q_{wa} Wave excitation

q_{wi} Wind excitation

q_{cu} Current excitation

r Horizontal displacement in any direction

S_x Response spectrum

S_q Excitation force spectrum

S_T Spectrum of top end line tension

S_w Wind velocity spectrum

T Period of oscillation

T Tension in mooring line

T_C Characteristic tension

T_P Peak period

t time

$\bar{U}$ Mean wind or current velocity

$u(t)$ Dynamic wind gust velocity

w Unit weight in air

$\ddot{x}$ Vessel acceleration

$\dot{x}$ Vessel velocity

x Vessel displacement or offset

$\bar{x}$ Static vessel displacement or offset

Greek Characters

ϵ Phase angle

λ Lagrange multiplier

Λ Logarithmic decrement

μ mean value

∇ Nabla-operator, or partial derivative symbol

∇f Gradient of function f

ρ Density

σ Standard deviation, subscript refers to the response

ω Frequency or angular velocity

ζ_a Wave amplitude

ξ Damping ratio

Commonly used expressions

Surge: Translation along x-axis

Sway: Translation along y-axis

Heave: Translation along z-axis

Roll: Rotation about a x-axis

Pitch: Rotation about a y-axis

Yaw: Rotation about a z-axis

Pretension: Tension in the lines at initial position, without excitation from environment

Fairlead: The connection from the mooring line to the vessel

Chapter 1

Introduction

1.1 Background and Literature Survey

Mooring systems are complex systems designed to maintain the desired position of an offshore vessel. Offshore vessels are typically moored with 8-16 mooring lines and consist of heavy chain, steel wire and/or polyester rope that are connected to an anchor. Mooring systems consider both the safety of environment and the people working at the offshore structure, and are therefore of critical importance.

As the offshore industry is moving towards new areas with potentially severe environmental conditions and environmentally sensitive areas, e.g. the arctic, mooring system failures present a greater risk. The requirements of mooring systems, for both permanent and mobile units, have therefore become more complex. Mooring systems are designed according to the regulations established through standards such as DNV (2013) and ISO (2013). More operations take place in proximity to other structures, such as support vessels and flotels. New mobile units have become larger and many have reached the end of their lifetime. Up until now, there were too many mooring line failures that lead to unwanted consequences, as described in works from Fontaine et al. (2014) and Ma et al. (2013). The utilization of correct numerical simulation methods to achieve mooring system response is therefore important to the design of mooring systems. This work studies the differences in terms of vessel response obtained through the utilization of different analysis theory and software.

A dynamic mooring line system is exposed to two types of inherent dynamic coupling: a) dynamic interaction between vessel and mooring lines; b) and coupling of mean, wave frequency response due to interaction with incident waves and low frequency response that is caused by second order difference frequency forces. The coupling in a) is more pronounced in deeper waters, and the coupling effect in b) is influenced by the geometric nonlinearity in the mooring lines and nonlinear drag forces (Low and Langley, 2008). A mooring system can be analyzed in the frequency or the time domain. This analysis involves the estimation of maximum mooring line tension and vessel offset. There are two fundamental differences between performing an analysis in the frequency domain in comparison to performing an analysis in the time domain. The non-linear restoring terms and damping terms must be linearized, and the low frequency (LF) and wave frequency (WF) load effects are separately analyzed. In order to correctly add these contributions together, the superposition principle must be valid, which requires a linear system. The presence of coupling described in b) indicates that the mean, WF and LF motions should preferably not be separated. The time domain approach directly accounts for all non-linearities in the dynamic system and yields simultaneous simulations of the LF and WF response, but requires significantly more computer power. Both methods use statistical properties to provide an estimate of the characteristic load effect.

Fylling (1980) studied issues in relation to a frequency domain simulation of mooring systems with pronounced LF response. The state of the art option to overcome these issues is a time domain simulation, which properly treats the non-linearities in the systems. A time-domain analysis, however, leads to the challenge of significant computational capacity and time. Researchers have investigated several methods to overcome these obstacles. Work from Low and Langley (2008) presents a hybrid method, in which the WF response is simulated in the frequency domain and the coupled LF response is solved in the time domain allowing larger time steps in the numerical procedure and thus less computational time. Several frequency domain simulations of the WF response are executed at certain time intervals, utilizing the instantaneous position of the coupled system from the time domain simulation. A decoupled time domain approach is another widely-used procedure, in which the effects from mooring line dynamics are included in the simulation of the vessel response in a simplified manner. Research from Ormberg and Larsen (1998) demonstrated that such

a decoupled approach yields an adequate representation of the vessel response in relatively shallow water depths.

The present market place significant pressure on the cost to design a mooring system. It is therefore important to be able to produce a mooring system at the lowest possible cost, and at the same time, to ensure a safe design that meets the requirements set by standards. Various optimization procedures are available for this purpose, although limited work has been conducted regarding the cost optimization of mooring systems. The constrained optimization is typically utilized for mooring system analyses, as the constraints on design are typically set by requirements from standards. Nocedal and Wright (2006) present the basic theory of constrained optimization, in conjunction with different linear and quadratic programming methods to solve the constrained problem. In terms of cost optimization of a combined mooring and riser systems, Fylling (2003) describes how to establish a cost function that is minimized with optimized variables, and how the constraints on mooring line tension and vessel offset may be implemented. Different automatized algorithms have been developed for optimization purposes. The NLPQL algorithm is a Fortran implementation of a sequential quadratic programming method described in Schittkowski (1986), and is today widely used in automatic optimization procedures. The NLPQL algorithm is implemented in the SIMA workbench, which is utilized to formulate the optimization problem in this thesis.

1.2 Objectives

The main objectives of this thesis are as follows:

1. Review relevant literature for mooring systems. Describe the theory and methods related to coupled and separated analysis methodology; focus shall be on time domain methods, but frequency domain method shall be briefly described. Describe the relevant time domain simulation tools available in SIMA as well as how SIMA may effectively be utilized.

2. Establish an appropriate simulation SIMO/Riflex model for Safe Scandinavia, and perform a time domain analysis in SIMO, whereby the results shall be compared to the results obtained from a frequency domain analysis performed in MIMOSA in the project thesis.

3. Study and describe theory related to automated optimization based on relevant literature and papers. A recipe on how automated optimization can be performed when using the SIMA workbench shall be described.

4. Mooring systems based on steel components like chain and steel wire rope as well as a system based on chain and synthetic ropes (polyester) shall be optimized and compared. Sensitivity studies shall be carried out as agreed with the supervisor.

5. Quantify and compare the load effects of the selected mooring systems by comparing results from quasi-static analysis using SIMO with results from dynamic analysis using RIFLEX. The time domain results shall also be compared with results from frequency domain using MIMOSA.

Based on the points listed above, a conclusion follows with recommendations for further work.

1.2.1 Approach

This work presents basic theory related to excitation loads on a moored vessel, in conjunction with a description of damping and restoring forces, based on the studies executed in the project thesis with some modifications. It provides a description of both the frequency and time domain analysis to understand the differences in comparison to the results yielded from different software.

The theory related to the optimization of a mooring system was briefly assessed in the project thesis, and is described more in depth in this thesis.

This study assesses three different case studies, whereby the analyses are based on realistic environmental data, although from a different geographic location than the field the considered mobile

unit is designed to operate at. The analyses in Case Studies 1 and 2 are performed in SIMO, with separated WF and LF response. The analysis utilizes a quasi-static approach to compute the tension in the mooring lines. In Case Study 3, the analyses are performed in SIMO, Riflex and MIMOSA, and the responses from each software are compared and discussed.

1.3 Report Structure

The organization of the report is as follows. Chapter 2 introduces the equation of motions for a mooring system. It additionally presents the governing loads on a mooring system, such as damping and restoring forces and environmental loads. Afterward, it explains and briefly compares two methods of analyzing a mooring system, frequency and time domain approach.

Chapter 3 assesses basic theory regarding the optimization of mooring design. The theoretical background for optimization algorithms is quite complex, and is therefore only described on a superior level.

Chapter 4 provides a description of the vessel and its properties utilized in every analysis, in conjunction with the environmental conditions considered in each analysis. It further describes various software such as MIMOSA, SIMO and Riflex. It presents the theory related to the different computer programs qualitatively, in order to compare the analyses performed in the respective software. Finally, in Chapter 5, provides a presentation of how to efficiently use the SIMA workbench and its programs in order to adequately analyze mooring systems.

This thesis' main work is divided into three different case studies. Case Study 1, provided in Chapter 5, includes the implementation of the vessel, Safe Scandinavia, and its initial mooring system in SIMO. A ULS time domain analysis of the vessel response performed in SIMO is compared to the results obtained from analyses performed in MIMOSA in the project thesis.

Case Study 2 in Chapter 6 presents the optimization of two different mooring systems with respect to hardware cost. One system is comprised of heavy chain in combination with steel wire, hereby referred to as the steel system. Another system is comprised of a combination of heavy chain and polyester rope, and is known as the polyester system. The first portion of Chapter 6 presents a detailed description of how the optimization problem is formulated in SIMA. This optimization procedure is then applied to both systems. The analysis then compares four different optimization cases with various constraints, for both the polyester and steel systems, in terms of the resulting cost and mooring line configuration. Following this comparison, Chapter 6 presents a sensitivity study of the optimization formulation to explore the robustness of the formulation. Afterwards, it includes a verification of the optimization results and a discussion of the results. The chapter concludes with a section that presents the experiences from the formulation of an optimization problem in SIMA.

Chapter 7 presents the last study, Case Study 3. This case study involved the analysis of one single mooring line from both an optimized steel system configuration and a polyester system configuration in Riflex. For this purpose, the heaviest loaded line was selected. This chapter compares and discusses the response in terms of the vessel motion and line tension in the heaviest loaded line found from MIMOSA, SIMO and Riflex.

Finally, Chapter 8 concludes the work performed in this thesis, and recommendations for further work is presented.

Chapter 2

Theoretical Background - Mooring Systems

This chapter focuses on understanding the dynamic and static behavior of a moored vessel. It briefly describes and discusses the environmental loads, which result in both excitation forces and damping contributions as well as restoring and damping forces. Afterward, this chapter describes and compares a solution of the equation of motion, given in Eq. 2.6, for a moored vessel in both the frequency and time domain. The frequency domain will only be assessed briefly as it was thoroughly described in the project thesis.

2.1 Governing Loads and Vessel Motions

A mooring system for an offshore floater is designed against the overload of any mooring line. Overload is defined as the tension in a line that exceeds the breaking strength (MBS) included a given safety margin, as outlined in certain rules and regulations. The governing excitation mechanism for mooring line tension is the top end motion of the line, i.e. the static and dynamic motion of the floater itself. The forces induced on the mooring lines from the vessel are generally much larger than the forces that act directly on the mooring lines, and the latter forces can often be neglected. Figure 2.1 presents a simple two-dimensional schematic of the governing loads on a mooring system.

The resulting floater motion includes contributions from motions in all six degrees of freedom (DOFs); surge, sway, heave, roll, pitch and yaw. Figure 2.2 illustrates the definition of these rotations and translations..

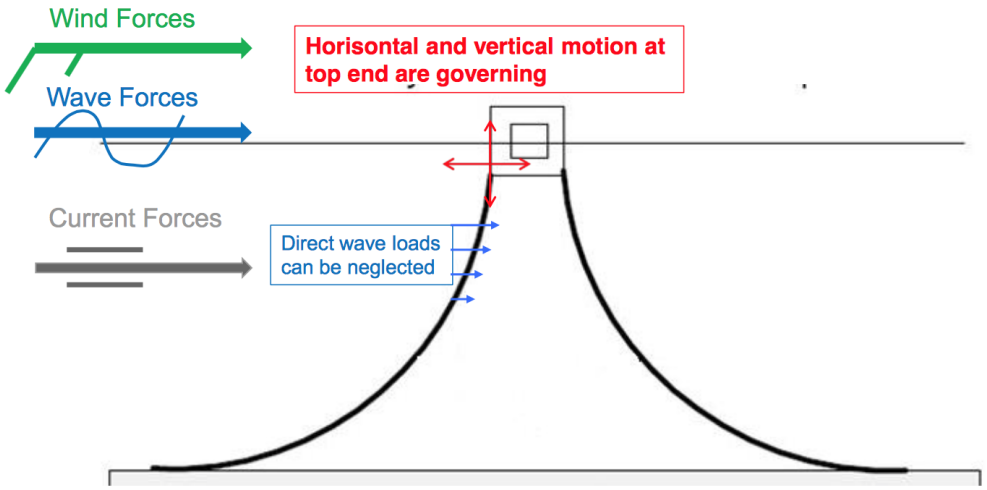

Figure 2.1: Forces on a moored vessel (Larsen, 2015)

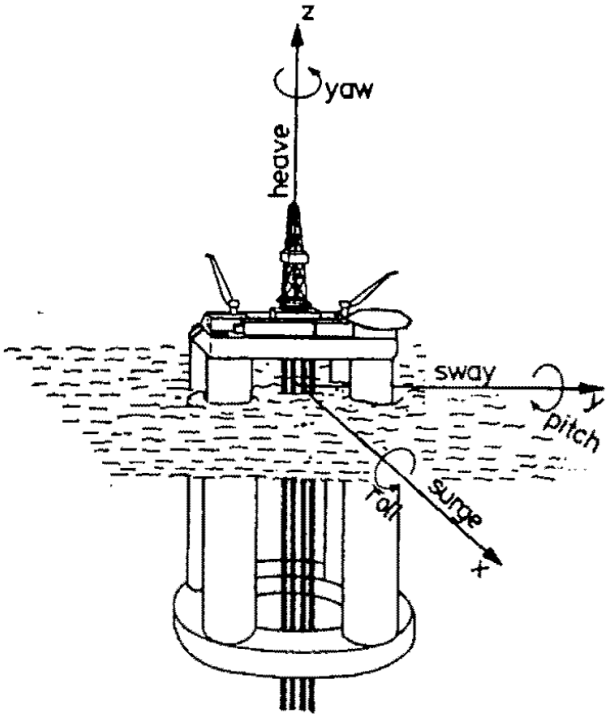

Figure 2.2: Definition of rigid body modes (Faltinsen, 1993)

Through an assumption of small motions, the coupled motion at any arbitrary point (x,y,z) on the vessel can be expressed in Eq. (2.1) (Faltinsen, 1993).

$$\boldsymbol{s} = \eta_1 \cdot \boldsymbol{i} + \eta_2 \cdot \boldsymbol{j} + \eta_3 \cdot \boldsymbol{k} + \boldsymbol{\omega} \times \boldsymbol{r} \tag{2.1}$$

η_1, η_2 and η_3 represent the translatory motions surge, sway and heave, respectively. Eq. (2.2) and (2.3) define $\boldsymbol{\omega}$ and $\boldsymbol{r}$.

$$\boldsymbol{\omega} = \eta_4 \cdot \boldsymbol{i} + \eta_5 \cdot \boldsymbol{j} + \eta_6 \cdot \boldsymbol{k} \tag{2.2}$$

$$\boldsymbol{r} = x \cdot \boldsymbol{i} + y \cdot \boldsymbol{j} + z \cdot \boldsymbol{k} + \boldsymbol{\omega} \times \boldsymbol{r} \tag{2.3}$$

η_4, η_5 and η_6 represent the oscillatory motions roll, pitch and yaw. The expression in Eq. (2.1) may be applied, for instance, when motions at the fairlead are of interest.

The total motion of the vessel, the top end motion of the line, can be found by solving the equation of motion, which will be explained further in Section 2.2 and is presented in Eq. (2.6).

The motion of a moored vessel can be divided into static and dynamic contributions. The static motion emerges from the mean forces that act on the vessel, which gives it a mean offset, whereas the dynamic motion is wave-, high- and low frequency motions. The mean wave drift-, current- and wind forces contribute to the static forces, and are described in Section 2.2.1. The mooring lines do not directly influence these forces, although the dimensions and orientation of the moored vessel do. They cause static tension in the mooring lines and lead the vessel to have a mean offset. Through a consideration of the line characteristics, which are described in Section 2.2.2, these forces may be directly computed (Fylling, 1980).

There are several sources that contribute to dynamic loads on the mooring system (Fylling, 1980):

- • Transient loads that are for instance caused by changes in line length or anchor displacement
- Wave frequency (WF) motions of the moored vessel
- Low frequency (LF) wind and wave drift forces
- Periodic vortex shedding causing high frequency (HF) oscillations on the mooring lines

A moored structure typically has a large eigenperiod, as the stiffness in the mooring system is relatively low in comparison to the structure's mass (Triantafyllou, 1999). Due to the large natural period, typically one to two minutes, the motions of interest are the mean, WF and LF, whereas HF forces are less important. The LF motions are of particular interest because they are resonant oscillations, and can be tuned by the mooring system. For a moored structure with large waterplane area LF resonance oscillations occur through surge, sway and yaw (Faltinsen, 1993). For a semi-submersible, with relatively small waterplane area, LF resonance oscillations may occur in surge, sway, yaw, pitch and roll.

2.1.1 Inertia versus Drag Dominated System

In the consideration of a marine structure, the dynamic response may be divided into different regimes. In order to evaluate these regimes, the dynamic load factor, or dynamic amplification factor, is particularly useful. Eq. (2.4) presents this factor (Larsen, 2014). The dynamic load factor provides the relation between the dynamic and the static response for a given excitation load.

$$DLF = \frac{1}{\sqrt{[1-(\frac{\omega}{\omega_0})^2]^2 + \omega^2 \frac{c^2}{k^2}}} \tag{2.4}$$

The frequency ratio $\frac{\omega}{\omega_0}$ is the ratio between the load frequency ω and the natural frequency ω_0 of the vessel. c and k represent the damping and stiffness of the system, respectively.

For a stiffness dominated system the load frequency is much lower than the natural frequency of the structure. Figure 2.3 illustrates the frequency range for a stiffness dominated system.

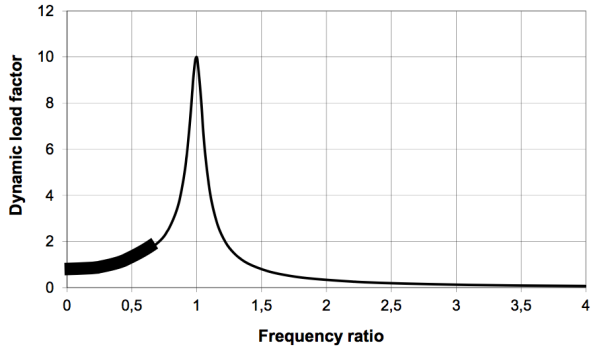

Figure 2.3: Stiffness dominated area (Larsen, 2014)

The variation in excitation appears as slow, and the system generates almost no inertia forces. The static forces nearly balance the excitation loads, and the construction behaves nearly quasi-static (Larsen, 2014). Due to the large natural frequency of a moored structure, a stiffness dominated system is rarely expected, but the static excitation from wind, waves and current are within this area and is balanced by the stiffness in the mooring system.

When the load frequency is very close to the natural frequency of the structure, the system is within the resonance area. The expression for the dynamic load factor reduces the what given in Eq. (2.5) provides the reulsintg expression for the dynamic load factor in this area.

$$DLF = \frac{1}{\sqrt{\omega^2 \frac{c^2}{k^2}}} \tag{2.5}$$

As made evident, the dynamic response of the system is mainly controlled by the damping force c. The damping force drains energy from the system and thus limits the response, as highlighted in Figure 2.4.

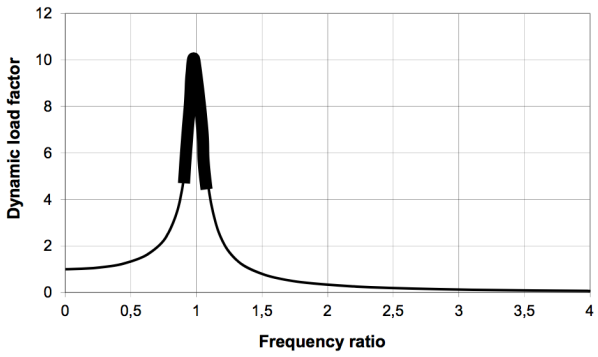

Figure 2.4: Resonance area (Larsen, 2014)

In the case of zero damping, the dynamic load factor approaches infinity at resonance. In the resonance area, the excitation on the structure cannot be balanced by either stiffness or inertia forces. The frequency of slowly varying wind and wave forces is close to the natural frequency of a moored vessel. Typical resonant response in surge, sway and yaw for a moored structure with large a eigenperiod is excited by the slowly varying wave drift force and the wind gust force, as presented in Table 2.1. The damping of the LF response is therefore of great importance. Section 2.2.3 describes the different damping mechanisms on a moored vessel.

A structure exposed to first order wave forces with a frequency significantly higher than its natural frequency is inertia-dominated. Figure 2.5 illustrates that the frequency ratio is high and the response appears in the inertia dominated area.

The load frequency is too high in order to achieve large enough offsets to generate stiffness forces to balance the excitation. The excitation forces are this balanced by the system's inertia forces (Larsen, 2014). For a moored vessel, similar balances are achieved for surge, sway and yaw responses induced by first order wave forces.

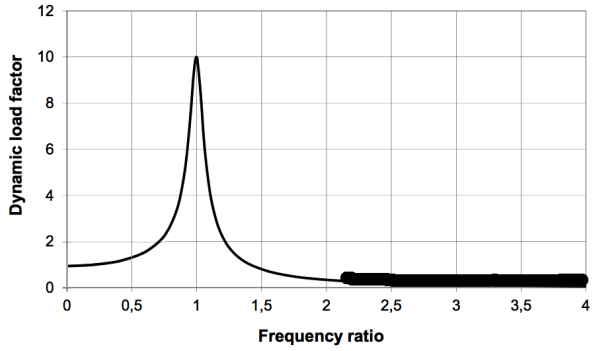

Figure 2.5: Inertia dominated area (Larsen, 2014)

2.2 Equation of Motion

In order to find the top end motion, the equation of motion provided in Eq. 2.6 must be solved for all six DOFs.

$$(\boldsymbol{M} + \boldsymbol{A}(\omega))\ddot{\boldsymbol{x}} + \boldsymbol{C}(\omega)\dot{\boldsymbol{x}} + \boldsymbol{D_l}\dot{\boldsymbol{x}} + \boldsymbol{D_q}\dot{\boldsymbol{x}}|\dot{\boldsymbol{x}}| + \boldsymbol{K}(\boldsymbol{x})\boldsymbol{x} \;=\; \boldsymbol{Q}(\boldsymbol{t}, \boldsymbol{x}, \dot{\boldsymbol{x}}) \tag{2.6}$$

In the above equation $\boldsymbol{x}$ is defined as the motion vector. $(\boldsymbol{M} + \boldsymbol{A}(\omega))$ is the structural and added mass matrix, $\boldsymbol{C}(\omega)$ is the potential damping matrix, $\boldsymbol{D_l}$ and $\boldsymbol{D_q}$ are linear and quadratic damping matrices, $\boldsymbol{K}(\boldsymbol{x})$ is the stiffness matrix and $\boldsymbol{Q}(\boldsymbol{t}, \boldsymbol{x}, \dot{\boldsymbol{x}})$ is the excitation load matrix. The following sections describe the restoring, damping and excitation terms.

2.2.1 Environmental Conditions and Corresponding Excitation Forces

Environmental loads on the vessel include forces from wind, waves and current. The loads may be dynamic, time-varying, or static. The excitation force from the environment is identified through the sum of these loads, as indicated Eq. (2.7), which is then simplified to a single DOF for convenience.

$$Q(t, x, \dot{x}) \;=\; q_{wi} + q_{wa} + q_{cu} \tag{2.7}$$

q_{wi}, q_{wa} and q_{cu} represents the forces from wind, waves and current, respectively. These environmental loads are divided into excitation regimes, as presented in Table 2.1. The high frequency motions are of less importance in the consideration of a moored vessel, and are therefore omitted from the table.

	Static	**Wave frequency**	**Low-frequency**
Waves	Mean wave drift force	1^{st} order wave forces	LF wave drift forces
Wind	Mean wind force	-	Wind gust forces
Current	Mean current force	-	-

Table 2.1: Excitation regimes for environmental loads

The following sections describe the different contributions within each regime. The wind and current forces are usually estimated based on small scale wind tunnel tests, small scale towing tank tests or by computational fluid dynamics numerical simulations.

Wind Forces

Wind forces are characterized by a mean value due to average wind velocity and a slowly varying value caused by wind gusts. The wind gusts have significant energy in the same order of magnitude as the natural oscillation periods in surge, sway and yaw. Wind is often modeled as a constant speed with an additional varying speed component, which has a zero mean. A gust spectrum is used to model the varying portion of the wind. Different spectra are available for this calculation. Figure 2.6 provides some examples. The reference wind speed for these spectra are taken $10m$ above water level.

The wind force may be expressed as shown in Eq. (2.8)

$$q_{wi}(t) \;=\; C_{wi}(U(t) - \dot{x}^{LF})^2_{LF} \;=\; C_{wi}[(\bar{U} + u(t)) - \dot{x}^{LF}]^2 \tag{2.8}$$

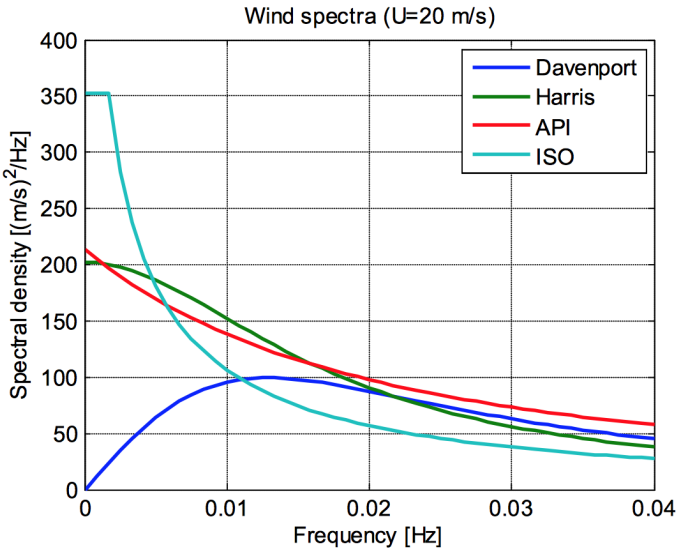

Figure 2.6: Four different wind spectra for a mean wind speed = $20m/s$ (Kaasen et al., 2012)

C_{wi} is the direction dependent wind force coefficient, as shown in Eq.2.9. $\dot{x}^{LF}$ is the vessel LF velocity, $\bar{U}$ is the mean wind velocity and $u(t)$ is the dynamic wind gust velocity. From this equation, it is evident that the wind force is proportional to the relative velocity between the vessel and the wind.

$$C_{wi} = \frac{1}{2}\rho_{air} C_D A \tag{2.9}$$

ρ_{air} is the air density, C_D is the global drag coefficient of the vessel and A is the area of the vessel that the wind "meets".

Through an assumption that mean wind velocity is much bigger than both the LF velocity and the wind gust velocity, the terms $\dot{x}^{LF^2}$ and $u(t)^2$ may be neglected, and therefore, the above equation can be written as presented in Eq. (2.10).

$$q_{wi}(t) = C_{wi}\bar{U}^2 + 2C_{wi}\bar{U}u(t) - 2C_{wi}\bar{U}\dot{x} \tag{2.10}$$

Here, the first term represents the static wind force, the second represents the LF excitation force and the last term represents the LF damping force.

Waves Forces

The wave forces that act upon a moored vessel may be characterized as follows (Larsen, 2015):

- 1^{st} order forces proportional to the wave amplitude
- Mean value forces due to 2^{nd} order wave loads proportional to the wave amplitude squared
- LF forces excited by 2^{nd} order wave loads proportional to the wave amplitude squared

The first-order forces contribute to the WF response of a moored vessel. First-order implies that the wave-induced motion and load amplitudes are proportional to the wave amplitude, and that linear theory is valid (Faltinsen, 1993). A basic assumption of linear theory includes small wave steepness, i.e. the waves are not near breaking. The first-order wave forces may be calculated by hand based on potential theory, or, alternatively, by potential theory computer programs, such as WADAM or WAMIT. The response of a vessel exposed to first-order wave forces are described by response amplitude operators (RAOs).

The second-order wave loads are known as wave drift excitation forces. The LF wave forces and moments are proportional to the wave amplitude squared. The LF excitation forces are typically smaller than the WF forces in terms of magnitude. However, they are still of significant importance as their period of oscillation is within the range of the natural frequency of a moored vessel.

The wave drift excitation gives rise to both slowly varying and mean forces. The mean wave drift force is caused by the relative vertical motion between the vessel and the waves, and is due to the body's capability to generate waves. The mean wave drift force is largest for short waves, i.e. high frequency waves, whereby the structure acts as a rigid wall that reflects all the waves. For very long waves, this force is small, as the waves are not affected by the presence of the structure, i.e. the vessel behaves like a cork.

Maruo derived formulas for wave drift forces on a three-dimensional body (Faltinsen, 1993). Through his assumption of zero average energy flux throughout the surface of the structure, he found that the reflected wave amplitude could never be larger than the wave amplitude ζ_a (Faltinsen, 1993). This results in a maximum possible wave drift force amplitude of $\frac{\rho g}{2}\zeta_a^2$. The direct pressure integration method constitutes another method to calculate the mean wave forces and moments, which results in the same maximum value found by Maruo's formula. Faltinsen (1993) thoroughly describes both these methods..

Faltinsen (1993) states that the LF excitation forces are large when the mean wave forces are large, which again leads LF motions to be most important for large volume structures. Faltinsen (1993) derived an expression for the slowly varying excitation forces in any translation or rotation i, which is provided in Eq. (2.11) for N wave components.

$$F_i^{SV} = \sum_{j=1}^{N}\sum_{k=1}^{N} A_j A_k [T_{jk}^{ic}\cos[(\omega_k-\omega_j)t+(\epsilon_k-\epsilon_j)] + T_{jk}^{is}\sin[(\omega_k-\omega_j)t+(\epsilon_k-\epsilon_j)]] \quad (2.11)$$

A is the wave amplitude, ω is the wave frequency and ϵ is the random phase angle. F_1^{SV}, F_2^{SV} and F_3^{SV} are the surge, sway and heave components of the slowly varying force. F_4^{SV}, F_5^{SV} and F_6^{SV} are the roll, pitch and yaw moments. T^{ic} and T^{is} are the second order transfer functions of the LF loads. Faltinsen (1993) provides a further explanation of this expression, in conjunction with a simplification of the expression through the application of Newman's approximation. This thesis does not further describe this equation.

Current

Forces caused by current are characterized by a mean value, as a result of the mean current velocity and negligence of the current turbulence. The current speed near the surface is of interest in order

to find the motion response of a vessel. Eq. (2.12) presents the excitation force from the current for a given degree of freedom and direction.

$$q_{cu}(t) \;=\; C_{cu}|\bar{U} - \dot{x}|(\bar{U} - \dot{x}) \tag{2.12}$$

Eq. (2.13) defines he current force coefficient C_{cu} as a function of seawater density ρ_{water}, drag force coefficient C_D and the vertical submerged area A.

$$C_{cu} \;=\; \frac{1}{2}\rho_{water} C_D A \tag{2.13}$$

Through an assumption that the mean current velocity $\bar{U}$ is larger than the vessel LF velocity $\dot{x}$, this expression in Eq. (2.12) may be written as in Eq. 2.14.

$$q_{cu}(t) \;=\; C_{cu}(\bar{U} - \dot{x})(\bar{U} - \dot{x}) \tag{2.14}$$

Through multiplication of the two terms in parentheses, the term $\dot{x}^2$ can be omitted, as the two other terms are of a much larger magnitude. Eq. (2.15) presents the final expression for the current excitation force.

$$q_{cu}(t) \;=\; C_{cu}\bar{U}^2 - 2C_{cu}\bar{U}\dot{x} \tag{2.15}$$

In this expression the first term represents the mean current force and the second term represents the LF damping force.

2.2.2 Restoring Forces

The stiffness provides the restoring forces of the system. For a freely floating body, the restoring forces in heave, roll and pitch follow from hydrostatic and mass considerations (Faltinsen, 1993). No stiffness exists in surge, sway and yaw, as there are no restraints against these motions. For a moored system, however, these restraints are induced through the mooring lines. This stiffness

consequently controls the mean offset of the vessel, and in turn, influences the LF motion.

There are two basic principles to provide restoring forces:

1. Geometric stiffness of the line
2. Elastic stiffness of the line

Geometric stiffness is the most important for a catenary chain/steel wire line. Geometric stiffness is provided through a change in tension due to change in line geometry, the weight of the line and/or separate clump weights, or line buoyancy and/or separate buoys. Elastic stiffness is most important for taut moorings with fiber ropes. The stiffness is then provided by axial elongation, i.e. stretch, of the line. The mooring line has an effective stiffness provided by both elastic and geometric stiffness as presented in Eq. (2.16).

$$\frac{1}{k_{tot}} = \frac{1}{k_{geometric}} + \frac{1}{k_{elastic}} \tag{2.16}$$

Figure 2.7 presents a schematic of elastic and geometric stiffness.

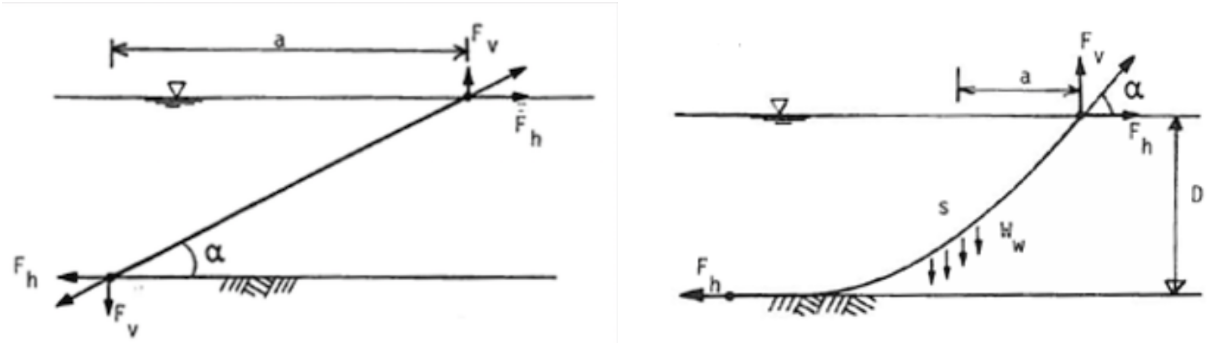

2.7.a Elastic stiffness 2.7.b Geometric stiffness

Figure 2.7: Mooring line stiffness (Larsen, 2015)

Eq. (2.17) and (2.18) provide the equilibrium of a mooring line for geometric and elastic stiffness, respectively.

$$F_H \cdot d \; = \; W_w \cdot a \tag{2.17}$$

$$F_H \cdot d \;=\; F_v \cdot a \tag{2.18}$$

In this case, $F_H[N]$ is the horizontal tension at the top end of the line, $d[m]$ is the vertical distance from sea surface to seabed, $W_w[N]$ is the weight of the line, $F_v[N]$ is the vertical tension and $a[m]$ is the distance from the top end line position to the point of attack of the weight for geometric stiffness and for elastic stiffness, the distance from fairlead to anchor

When a catenary moored vessel is displaced a distance from equilibrium position, two effects emerge: a change in weight due to a portion of the line being lifted off the seafloor and an increase in a. Both these effects work against the displacing motion and try to restore equilibrium position, and consequently, are termed restoring forces. For an elastic line, the line is elongated and behaves like a spring to restore the equilibrium position.

The static equilibrium of a mooring line segment may be derived from Figure 2.8. As illustrated in

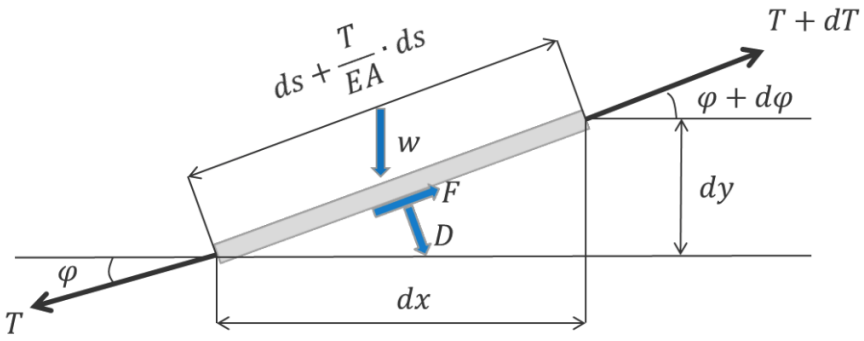

Figure 2.8: Forces acting on a two dimensional mooring line (Larsen, 2015)

this figure, whereby zero bending stiffness is assumed, T is the tension in the line, F and D are the external forces that act on the line segment in the tangential and radial directions: w and EA are the weight in water and axial stiffness, respectively, per unit length. Eq. (2.19) and (2.20) provides the static equilibrium of a line segment in the tangential and normal directions.

$$\mathrm{d}T \;=\; \left[\sin\phi - F\left(1 + \frac{T}{EA}\right)\right]\mathrm{d}s \tag{2.19}$$

$$T\mathrm{d}\phi \;=\; \left[w\cos\phi + D\left(1+\frac{T}{EA}\right)\right]\mathrm{d}s \tag{2.20}$$

These equations are nonlinear and it is generally not possible to find an explicit solution.

Through the utilization of these equations, a relation between the horizontal tension T_x and vessel offset X_l may be established for both an inelastic and elastic line. This relation is known as the line characteristics and is illustrated in Figure 2.9.

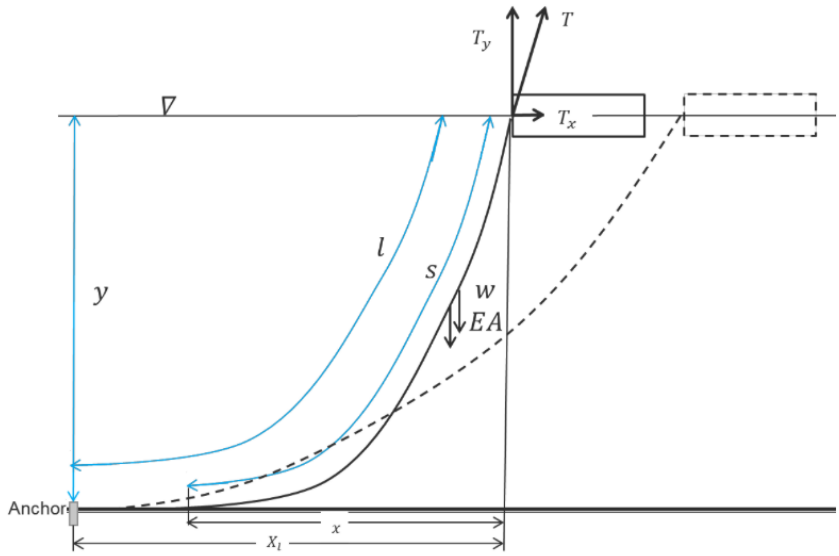

Figure 2.9: Notation defining the line characteristics (Larsen, 2015)

For an inelastic line ($\frac{T}{EA} \ll 1$), Eq. (2.21) provides the line characteristics. The complete derivation of this equation is found in Larsen (2015).

$$X_l \;=\; l + \frac{T_x}{w}\cosh^{-1}(1+\frac{wy}{T_x}) - \sqrt{y(y+\frac{2T_x}{w})} \tag{2.21}$$

Eq. (2.22) and (2.23) present the line characteristics for an elastic line.

$$T_x \;=\; EA\left[\sqrt{\left(\frac{T}{EA}+1\right)^2 - \frac{2wy}{EA}} - 1\right] \tag{2.22}$$

$$x = \frac{T_x}{w}\sinh^{-1}\left(\frac{T_y}{T_x}\right) + \frac{T_x T_y}{wEA} \tag{2.23}$$

The static environmental loads that act on the vessel provide the equilibrium position. Dynamic forces from wind and waves cause the vessel to oscillate about this mean offset. The system's stiffness limits the range of these oscillations.

2.2.3 Damping

The first order wave excitation loads are typically much larger than the contribution from the wave drift forces.The LF wave drift forces, however, excite the resonance oscillations of the moored vessel, and in this way, cause large responses. The potential damping from wave radiation can often be neglected as this effect is small near the slow drift resonance. The damping of the LF motions is therefore very important in mooring design. API (2005) presents the following sources of damping for a moored vessel:

- Viscous damping of the vessel, including wind, wave and current drag
- Wave drift damping of the vessel
- Mooring system damping
- Wave radiation damping - small

The viscous damping from wind arises from frictional drag between the vessel and the air. This contribution constitutes a steady state component that allows for linearization procedures in the estimation of the damping coefficient (Brown, 2005). The relative motion between the water and hull, which is a result of current and the LF motion of the vessel, provides viscous flow damping of the structure. The wave-drift damping of the vessel is due to its interaction with incident waves. The quantification of this damping contribution may, for instance, be found in model testing. The model test may involve a free decay test, in the desired directions, in both calm water and in regular waves. In the case of regular waves, the decay in motion is more rapid than the decay observed in calm water. Figure 2.10 highlights this fact.

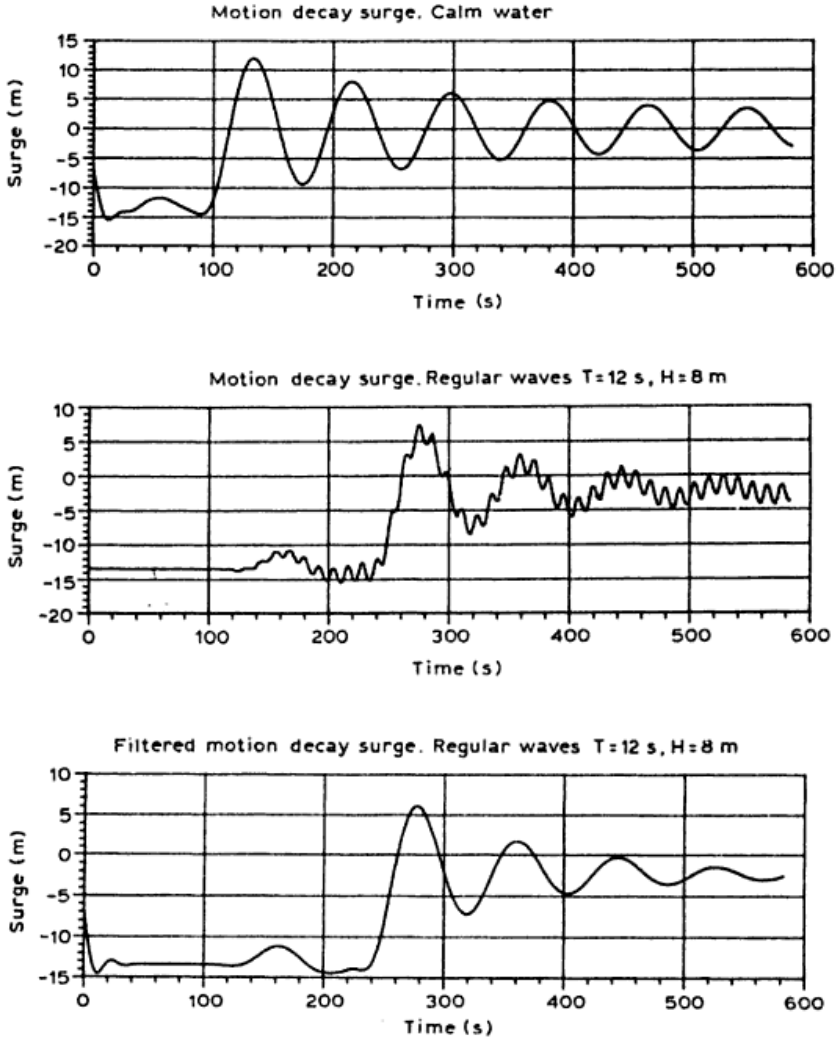

Figure 2.10: Influence of wave drift damping (Faltinsen, 1993)

This additional damping represents the wave drift damping. Depending on the wave frequency, there is also a linear damping contribution, which is related to wave radiation, and is based on potential theory. This contribution, however, is quite small in comparison to the resonance oscillations, as the incoming wave frequency is much greater than the resonance frequency.

The mooring system damping makes several contributions, therefore, much research has placed effort into understanding and estimating these contributions. According to Johanning et al. (2007),

the damping on a catenary line results from friction between the line and the seabed, internal friction within the chain and the drag force on the line caused by transverse motion. Huse (1991) extensively researched this area, and his work concludes that up to 80% of the total damping arises from the mooring line damping.

2.3 Time and Frequency Domain Analysis

There are two approaches to solving the equation of motion, which is presented in Eq. (2.6). It can be solved in the time domain or in the frequency domain. The following sections describe and compare these two methods.

2.3.1 Frequency Domain

A complete description of how to analyze mooring systems in the frequency domain was included in the project thesis, and is compiled here to illustrate the difference between a frequency and time domain method.

An energy spectrum can describe a stochastic process. The spectrum expresses the energy as a function of the frequency. It yields a complete description of the statistical parameters of a Gaussian Process, such as the standard deviation, extreme values and zero up-crossing period. Provided that all the spectral moments may be accurately found, a complete statistical description can be calculated without statistical uncertainty. Consequently, the frequency domain description of a stochastic process is directly given by the spectrum (Larsen, 2014).

In order to solve the equation of motion, Eq. 2.6, the load must be harmonic and the principle of linear superposition must be valid. This solution requires separation of the WF and LF motions, as

expressed in Eq. (2.24), as well as the linearization of the nonlinear damping and stiffness terms.

$$\begin{aligned} x &= x^{LF} + x^{WF} \\ Q &= Q^{LF} + Q^{WF} \end{aligned} \tag{2.24}$$

Eq. (2.25) provides the linearized equation of LF motion for a single degree of freedom.

$$(M + A(0))\ddot{x}^{LF} + D^*_{lin}\dot{x}^{LF} + K^*_{lin}x^{LF} = Q^{LF} \tag{2.25}$$

The LF force spectrum is found through the use of the superposition principle; addition of the force spectra for LF wind and the wave drift. The LF wave spectrum, with a difference-frequency μ for a given degree of freedom and wave direction, is expressed as presented in Eq. (2.26). μ is the difference-frequency $\omega_i - \omega_j$, given for $i \neq j$, where ω_i and ω_j are the circular frequency for two incident waves.

$$S_{qwd}(\mu) = 8\int_0^\infty C_{wd}(\omega + \frac{\mu}{2})C_{wd}(\omega + \frac{\mu}{2})S_\zeta(\omega)S_\zeta(\omega + \mu)\mathrm{d}\omega \tag{2.26}$$

Eq. (2.27) provides the LF wind force spectrum.

$$S_{qwi} = (2C_{wi}\bar{U})^2 S_w(\omega) \tag{2.27}$$

C_{wi} is the wind force coefficient, $\bar{U}$ is the mean wind velocity and $S_w(\omega)$ is the wind velocity spectrum, as described in Section 2.2.1.

The relation between the LF force spectrum and the LF response spectrum is the transfer function, given in Eq. (2.29), squared, as expressed in Eq. (2.28).

$$S_{x^{LF}} = |H_{LF}(\omega)|^2 S_{Q_{LF}} \tag{2.28}$$

$$|H^{LF}(\omega)|^2 \;=\; \frac{1}{K^*_{lin} - [(M + A(0))\omega^2]^2 + D^{*2}_{lin}\omega^2} \tag{2.29}$$

Through the assumption of a low damping level, the standard deviation of LF motion $\sigma_{x^{LF}}$ can be simplified as presented in Eq. (2.30). μ_n represents the resonance frequency.

$$\sigma^2_{x^{LF}} \;=\; \int_0^\infty S_{x^{LF}}(\omega) \;=\; S_{Q_{LF}}(\mu_n)\frac{\pi}{2K^*_{lin}D^*_{lin}} \tag{2.30}$$

The response spectrum that results from first order wave excitation is described by the RAOs and the wave spectrum. The RAO $H^{WF}(\omega)$ provides the ratio between the response amplitude x^{WF}_a and the incident wave amplitude ζ_a, as shown in Eq. (2.31).

$$H^{WF}(\omega) \;=\; \frac{x^{WF}_a(\omega)}{\zeta_a(\omega)} \tag{2.31}$$

$$S_{x^{WF}} \;=\; |H^{WF}(\omega)|^2 S_\zeta(\omega) \tag{2.32}$$

Eq. (2.32) presents the resulting response spectrum. The RAOs can be obtained through the utilization of various software, for instance WADAM.

The total motion x^{tot}_{max} can be found through the use of the "combination rule" provided in Eq. (2.33), here given for one DOF.

$$x^{tot}_{max} \;=\; max \begin{cases} \bar{x} + x^{LF}_{max} + x^{WF}_{sign} \\ \bar{x} + x^{WF}_{max} + x^{LF}_{sign} \end{cases} \tag{2.33}$$

$sign$, i.e. twice the standard deviation, is the significant value and is defined as the mean of the largest one third of all maxima, and max is defined as the most probable maximum. Through the assumption that the response is a narrow-banded Gaussian process, with Rayleigh distributed

maxima, x_{max}^{LF} and x_{max}^{WF} is provided by Eq. (2.34) and (2.35).

$$x_{max}^{LF} = \sigma_{x^{LF}}\sqrt{2\ln N^{LF}} \tag{2.34}$$

$$x_{max}^{WF} = \sigma_{x^{WF}}\sqrt{2\ln N^{WF}} \tag{2.35}$$

N^{LF} and N^{WF} represent the number of LF and WF oscillations, respectively, during a three hour sea state, typically. As the wave drift excitation that contributes to the LF response is generally non-Gaussian, the deviation, or skewness, of the LF response spectrum from the assumed Gaussian shape determines the extent to which the estimated LF motions are correct.

In order to estimate the line tension one can either use a quasi-static approach or a dynamic approach. In the quasi-static approach, the line tension is only dependent on the top end position, whereas in the dynamic approach, the tension is dependent on the top end position, velocity and acceleration. The dynamic approach is based on a "base" tension T_{base}, which corresponds to the offset $x_{base} = x_{max}^{tot} - x_{max}^{WF}$. The dynamic WF motions in all DOFs are simulated based on the base position. Eq. (2.36) expresses the characteristic tension T_C, which is defined as the most probable maximum value for a three hour duration in the worst 100-year sea state. This expression is obtained by assuming that the response is a narrow-banded Gaussian process with corresponding Rayleigh distributed maxima.

$$T_C = T_{base} + \sigma_T\sqrt{2\ln N} \tag{2.36}$$

N is the number of zero up-crossing in the process and σ_T is the standard deviation of the top end line tension and given in Eq. (2.37), whereby $S_T(\omega)$ is the spectrum of the top end line tension.

$$\sigma_T = \sqrt{\int_0^\infty S_T(\omega)\mathrm{d}\omega} \tag{2.37}$$

2.3.2 Time Domain

In this case, the stochastic process is a realization of the response in time domain. Measurements within a certain time interval provide a time series of the process. The statistical parameters of the process can be determined by estimating the distribution parameters of the realization process. In order to reduce the statistical uncertainty of these estimations, one must consider the process over a sufficiently long time interval (Larsen, 2014).

If the spectrum of the response is known, a time realization can be obtained through the utilization of an inverse Fourier transformation. This process entails a transformation from the frequency domain to the time domain. Accordingly, if the time realization is known, then the spectrum may be obtained through a Fourier transformation.

In the time domain the equation of motion, as provided in Eq. 2.6, may be solved through direct numerical integration. Unlike the frequency domain approach, this method allows for the WF and LF motions to be solved simultaneously, and non-linearities are directly accounted for in the damping and restoring force terms. MARINTEK (2013) provides two different methods to solve the equation of motion, through the use of convolution integral and the separation method. By utilizing the convolution integral, the equation of motion for a single DOF may be written as provided in Eq. (2.38). The added mass A_∞ is given for infinite frequency.

$$(m + A_\infty)\ddot{x} + D_l\dot{x} + D_q\dot{x}|\dot{x}| + Kx + \int_0^t h(t-\tau)\dot{x}(\tau)\mathrm{d}\tau \;=\; q(t, x, \dot{x}) \tag{2.38}$$

In this case, the frequency dependent added mass and damping are Fourier transformed to yield the retardation function $h(\tau)$, which is given in Eq. (2.39).

$$h(\tau) \;=\; \frac{2}{\pi}\int_0^\infty C(\omega)\cos(\omega\tau)\mathrm{d}\omega = \; -\frac{2}{\pi}\int_0^\infty \omega A(\omega)\sin(\omega\tau)\mathrm{d}\omega \tag{2.39}$$

The full derivation of these two equations can be found in MARINTEK (2013). In the establishment of this relation, the added mass and damping terms can be identified through the retardation function. In order to calculate the retardation function, one needs either the frequency dependent added mass or the damping, in conjunction with one value of the added mass. The damping is typically used to compute the retardation function.

The separation of motions is the other approach to solve the equation of motion in time domain. The motion is separated into a low frequency part and a wave frequency part. The WF part is then solved in the frequency domain, which requires that the motions are linear responses of the excitation loads (MARINTEK, 2013). This approach results in setting the quadratic damping term to zero and assuming constant stiffness. The excitation forces are separated into WF, first order wave forces, and LF, second order forces that arise from wind, waves and current. This separation allows for the separation of the position in the same manner, as presented in Eq. (2.40).

$$x = x^{WF} + x^{LF} \tag{2.40}$$

As already mentioned x^{WF} is solved in the frequency domain, whereas x^{LF} is solved in the time domain. Through the use of Fast Fourier transformation the WF response is converted into a time realization of the response. MARINTEK (2013) provides a complete derivation of this process.

Vessel Motion and Corresponding Line Tension

Two methods are generally used to find the motions of a moored vessel: coupled and decoupled analysis. The traditional method is decoupled analysis, which includes a two-step procedure (Ormberg et al., 1997):

1. The first step involves the simulation of the vessel response, both WF and LF response, whereby the load effects from mooring lines are included as nonlinear position dependent forces.

2. The second step involves the analysis of the dynamic response in the mooring lines. The top

end excitation is the motion response of the vessel, which is found in step one.

The main simplifications in the first step involve how the velocity dependent forces, damping, and the influence of mooring current forces on the position dependent forces, stiffness, are accounted for. These aspects can either be neglected or included in an approximate manner. The damping, which in general is critical for the correct calculation of the LF response, can be included by a linear damping force acting directly on the vessel. An additional current force on the vessel can be implemented to account for the current forces that acts directly on the mooring lines. Both these effects must be estimated by separate programs, and are typically included as vessel coefficients in the vessel response analysis (Ormberg and Larsen, 1998).

As described in the preceding subsection, the vessel response can be found by either solving the WF and LF response simultaneously or by separation of the response. The response in the mooring lines, the tension, can be calculated by dynamic or quasi-static methods. Figure 2.11.a provides an illustration of the decoupled approached.

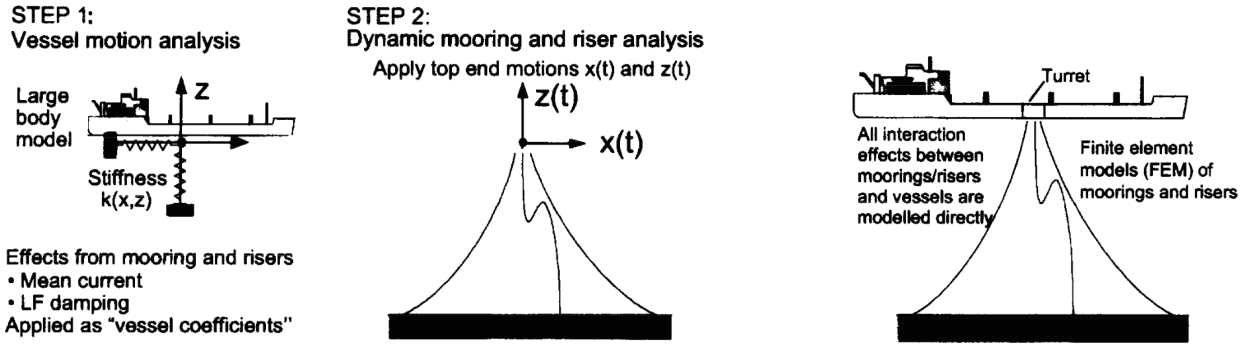

2.11.a Decoupled method

2.11.b Coupled method

Figure 2.11: Illustration of decoupled and coupled analysis methods (Ormberg and Larsen, 1998)

The main limitations of a decoupled approach include:

1. Insufficient representation of the mean current forces that act directly on the mooring lines:
2. and inaccurate estimates of the important damping effects from mooring lines on the LF

response, as they may only be included in a simplified manner.

With increasing water depth, the effects from these simplifications become more pronounced. Thus, in deep water the decoupled approach may be too inaccurate (Ormberg and Larsen, 1998). In shallow water, however, these simplifications may provide a somewhat adequate representation of the above mentioned effects, as the current drag on the mooring lines is not too pronounced. The work of Ormberg and Larsen (1998) substantiate this argument, in which a coupled and decoupled analysis of the vessel motions of a FPSO moored by a catenary system at $150m$ water depth were evaluated and compared. On the other hand, to completely neglect the influence of mean current forces and LF damping on the mooring lines over-predicts the vessel motion. The influence of increasing water depth was also studied, and it was found that the importance of mean offset increases with increasing water depth, which confirms the importance to include current effects on the mooring lines for deeper water moorings.

The shortcomings described with respect to a decoupled analysis may be overcome by performing a coupled analysis, which is illustrated in Figure 2.11.b. This approach involves simultaneously analyzing the vessel motions and mooring line dynamics. More specifically, the forces and motions for one time step are simulated and used as input for the next time step. The interaction between vessel response and mooring line dynamics are thus fully accounted for at each time step. A coupled analysis is consequently the most accurate analysis method to correctly predict the response of a moored vessel. A comparison of the vessel response obtained from experiments and the coupled time domain approach for a FPSO moored at $330m$ was found to correspond well by Ormberg and Larsen (1998).

In summary, the following coupling effects are present for a moored structure with risers (Wang, 2010):

1. Static restoring force from mooring system as function of vessel offset

2. Current loads and their effects on the restoring force of the mooring and riser system

3. Friction between seafloor and mooring lines or risers (if this interaction exists)
4. Damping from mooring and riser system due to, for instance, current and dynamics in the line
5. Friction contact between the vessel hull and riser
6. Additional inertia forces as a result of the mooring and riser system

Points 1) to 3) influence the restoring force in the system, points 4) to 5) involve the damping of the response and point 6) is related to the inertia forces. Through the performance of a decoupled time domain analysis, 1) is accurately treated, 2), 4) and 6) may be accounted for in a simplified manner and 3) and 5) cannot generally be accounted for. All the above mentioned effects are properly accounted for through the performance of a coupled time domain analysis.

As already mentioned, the mooring line tension may be calculated by a dynamic or a quasi-static method. A quasi-static approach to calculate the line tension neglect the dynamic effects in the mooring lines. These dynamic effects includes the nonlinear drag on the mooring lines and the inertia of the line. Drag forces on the mooring lines that results from the presence of current that acts directly on the lines arise from the square of the relative velocity between the line and the current. In the case of no current that acts on the mooring lines, the drag force is proportional to the square of the velocity of the line due to the forced vessel motions. An experimental study performed by Zhang et al. (2012) provided that the dynamic tension in the mooring line was significantly amplified when the line configuration changed from a slack to a taut state. Thus, for a catenary system that experience both taut and slack configuration when exposed to extreme weather, a dynamic method should be utilized to calculate the tension in the mooring lines.

2.3.3 Comparison of Time- and Frequency Domain Methods

In time domain, the equation of motion is solved by direct numerical integration, which results in significant computation time. The non-linearities in the system are directly taken into consideration

through the performance of the integration at each time step. This aspect constitutes the main difference between the time and frequency domain approach. In the frequency domain, the nonlinear terms need to be linearized and the motion is separated into a WF and LF part. As already mentioned, the linear superposition principle must be valid and harmonic loading is necessary within the frequency domain. The important nonlinear effects that result from drag loads and horizontal restoring force, which are significant for severe sea states, may be lost in this linearization procedure. On the other hand, a frequency domain analysis requires much less computational power and yields good results in moderate sea states. The frequency domain method does not discriminate between a completely Gaussian or a skewed response, as found in Fylling (1980). The skewness of a response can be seen from the lack of symmetry in the time series. Through an assumption of a positive static offset, and the LF and total motions demonstrate a negative skewness, the resulting response in terms of positive extreme amplitudes from a frequency domain simulation is overestimated. A positive skewness indicates higher positive extreme response amplitudes than provided by the frequency domain simulation.

2.4 Extreme Value Statistics

When the equation of motion is solved in the time domain, the response is given as a time series within a certain interval. The extreme value statistics are used to estimate the characteristic value from the time series. For mooring systems, this characteristic value is termed the most probable largest value. Leira (2014) presents the theory of such extreme value statistics which is briefly described in this section.

The wave elevation is assumed to be a narrow-banded and Gaussian process. The maxima of the process are then Rayleigh distributed and assumed to be statistically independent. When these assumptions are satisfied, one can utilize the Gumbel distribution to obtain the characteristic values from the response. The Gumbel distribution are typically applied to the maxima, provided that the initial response curves have an upper tail that has a normal, log-normal, exponential, Weibull,

Rayleigh, Rice etc. distribution. The most probable largest value, which is used as the characteristic value in mooring designs, correspond to a probability level of 0.37. This level is found through the integration of the cumulative distribution twice with respect to the response, by setting the obtained expression equal to zero and then solving for the response. Eq. (2.41) and (2.42) provide the expressions for the cumulative and probability density functions. The extreme value samples are $y_1, y_2, ..., y_N$, where $y = max(x_1, x_2, ..., x_n)$. n is the total number of samples from one time series and N is the number of the extreme value samples.

$$F_y(y) \;=\; e^{-e^{-\alpha(y-u)}} \qquad -\infty \leq y \leq \infty \tag{2.41}$$

$$f_y(y) \;=\; \alpha e^{-\alpha(y-u)-e^{-\alpha(y-u)}} \tag{2.42}$$

Eq. (2.43) and (2.44) presents the moments of the distribution, which are the mean value μ_y and standard deviation σ_y.

$$\mu_y \;=\; u + \frac{0.57722}{\alpha} \tag{2.43}$$

$$\sigma_y \;=\; \frac{\pi}{\sqrt{6}}\frac{1}{\alpha} \tag{2.44}$$

From the above equations the moment estimators $\hat{\alpha}$ and $\hat{u}$ are established, as provided in Eq. (2.45) and (2.46). The standard deviation $\hat{s}_y$ and mean $\hat{u}_y$ are found from the sample of extreme values $y_1, y_2, ..., y_N$.

$$\hat{\alpha} \;=\; \frac{1}{\hat{s}_y}\frac{\pi}{\sqrt{6}} \;=\; \frac{1.28255}{\hat{s}_y} \tag{2.45}$$

$$\hat{u} \;=\; \hat{\mu}_y - \hat{s}_y\frac{\sqrt{6}}{\pi}0.57722 \;=\; \hat{\mu}_y - 0.45\hat{s}_y \tag{2.46}$$

Chapter 3

Theoretical Background - Optimization

A mooring system can be optimized with respect to cost, minimum offset or line tension. Optimization with respect to cost is utilized to ensure the best possible mooring solution in terms of cost, without exceeding the MBS of the lines and to ensure that feasible solutions meet the given requirements and constraints. An optimum mooring system may also be defined as the solution that gives the minimum responses of the floating vessel (Shafieefar and Rezvani, 2007). This chapter consists of a brief description of the theory behind optimization and solution methods, together with an overview of a commonly used optimization algorithm: the NLPQL algorithm.

3.1 Introduction to Optimization

Shafieefar and Rezvani (2007) define the following aspects for optimal mooring design with respect to cost:

- Optimization of platform heading with respect to the environmental forces
- Optimization of mooring line layout, i.e. direction and spreading, with respect to directional variations in weather and fairlead arrangement
- Optimization of line tension or line length
- Optimization of materials
- Minimize the time required to perform the optimization through the automation of the design procedure

Other factors that should be considered in the design of an optimal mooring system may include anchor type, and consequently soil conditions, the use of clump weight or buoyancy elements and the design life. The cost of installation is another important cost to consider before deciding upon a final design. A full catenary chain - steel wire - chain system is typically more time demanding to install than a chain - polyester rope - chain system. The installation cost is thus higher for the steel system. A mooring optimization procedure may also involve risers along with the mooring lines. When risers are attached to the moored vessel, strict requirements are set for the vessel motion.

Three points are generally included to formulate an optimization problem:

1. A function or quantity to be minimized, often denoted as the *objective function*
2. Design requirements, referred to as *constraints*
3. Design parameters subjected to variation, which are denoted as *variables*

The above items are described in the proceeding sub sections.

A typical optimization procedure whereby the aim is to minimize the mooring line cost is executed as follows:

- Choose a starting point for the mooring system
- Perform a dynamic analysis to check if the system satisfies the given constraints
- Calculate the cost from the objective function
- Change the system and perform a new design check

This procedure is illustrated in Figure 3.1 where where the cost function is to be minimized while subjected to constraints on maximum allowable offset and minimum allowable safety factor on the mooring line tension.

Such a procedure may be automatically repeated by utilizing an automated optimization algorithm. This algorithm has certain defined convergence criteria with respect to both the cost and constraints.

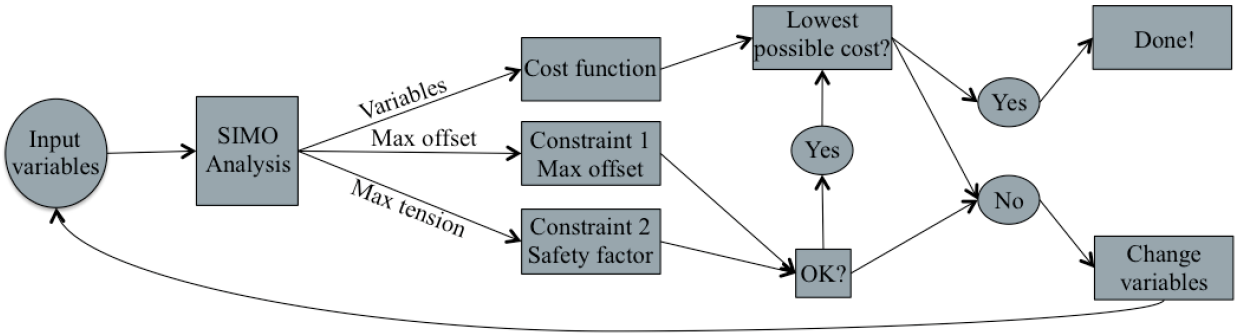

Figure 3.1: Schematic illustration of optimization procedure

The automated procedure continues to run until a minimum cost is obtained and specified constraints are satisfied.

3.1.1 Objective Function

In the optimization of a mooring system with respect to the total cost, the objective function is defined as a cost function. When a combined mooring and riser solution is designed, the minimization of the objective function corresponds to the minimization of costs related to mooring and riser materials (Fylling, 2003). Eq. (3.1) presents this aspect.

$$CF = CF_{moor} + CF_{riser} \tag{3.1}$$

The mooring cost CF_{moor} includes the cost of all components and segments in the line, e.g. material, buoys, clump weights and other hardware components. Fylling (2003) presents two different models of how to represent the riser cost CF_{riser}. The first model involves that the riser cost is offset dependent, meaning that a greater vessel offset is expected to yield higher cost. The second model represents the material cost of the riser pipe and buoyancy material. The latter model requires that the relations between the critical response in the riser and design variables are reflected in the riser modeling, whereas a detailed riser analysis within the optimization program is not required for the first model. This first model thus allows for a separate design optimization to be executed for the

riser, in which the cost optimization is only based on the riser offset.

The cost related to the riser system is naturally excluded when only the optimization of a mooring system is sought. The objective function becomes a mathematical function that describes the cost related to mooring line length, materials and cross-section dimensions.

3.1.2 Constraints

The constraints for an optimization procedure are typically established by certain rules and regulations. For the mooring lines, the requirements are typical set for maximum and minimum tension in line segments, maximum line slope at anchor, minimum fatigue life, clearance to other structures, maximum pretension in the lines and maximum vessel offset, according to Fylling (2003). The requirements for the risers are similar: maximum tension in line segments, maximum curvature of line segments and the slope range at the lower end of the line. The actual values of these requirements are case dependent. Different cases comprise mobile and permanent mooring systems, in which different requirements apply for both cases of an intact system design and one, and two, line failure design. For both mobile and permanent units, the restrictions from standards are divided into consequence classes. These consequence classes were thoroughly described in the project thesis.

The relevant responses that the constraints are checked against may be calculated by different software, and are stored. They are then, together with the requirements, converted into constraint functions (Fylling, 2003). The constraint function must be positive in order to obtain an allowable design.

The constraint functions for maximum line tension and fatigue life are derived in Fylling (2003). Eq. (3.2) presents the constraint function for maximum tension as an example of a constraint

function.

$$g_{plf} = \frac{(F_b - (f_s F_{stat} + f_d F_{dyn}))}{F_b} \tag{3.2}$$

In this equation, the partial load factors are implemented. The static and dynamic loads are provided as F_{stat} and F_{dyn} respectively, with corresponding load factors f_{stat} and f_d. In order to ensure an acceptable, design this constraint function must be non-negative.

3.1.3 Variables

The variables that can be modified during an optimization procedure are termed the optimization variables. Fylling (2003) defines the following three types of variables:

- Vessel variable - neutral heading is specified
- Line variables - direction and pretension or anchor coordinates
- Segment variables - length and cross-section parameters

For a single point mooring system the direction of each line can be varied or for a semi with line clusters in each corner the relative angle between each line in the cluster can be varied. If the mooring configuration consists of buoys or clump weights the forces from these weights may also be included as variables.

Fylling (2003) states how these parameters can be varied, and provides guidance about how to avoid error conditions in the mooring analysis.

3.2 Constrained Optimization Problems - Solution Methods

The theory in this section is mainly gathered from the work of Aksnes and Levold (2013) and Nocedal and Wright (2006). An optimization problem formulated for mooring systems is typically constrained by design requirements, as explained above. An optimization problem can also be un-

constrained, but this is not assessed in this thesis.

Eq. 3.3 presents the formulation of a constrained optimization problem in mathematical terms (Nocedal and Wright, 2006).

$$\min f(x) \quad \text{subject to} \quad \begin{cases} g_i(x) = 0,\ i \in \mathcal{E} \\ g_i(x) \geq 0,\ i \in \mathcal{I} \end{cases} \tag{3.3}$$

f is the objective function, x is the vector of optimization variables, and $g_i(x) = 0,\ i \in \mathcal{E}$ is the set of *equality constraints* and $g_i(x) \geq 0,\ i \in \mathcal{I}$ is the set of *inequality constraints*, where $\mathcal{E}$ and $\mathcal{I}$ are sets of finite indices. A *feasible point* is a point x that satisfies the given constraints. Consequently, a set of all feasible points are known as a *feasible set*. The optimization variables are typically given with upper and lower bounds.

A local optimization algorithm finds the local minimum of the objective function. It should be noted, however, that an objective function may have more than one local minimum. This aspect must be considered in the performance of an optimization with a local optimization algorithm. This procedure is termed local optimization.

Global optimization procedures may be used to find the global minimum of the objective function subjected to given constraints. It is generally difficult to find this global minimum in cases in which the problem is subjected to a large number of variables. ”In the special case where both the objective function and the constraints are convex (so-called convex optimization), a local minimum is in fact a global minimum.” ” (Aksnes and Levold, 2013).

When the objective function and constraints are differentiable, gradient methods may be utilized for optimization problems. These methods utilize the gradients of the objective function and con-

straints in order to localize "good" directions to search for local minimums. In the case that the mentioned functions can not be differentiated, or they might be discontinuous, the gradient method should be replaced with derivative-free methods. A derivative-free method is only required to evaluate the objective function. This kind of method usually consists of a large number of evaluations, and is therefore applicable to small problems with limited number of variables.

Gradient methods can be separated into two main classes for nonlinear constrained problems:

- Barrier, penalty and augmented Lagrangian methods
- Sequential quadratic programming methods (SQP methods)

The first item's concept is to replace the constrained optimization problem with a number of unconstrained problems. This replacement can be done by introducing barrier and penalty parameters. Eq. (3.4) represents a quadratic penalty function.

$$Q(x;\mu) \;=\; f(x) + \frac{1}{2\mu}\sum_{i\in\mathcal{E}} g_i^2(x) \tag{3.4}$$

The second term in this equation is the penalty term, which will increases if the constraints are breached. f is the objective function that contains x variables, g_i is the constraint function, $\mu > 0$ is the penalty parameter and $\mathcal{E}$ is the set of equality constraints.

On the other hand, if problems contain inequality constraints, barrier methods are typically utilized. Eq. (3.5) presents a typical barrier function.

$$P(x;\mu) \;=\; f(x) - \mu\sum_{i\in\mathcal{I}} \log g_i(x) \tag{3.5}$$

The set of inequality constraints are given as $\mathcal{I}$, and $\mu > 0$ represent the barrier parameters. The second term represents the barrier term and becomes very large as x approaches the boundary of the feasible set. The calculation procedures for both the penalty and the barrier method is similar; the unconstrained problem is solved for a decreasing arrangement of μ.

These two methods need to be combined in order to handle nonlinear problems. Aksnes and Levold (2013) describe issues and challenges related to the penalty and barrier methods. The augmented Lagrangian method may be used in order to overcome some of these issues. This section does not describe this method, but it is based on the same idea as the two above methods; it solves an unconstrained problem rather than a constrained problem.

SQP methods are based on the idea of formulating a quadratic sub-problem at each iterate, and then employing the solution of the sub-problem as a new search direction. The problem provided in Eq. (3.3) is modeled by linearizing the constraints, obtaining a typical quadratic subproblem as presented in Eq. (3.6).

$$\begin{aligned} \min_{p} \quad & f_k + \nabla f_k^T + \frac{1}{2}\nabla^2_{xx}\mathcal{L}_k p \\ \text{subject to} \quad & \nabla g_i(x_k)^T p \;=\; 0,\; i \in \mathcal{E} \\ & \nabla g_i(x_k)^T p \;\geq\; 0,\; i \in \mathcal{I} \end{aligned} \tag{3.6}$$

The Hessian of the Lagrangian of the problem is defined in Eq. (3.7), whereby λ_i is the Lagrange multiplier for the constraint g_i.

$$\nabla^2_{xx}\mathcal{L}(x,\lambda) \;=\; \nabla^2_{xx}\left(f(x) - \sum_{i\in\mathcal{L}} \lambda_i g_i(x)\right) \tag{3.7}$$

The utilization of the Lagrange multiplier provides a strategy for finding loacal minimum or maximum points in mathematical optimization, whereby the objective function is exposed to constraints. Active set methods, described in Nocedal and Wright (2006), are quadratic programming algorithms applied to solve Eq. (3.6). Further study of SQP methods and solution algorithms will not be assessed in this thesis, but a reference is made to Nocedal and Wright (2006). The SQP methods are suitable for both small and large problems.

3.2.1 Optimization Algorithms

The software to be utilized in the optimization in this thesis is known as SimOpt and is implemented in the SIMA workbench. SimOpt is an external program and an interface to the FORTRAN subroutine NLPQLP. NLPQLP performs the actual optimization, and is a specified version of the NLPQL routine developed by Schittkowski (1986). Other routines are also available for optimization purposes, but is only mentioned briefly as the NLPQL is the basis for the optimization work in this thesis.

NLPQL is a FORTRAN implementation of a SQP method used to solve nonlinear constrained optimization problems. The following assumptions determine its applicability:

1. A smooth problem: Both the cost function, or another objective function, and the constraint functions must be continuously differentiable within the area of specified variable limits. The functions only need to be defined within these variable boundaries, since the routine does not search for a solution outside these.

2. A small problem: The problem size will depend on e.g. storage capacity, and on the quadratic programming routine's capability to solve large problems. The more variables that exist in the optimization, then the larger problem becomes. Extensive testing has been executed on the NLPQL routine with up to 100 variables (Schittkowski, 1986).

Schittkowski (1986) provides a more mathematical explanation of the NLPQL program, together with a formulation of a quadratic programming sub-problem. The results obtained from the NLPQL program were by Schittkowski (1986) compared to the results from seven other frequently used optimization programs. The comparative results found that the NLPQL program was the most efficient in terms of calculation time.

The quadratic programming algorithms used for solving SQP problems are gradient based, or derivative-based, which means that they utilize the information of the derivatives when solving the problem. Yang (2011) describes the disadvantage of such algorithms; they are efficient for local minimum search, but may be trapped in a local minimum point if the considered problem is not convex. Certain requirements are thus induced on the objective function. Other algorithms described in Yang (2011) is derivative-free algorithms, which may be more efficient if discontinuities are present in the objective function, and metaheuristic algorithms. These algorithms are not further described in this thesis.

Chapter 4

Analysis Description

Section 4.1 describes the vessel considered throughout the analyses performed in Case Studies 1, 2 and 3. The main differences between the cases is the mooring system configuration, which is presented specifically for each case.

The analysis performed in each case study is based on certain design limit states and environmental conditions. Section 4.2 provides a brief description of the design restrictions. Section 4.3 describes the environmental conditions. Several simulations tools and software are available to analyze moored structures in terms of vessel response and tension in the mooring lines. This thesis utilizes MIMOSA, SIMO and Riflex to perform mooring system analyses. The basic theory of each of these programs is described in sections 4.4.1, 4.4.2 and 4.4.3, respectively.

4.1 Description of Safe Scandinavia

The work in this thesis considers the semi-submersible Safe Scandinavia, which is presented in Figure 4.1. It is a moored support and accommodation unit, converted to function as a tender support vessel for Statoil's Oseberg Øst platform in 2015. The semi functions as an accommodation unit, in addition to supplying the permanent platform with bore oil (Prosafe, 2016b).

Browne (2015) listed the data on Safe Scandinavia. It consists of two pontoons, eight columns and a topside. Table 4.1 presents the dimensions with a draft equal to $17.5m$ for the "survival" condi-

Figure 4.1: Safe Scandinavia (Prosafe, 2016a)

tion. For each case, this draft is kept fixed. The semi-submersible operates in relatively shallow water or 157m water depth. The structural mass of the semi is $2.684 \cdot 10^7 kg$ or 26,840 tons.

Parameters	**Unit**	**Topside**	**Hull**
Area, Ax	m^2	2400.0	1320.0
Area, Ay	m^2	3200.0	1760.0
Area, Az	m^2	4800.0	4800.0
Length, Lx	m	80.0	60.0
Length, Ly	m	60.0	60.0
Length, Lz	m	40.0	22.0

Table 4.1: Dimensions of topside and hull for Safe Scandinavia

Statoil provided the RAOs and wave drift force coefficients for the semi, in terms of the output from a WAMIT analysis. Plots of RAOs in all DOFs and wave drift force coefficients in surge, sway and yaw are presented in Appendix A.1 and A.2. Statoil also provided the current- and wind force coefficients, which are found from a small scale wind tunnel test. Plots of the wind- and current force coefficients against weather direction in surge, sway and yaw are included in Appendix A.3. The RAOs, wave drift-, current- and wind force coefficients are implemented in each case study to ensure consistent vessel representation and properties.

4.2 Design Limit States

Standards such as ISO (2013) and DNV (2013) set the design criteria for a moored vessel and the mooring lines. There are typically three different limit states against which a mooring system has to be checked:

- Ultimate Limit State (ULS)
- Accidental Limit State (ALS)
- Fatigue Limit State (FLS)

The design for these three different states are respectively: design against overload for an intact system, design against overload for a damaged system and design against fatigue failure, in which all possible sea states are taken into account (Larsen, 2015). Overload is characterized as any tension that exceeds the limits for either mooring lines or anchor. The avoidance of overload of an intact system indicates that the mooring lines shall resist known loads with a given safety margin. The ALS design is utilized to ensure that an accidental event shall not develop into a direct collapse, and is ordinarily checked by one or two line failures. Both ULS and ALS should be checked in extreme weather conditions. The FLS should ensure that the mooring lines individually have the adequate capacity to withstand cyclic loading (DNV, 2013). The mooring system should be evaluated with respect to these criteria with specified safety margins.

This section does not further explain design with respect to the FLS, as this thesis did not execute a fatigue assessment. In the designing of a final mooring system, an assessment of the FLS design should naturally be included.

In standards, criteria are specified for either permanent or mobile moorings with respect to the operational environment, design life, clearances to other structures and redundancy. There are also certain requirements for the hardware components in the mooring system, such as winches, con-

nection links, anchors, chains, steel wires and polyester ropes.

The design criteria utilized in the mooring analyses performed in this thesis is based mainly on the maximum line tension. The manufacturer provides the minimum breaking strength (MBS) of a mooring line or mooring component. The design load F_D on the mooring lines have to be less than the design resistance F_R, which results in a limit for the line tension. This load is often expressed as a percentage of the MBS and results in a certain safety factor, as presented in Eq. (4.1).

$$\begin{aligned} F_D &\leq F_R \\ \Rightarrow F_{MPM} \cdot sf &\leq MBS \end{aligned} \tag{4.1}$$

F_{MPM} is the most probable maximum load. A tension limit of 50% MBS will consequently result in a safety factor of 2.

DNV (2013) and ISO (2013) states that in the Norwegian and UK sector, a combination of both wind and waves for a 100-year return period, together with a 10-year return period for current, is generally applicable. Typically, the 100-year design criteria should be used for both permanent and mobile mooring systems.

Table 4.2 and 4.3 present safety factors valid for vessels that operate at the Norwegian Continental Shelf are found in ISO (2013).

Consequence Class	**3**	**2**	**1**
Intact	2.20	2.00	1.50
One line failure	1.50	1.35	1.20
Two line failures	1.50	1.35	N/A

Table 4.2: Safety factors for permanent mooring systems at the NCS (ISO, 2013)

In Table 4.2 the intact and one line failure system should be designed with respect to a design storm

with a 100-year return period, whereas the two line failure system should be designed with respect to a 10-year return period.

Consequence Class	**3**	**2**	**1**
Intact	1.90	1.80	1.50
One line failure	1.30	1.20	1.10

Table 4.3: Safety factors for mobile mooring systems at the NCS (ISO, 2013)

The safety factors for the latter table are provided for extreme weather conditions with a 100 year return period.

The consequence classes represented in Table 4.2 and 4.3 are defined as:

- *Class 1* - Failure of the mooring system is not likely to lead to catastrophic consequences
- *Class 2* - Failure of the mooring system may lead to undesired consequences
- *Class 3* - Failure of the mooring system is likely to lead to catastrophic consequences

A catastrophic consequence may be a collision between two installations, any event leading to loss of human life or any event leading to severe environmental impact. For a mobile flotel, or a tender support vessel, *Class 3* is applicable when the unit is in operating condition, i.e. when it is connected to a production platform. *Class 1* is applicable during survival condition, typically in extreme weather conditions, and the unit is disconnected from the production platform and moved a required distance away from the permanent unit. Other examples the suitability of *Class 3* is for a drilling platform or a production unit during operation, and *Class 2* may for instance be relevant for a drilling rig or production unit in which the operation is temporary stopped, but the riser(s) are still connected to the seafloor. *Class 1* may be applicable for a drilling platform when the riser has been disconnected for survival in extreme conditions.

Sjøfartsdirektoratet (2011) includes additional requirements for mobile units that operate as tender support vessels. They state that when the unit is operating close to a another installation, a safety

factor of 2.2 should be applied to the lines that are critical with respect to collision. For Safe Scandinavia this procedure involves the heaviest loaded lines when the weather is directed northwards, since the permanent installation lies north of Safe Scandinavia. The next requirement is if three of the most loaded lines in one corner of the vessel fail, then the mobile unit should steer clear of the permanent platform with a minimum $10m$ clearance. The calculation of the motions for both the permanent and mobile unit should be executed in the case of the largest failure mode of both such that this requirement, minimum $10m$ distance between the two structures is maintained.

The additional design requirements introduced above were not accounted for in the performance of a mooring system analysis in MIMOSA in the project thesis. They are thus not included in the analysis in Case Study 1 where the objective is to correctly implement the mooring system from MIMOSA to SIMO, and to compare the analysis results from these two different types of software. In Case Study 2, however, the impact of designing a mooring system with a safety factor of 2.2 is studied with respect to the hardware cost.

4.3 Environmental Conditions

This section presents the environmental conditions utilized in Case Studies 1, 2 and 3. In accordance with regulations introduced in the preceding section, the design weather is based on a 100-year extreme condition or design storm. In this way, the wind and waves were expected to be their worst over a 100-year period, with a corresponding expected worst current over a 10-year period.

All environmental data is found from the Metocean Design Basis for the Heidrun field provided in Eik and Nygaard (2004).

Waves

The wind-generated sea was modeled through a doubly peaked spectrum, which is also known as the Torsethaugen spectrum, in both MIMOSA and SIMO. The spectrum includes two parameters; significant wave height H_S and peak period T_P. These values are gathered from the 100-year contour line provided in Figure 4.2, and are presented in Table 4.4. Additionally, the wave direction needed to be specified in both MIMOSA and SIMO.

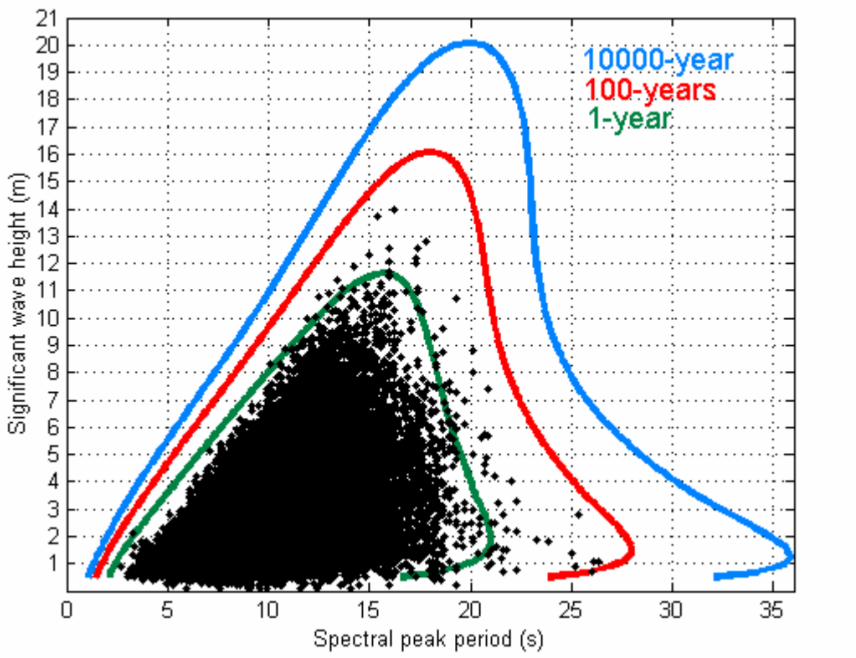

Figure 4.2: Contour plot of extreme value waves (Eik and Nygaard, 2004)

Significant wave height	Peak period
16.0 $[m]$	18.2 $[s]$

Table 4.4: Parameters describing the wave condition

The mean wave forces are given from the wave drift coefficients, defined for different frequencies and directions, and are included in the vessel description. The LF wave force is calculated from Newman's approximation in both SIMO and MIMOSA (MARINTEK, 2013) (Kaasen et al., 2012)

and is based on certain assumptions with respect to the second order transfer functions. The slowly varying wave force spectrum in MIMOSA is calculated by the expression provided in Eq. (2.26) from section 2.3.1, which includes both frequency and direction as variables. The first order wave forces are calculated based on the doubly peaked wave spectrum in both SIMO and MIMOSA.

Wind

The wind generated in MIMOSA and SIMO is modeled as a constant speed with a varying speed component with zero mean added. The gust spectrum used in the analyses to model the varying part of the wind was the ISO spectrum, which is also referred to as an NPD spectrum. Figure 2.6 in section 2.2.1 illustrates the ISO spectrum. This spectrum is defined on the domain [1/600,0.5]Hz in MIMOSA. The input parameters for an ISO spectrum are the mean wind speed and reference height for this parameter as well as direction. Eik and Nygaard (2004) provided the mean wind speed, which is a one-hour mean extreme wind velocity with a 100-year return period. Table 4.5 presents the specific wind condition utilized in the analyses. As various directions were utilized throughout this thesis, they are specified for each case study.

Mean wind speed	**Reference height**
36.0 $[m]$	10.0 $[m]$

Table 4.5: Parameters describing the wind condition

Current

The current does not vary in time, and is not represented by a spectrum. In both SIMO and MIMOSA, it is possible to model the current for several z-levels or depths, and thus to create a current profile. In this thesis's analyses, the current was defined for only one z-level, i.e. at the sea surface or $z = 0m$, and thus neglects the current drag on the mooring lines. The current is modeled as a constant horizontal velocity vector with an assumption of no current variation over the draft of

the vessel. The current condition defined in each analysis is given in Table 4.6, whereby the mean current velocity is taken from Eik and Nygaard (2004), as the ten-minute extreme value at the sea surface, with a 10-year return period.

Mean current speed	**z-level**
0.94 $[m/s]$	0.0 $[m]$

Table 4.6: Parameters describing the current condition

4.4 Simulation Tools

In order to qualitatively compare the differences in the results from MIMOSA, SIMO and Riflex, the following sections describe the basic theory about each software.

4.4.1 MIMOSA

MIMOSA is the preferred software for mooring analyses in the frequency domain, and the in- formation about the program provided in this section can be found in Kaasen et al. (2012). It is an interactive program to perform both static and dynamic mooring analyses. As it is a frequency domain computer program, the LF response is calculated through the utilization of a linear model of the nonlinear mooring and vessel model. In both the project thesis and in this master thesis, only a three DOF analysis was executed in MIMOSA.

MIMOSA is fully interactive, which enables the user to have control over the computations and to modify the input parameters during the analyses. Input files for the mooring system, to define the mooring line parameters, as well as the vessel motion are necessary. The input file that describes the vessel motion must include RAOs, wave drift force coefficients and wind- and current force coefficients. MIMOSA can read text files and result files from vessel motion computation

programs such as WAMIT. Results and plots computed by MIMOSA are directly presented within the interface, and the user may also save these elements to an external file.

The wind force is calculated from the wind velocity and its gust spectrum as already defined in section 2.3.1. . One should note that the wind in MIMOSA is not modeled with relative velocity, and damping from wind is not automatically included. The current, however, is modeled with translational relative velocity, which results in both driving and damping forces on the vessel. Both wind- and current force coefficients are included in the vessel description input file.

Vessel Motions and Corresponding Line Tension

As MIMOSA is a frequency domain program, the motion response is separated into a WF and a LF part. The WF motions are directly provided from the wave spectrum, in conjunction with the RAOs from the vessel description file. The *significant* value of the WF response is derived from the Rayleigh distribution, which is twice the standard deviation $\sigma_{x^{WF}}$. The static equilibrium of the system is found through a numerical procedure to solve an equation, whereby the addition of all the means, static, and forces on the system are set equal to zero. The static position is thus given as the position where the static mooring lines forces on the vessel are equal to the static environmental forces.

In MIMOSA, extreme WF response is defined as the most probable largest value, hereby denoted x_{max}^{WF} and presented Eq. (4.2).

$$x_{max}^{WF} = \sigma_{x^{WF}} \sqrt{2lnN^{WF}} \tag{4.2}$$

Where N^{WF} is the mean number of zero up-crossings of the respone x, which is determined from the mean zero up-crossing period.

The LF response is found by solving the linearized equation of motion, as presented in section 2.3.1. The principle of stochastic linearization is utilized to determine the damping and stiffness

matrix. The linearization is based on the assumption that the LF response is Gaussian, which is not necessarily the case. Kaasen et al. (2012) notes that the procedure to compute the stiffness and damping is expected to introduce some conservatism in the LF response.

Both slowly varying wind and wave drift excitation contributes to the extreme LF response. The wind's contribution to the extreme LF response may be estimated in the same manner as the extreme WF response because the wind excitation can be regarded as Gaussian. The wave-drift excitation is non-Gaussian, and the LF response lies somewhere in between a Gaussian and exponential distribution, depending on the dynamic properties of the mooring system (Kaasen et al., 2012). In order to account for the non-Gaussian LF response from wave drift, the most probable largest value of both LF wind and wave response becomes as expressed in Eq. (4.3)

$$x_{max}^{LF} = \sigma_{x^{LF}} \sqrt{2lnN^{LF}} \cdot f \tag{4.3}$$

The factor f accounts for the fact that the LF response is non-Gaussian, as a result of the fact that the wave drift excitation is non-Gaussian.

The tension in the lines that arises from the LF response is calculated quasi-statically and neglects the influence from line inertia and damping forces that act on the line. This LF tension and its standard deviation are found directly from the pre-calculated line characteristics in the execution of a three DOF analysis. In addition, the line characteristics in MIMOSA is only calculated for one z-level in the three DOF analysis. If the quasi-static method for WF tension is selected, the line characteristics directly provide the WF tension.

In addition to the quasi-static method, the WF tension in the line can be calculated through a simplified dynamic method or by a finite element method (FEM). As the simplified dynamic method was not utilized in any analyses, this section only describes the FEM. Eq. (4.4) presents the most

probable largest tension T_{max}.

$$T_{max} = T_{base} + T_{max}^{WF} \tag{4.4}$$

Section 2.3.1 describes the base tension T_{base}. The WF tension, and thus the most probable largest WF tension T_{max}^{WF}, found by FEM include dynamic effects, such as inertia and drag on the mooring lines. These dynamic effects are linearized as the analysis is performed within the frequency domain. T_{max}^{WF} is calculated in a similar manner to the maximum vessel response, as the WF top end motion is assumed to be Gaussian and narrow-banded and the peaks of nodal tension are expected to be Rayleigh distributed. Some modifications are included in the computation of T_{max}^{WF}, however, that try to capture the non-linear behavior of the dynamic cable model. Kaasen et al. (2012) explain these modifications.

4.4.2 SIMO

All theory related to SIMO presented in this section can be found and is explained more thoroughly in MARINTEK (2013). SIMO is a time domain software that is able to simulate total motions and station keeping behavior of complex marine operations. It allows for flexible modeling of multi-body systems and nonlinear simulation in the time domain. As described in section 2.3.2, in time domain analysis, the equation of motion can be solved through convolution integrals or by separation of motions. Infinite frequency added mass and retardation functions were not available for the model of Safe Scandinavia, and consequently, this analysis utilizes the separation of motions method.

The main difference between modeling environmental forces in SIMO and MIMOSA is that SIMO can compute the wind force with relative velocity between the wind and vessel, and the damping contribution from wind is directly included based on the wind force coefficients. Similar to MIMOSA, the current force is also modeled with relative velocity. Fast Fourier transformation (FFT) generate the time series of the wave and wind excitation.

The modeling of catenary lines in SIMO was based on the model used in MIMOSA; each line is described by a line type and initialized by either pretension and direction or global anchor coordinates, and prescribed a breaking strength. Cross section parameters and length are given for each segment together with the unit weight in air, the elasticity modulus and the transverse- and longitudinal drag coefficient for each line type. The mooring lines are assumed to form a catenary shape modeled through catenary equations. A ”shooting method” is used to calculate the initial configuration of the mooring lines. The basic principles of a shooting method is based on an iterative correction of unknown boundary conditions at one line end to satisfy the specified boundary conditions at the other line end (MARINTEK, 2015).

Vessel Motions and Corresponding Line Tension

As the equation of motion is solved by separation of motions, the WF motion response is solved in the frequency domain and the LF motion response is solved in the time domain by numerical integration. The 3^{rd}-order Runge-Kutta method is the numerical integration method utilized to solve the LF equation of motion, and is described in MARINTEK (2013). The results in terms of vessel motions are provided as separated time series of the WF and LF response, and the total response is found through a summation of the response time series. As the WF motions are solved in the frequency domain, the wave spectra in conjunction with the RAOs are utilized to simulate the WF response. FFT are then applied to generate the WF motion time series. The time series of both the WF and LF responses are based on the same sea state realization, which ensures the correct correlation between the two responses.

Both a quasi-static and a simplified dynamic model is available to calculate the mooring line tension. Only the quasi-static method is utilized in this thesis to calculate the tension in the line, and hence, the calculation neglects the transverse drag on the mooring lines. The line characteristics, from which the quasi-static line tension is found, are computed in the vertical plane and are a function of both the x and z coordinates. In addition, these characteristics are updated during the sim-

ulation, which ensures that the calculation properly accounts for the nonlinear geometric stiffness. In MIMOSA, the geometric stiffness is linearized as explained in the previous section. In addition, the line characteristics in SIMO are computed for more than one z-level, unlike MIMOSA.

4.4.3 Riflex

The theory presented in this section is found from MARINTEK (2015) and can be studied in depth in this theory manual. Riflex is a time domain finite element software based on small strain approximations, which makes it suitable to analyze slender structures, such as mooring lines.

The mooring lines are modeled as finite elements with nodes connected at each end of the element. The nodes have three translational and three rotational DOFs. Both beam and bar elements are available to describe the slender structure, but a bar element will typically be applicable to represent mooring lines as the bending stiffness is quite small and completely absent for chains. The axial stiffness in the element is described by a tension-elongation curve. A total Langrangian formulation describes the spatial bar element. The cross section of the element is assumed to be constant during elongation, and the strain is described by the Green strain tensor and the stress is described by Piola-Kirchhoff stress.

When performing a dynamic time domain analysis, the dynamic equilibrium equation of a spatial discretized finite element system model is presented by Eq. (4.5).

$$\boldsymbol{R}^I(\boldsymbol{r}, \ddot{\boldsymbol{r}}, \boldsymbol{t}) + \boldsymbol{R}^D(\boldsymbol{r}, \dot{\boldsymbol{r}}, \boldsymbol{t}) + \boldsymbol{R}^S(\boldsymbol{r}, \boldsymbol{t}) \;=\; \boldsymbol{R}^E(\boldsymbol{r}, \dot{\boldsymbol{r}}, \boldsymbol{t}) \tag{4.5}$$

$\boldsymbol{R}^I$ and $\boldsymbol{R}^D$ is the inertia and damping force vectors, $\boldsymbol{R}^S$ is the internal structural reaction force vector and $\boldsymbol{R}^E$ is the external force vector. $r,\ \dot{r}$ and $\ddot{r}$ is the structural displacement, velocity and acceleration vector.

The physical effects that contributes to the external force vector are;

- Weight and inertia, which are governed by line mass
- Hydrostatic force, which depends on pressure gradients
- Hydrodynamic forces that depends on waves, current and structure motions
- Forced line motion, which depends on vessel motions

The hydrostatic pressure effects are modeled by conservative, vertical forces. The hydrodynamic forces that depend on waves and current that act directly on the mooring lines ware omitted in the analyses, but the hydrodynamic forces that arise from the forced motions of the line's top end are included.

The mooring lines can be analyzed through a nonlinear or a linear time domain analysis. The nonlinear analysis is utilized in this thesis, through a step-by-step numerical integration of the incremental dynamic equilibrium equation based on the Newmark β-family method. This method allows for proper treatment of nonlinearities in the system, including:

- Geometric stiffness
- Nonlinear material properties
- Hydrodynamic loading from the generalized Morison equation given with relative velocities
- Contact problems (e.g. bottom contact for the mooring lines)

The sequence of calculations for a nonlinear integration procedure is summarized in MARINTEK (2015). The main points are to first calculate the static conditions. Then, at each time step the effective stiffness matrix, effective load vector, incremental displacements, velocities and accelerations are computed. At the same time step, an equilibrium iteration is executed until convergence is obtained. In this thesis, the mooring lines are analyzed without current that acts directly on the lines, and the hydrodynamic loads from the generalized Morison equation is thus not calculated from relative velocity, but only from the line velocity due to the forced vessel motions. The bottom contact is modeled by vertical bi-linear springs and horizontal springs combined with friction forces that result from sliding. For the analyses in this thesis, only vertical stiffness is included.

The main difference between SIMO and Riflex in terms of computing the mooring line response, is the calculation method. Riflex computes the tension through a FEM, which considers the dynamics of the mooring lines, whereas SIMO calculates the tension quasi-statically.

The main drawback of a full nonlinear time domain analysis is the computation time, as repeated assembly of the system matrices and triangularization at each time step is quite time consuming.

4.5 Efficient Use of SIMA Workbench

In order to efficiently use the SIMA workbench for mooring system analyses, there are different available options. The first option is to compute both vessel motions and line tension in SIMO, which results in a quasi-static or simplified dynamic calculation of the line tension. The vessel and mooring lines are both modeled in SIMO, and the damping effects from the mooring lines is included in the linear damping matrix. Case Studies 1 and 2 employ this method. In order to calculate the dynamic tension in the mooring lines, the FEM in Riflex should be chosen. A full nonlinear time domain analysis of the total response are available in SIMO, but the separation of motions method can also be utilized, whereby the WF response are computed in the frequency domain and the LF response is computed in the time domain.

The calculation of the dynamic line tension in Riflex can be done in two different ways, through either a decoupled or a coupled approach. The decoupled analysis involves the simulation of the vessel motion in SIMO, where the response is simulated without dynamic effects in the mooring lines that arise from drag and inertia, which again may influence the vessel motions. The mooring lines are modeled in Riflex as slender structures made from finite elements. The excitation of the dynamic mooring line tension is the top end motion of the line, i.e. the vessel motions simulated in SIMO. In this way, the motions are pre-simulated in SIMO for a three-hour sea state without consid-

ering the influence that the mooring dynamics have on the vessel response. These motions are then imported into Riflex and applied to the top node of the line. Figure 4.3.a illustrated this method. In this illustration, the stiffness and damping signs in the model represent the stiffness in the system, i.e. the geometric and elastic stiffness in the lines, in conjunction with the hydrostatic stiffness in heave, roll and pitch, the linear damping included in the vessel kinematics and the damping arising from relative current and wind velocity, which are provided by wind- and current force coefficients.

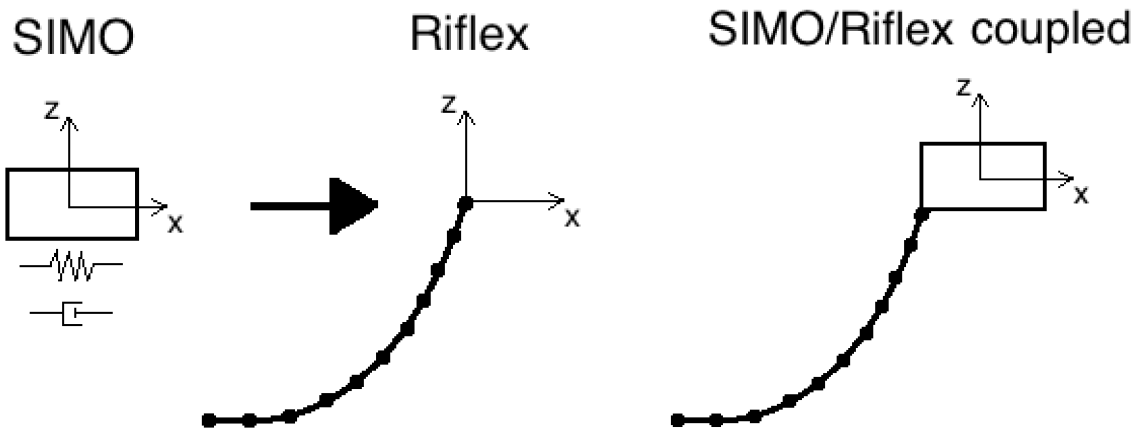

4.3.a Decoupled analysis in SIMA 4.3.b Coupled analysis in SIMA

Figure 4.3: Simplified 2-D illustration of decoupled and coupled method in SIMA

The motions in SIMO are either separated into WF and LF response, whereby the WF response is solved in the frequency domain and the LF response is solved in the time domain, or alternatively, are solved simultaneously within the time domain. Within this analysis, the motions are separated due to the lack of the needed retardation functions to solve the total motion in the time domain. Case Study 3 utilizes the method illustrated and described above.

The last option is to perform a coupled SIMO/Riflex analysis illustrated in Figure 4.3.b. This option in SIMA allows the vessel motions and dynamic tension in the lines to be solved simultaneously. The vessel properties, the vessel kinematics, and the mooring lines are modeled in a coupled

SIMO/Riflex task. The mooring lines are modeled in the same manner as in a Riflex task, i.e. made up from finite elements with supernodes that are defined at the upper and lower line end, which correspond to the fairlead and anchor position, respectively. The main advantage of this method is that at each time step the influence that the mooring line dynamics have on the vessel response is accounted for. A full time domain analysis is necessary in the coupled SIMO/Riflex analysis, and retardation functions must be included.

Chapter 5

Case Study 1: SIMO Analysis of Safe Scandinavia

A simplified analysis of Safe Scandinavia in the frequency domain was executed, as part of the project thesis work carried out during the autumn 2015, in the MIMOSA software. This chapter includes the procedure to implement the model in the SIMO software. This process leads to a comparison of the results from a SIMO analysis with the results obtained from the MIMOSA analysis.

5.1 Mooring System Configuration

Safe Scandinavia is moored with 12 lines. Figure 5.1 presents the mooring line configuration whereby the lines in each cluster are placed with 5° spacing.

The permanent platform, Oseberg Øst, lies north of Safe Scandinavia in "operational" condition. According to the supervisor, guidelines from Statoil state that the lines taking most of the load, when the vessel is exposed to weather in the direction towards the permanent structure in vicinity, must be made from steel. Consequently, lines 4 to 6 and 7 to 9 consist of a chain-steel wire-chain configuration, whereas lines 1 to 3 and 10 to 12 have a chain-fiber rope-chain configuration. Although this analysis only considers the response assuming that the vessel is displaced a distance away from Oseberg Øst in survival condition, the lines are defined by that same criterion. Browne (2015) derives the properties of the initial line materials, which are presented in Table 5.1.

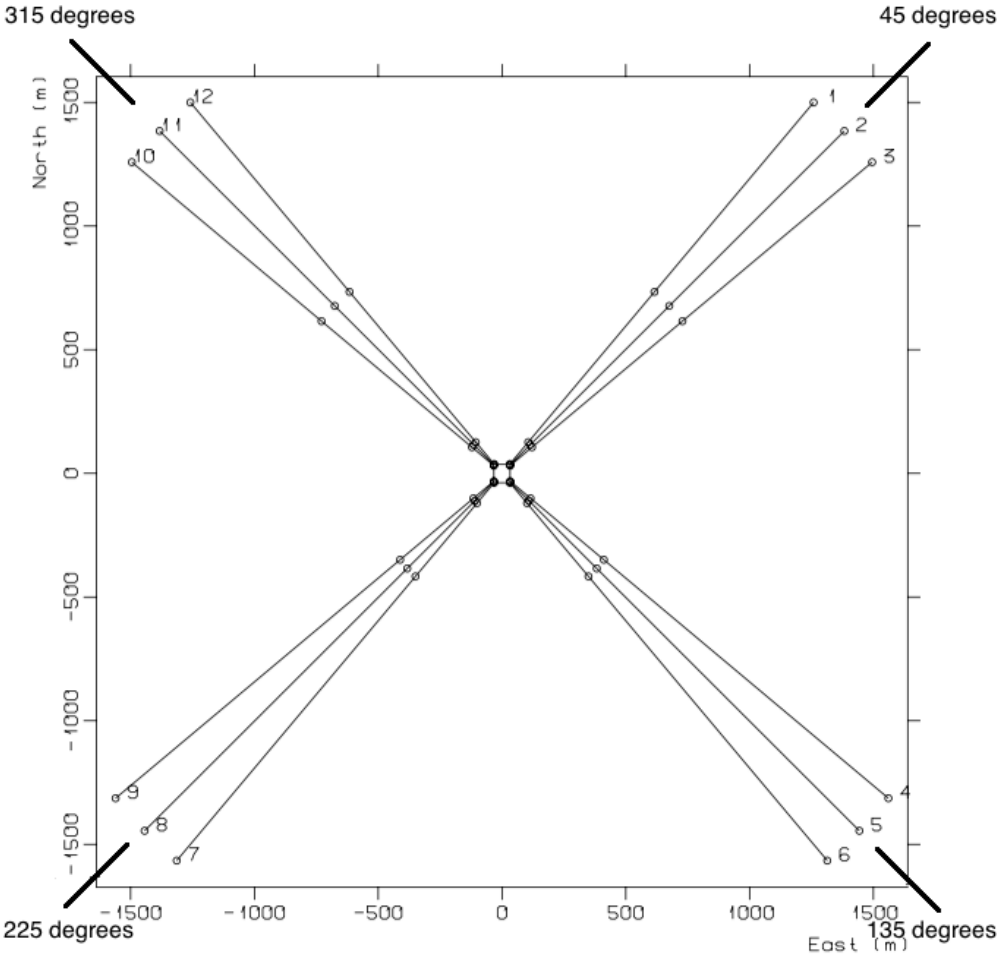

Figure 5.1: Horizontal projection of the mooring system from MIMOSA

Type	Diameter	Weight in water	E-modulus	MBS
	$[mm]$	$[kN/m]$	$[kN/m^2]$	$[kN]$
Chain R5, stud link	84.0	1.3	$640.0E+5$	8417.0
Wire rope, Diamond Blue	116.0	0.5	$664.0E+5$	8417.0
BexCo fiber	160.0	0.05	$118.0E+5$	8417.0

Table 5.1: Mooring line hardware properties

Each line- and segment length was initially chosen based on data provided in Browne (2015). In the project thesis, the line configuration was verified by checking that neither the steel wire segment nor the fiber rope segment interacted with the seabed. Line segment lengths and pretension in the lines were modified to ensure no interaction took place. Table 5.2 presents the resulting mooring line composition and pretension for the initial analysis..

Line	Pretension	Direction relative north	Bottom chain	Wire	Polyester	Rig chain
	$[kN]$	[°]	$[m]$	$[m]$	$[m]$	$[m]$
1	800.0	40.0	1000.0	-	800.0	120.0
2	800.0	45.0	1000.0	-	800.0	120.0
3	800.0	50.0	1000.0	-	800.0	120.0
4	900.0	130.0	1500.0	400.0	-	120.0
5	900.0	135.0	1500.0	400.0	-	120.0
6	900.0	140.0	1500.0	400.0	-	120.0
7	900.0	220.0	1500.0	400.0	-	120.0
8	900.0	225.0	1500.0	400.0	-	120.0
9	900.0	230.0	1500.0	400.0	-	120.0
10	800.0	310.0	1000.0	-	800.0	120.0
11	800.0	315.0	1000.0	-	800.0	120.0
12	800.0	320.0	1000.0	-	800.0	120.0

Table 5.2: Mooring line composition

This mooring line configuration is employed in the initial analysis in both MIMOSA and SIMO.

5.2 Method

Safe Scandinavia, as described in section 4.1, with a mooring system as described above was analyzed in MIMOSA in the project thesis, and this model is utilized in the analyses in this case study. The mooring and vessel description files were provided as output from MIMOSA, and is read directly into SIMO. The project thesis performed both a ULS and ALS analysis, as described in section 4.2. Only a ULS analysis is executed in SIMO, and thus only the results from the ULS analysis in MIMOSA is compared to those obtained from SIMO. The environmental conditions are defined as a 100-year extreme storm, as described in section 4.3. Figure 5.2 presents a screen shot of the mooring system from the SIMA workbench, where the coordinate system to the left represent the global coordinate system in SIMO.

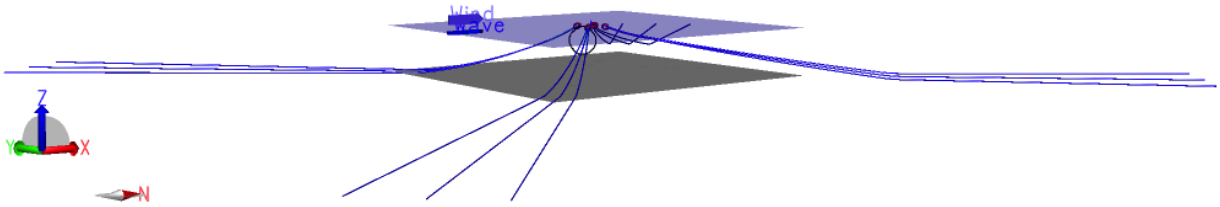

Figure 5.2: Screen shot of mooring system in SIMA

The proceeding provides a description of the implementation of the provided vessel and mooring system. This section highlights the differences in coordinate systems and include a verification of correct modeling of the vessel and mooring lines. Further, the procedure of extracting the most probable largest motions and line tension in SIMA is described.

5.2.1 SIMO Implementation of Model

In the implementation of the Safe Scandinavia model from MIMOSA into SIMO, some modifications and verifications are necessary to ensure that the model works correctly. The analysis in MIMOSA was executed with only three DOFs, whereas a full six DOF analysis is performed in

SIMO.

The first aspect to note is the difference in the coordinate system in SIMO in comparison to MIMOSA. Figure 5.3 presents the two different coordinate systems, including an illustration of Safe Scandinavia.

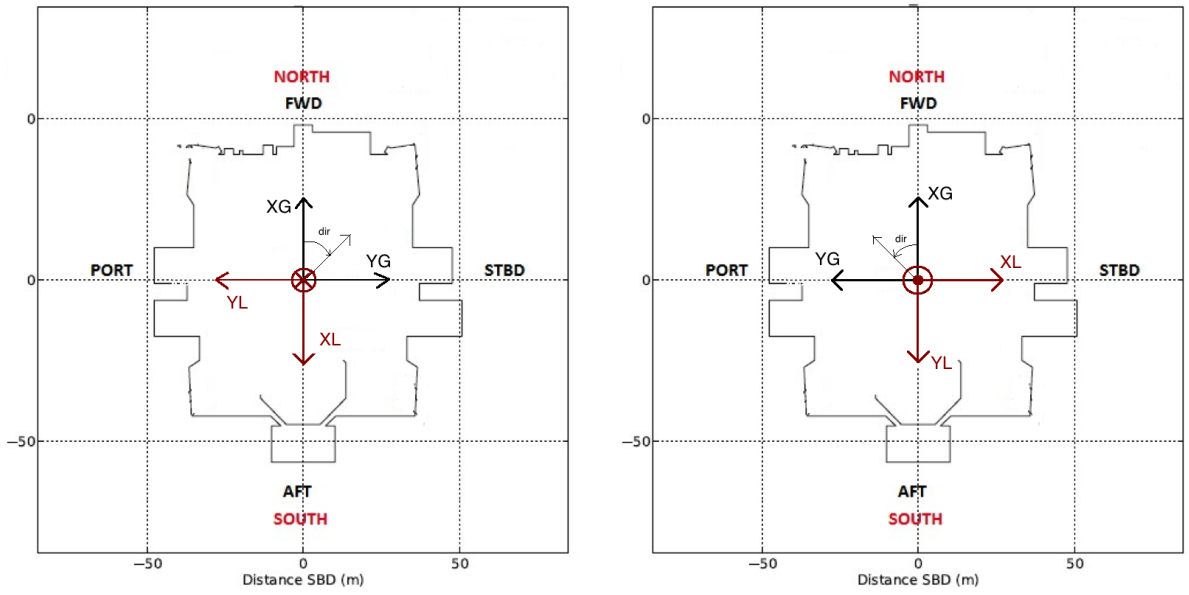

5.3.a Global and local coordinate system in MIMOSA 5.3.b Global and local coordinate system in SIMO

Figure 5.3: Coordinate systems

Both the local and global z-axis in MIMOSA points downwards, or into the paper, as illustrated in Figure 5.3.a, which leads to clockwise positive yaw moment. In SIMO, the global and local z-axis points upwards, out of the paper, as depicted in 5.3.b, which gives positive rotation about the z-axis counterclockwise. The local coordinate system in both figures is shifted 180°. This shift is due to the definition of current- and wind force coefficients that are found from model testing. These components are based on the local coordinate system illustrated in Figure 5.3.a, and are converted to follow the local coordinate system in Figure 5.3.b when the vessel is imported from MIMOSA into SIMO. A further important distinction is that the direction in terms of degrees is given as clockwise in in MIMOSA, whereas it is defined counterclockwise in SIMO. This implies that a

weather direction of 45° in MIMOSA corresponds to a weather direction of 315° in SIMO.

In the importation of the model from MIMOSA to SIMO, the rotation of the vessel was not included. The vessel rotation about the z-axis is manually set to 180° in SIMO to obtain the correct coordinates of each line end, e.g. the coordinates of line 6 in MIMOSA should be equal to the coordinates of line 6 in SIMO with respect to the north/south definition. This aspect simplifies the comparison of the results between MIMOSA and SIMO.

The vessel may be described by three different body types in SIMO, which correspond to different force models that can be applied to the vessel:

- Body Type 1: Large volume, total motion is simulated in time domain, 6 DOFs
- Body Type 2: Large volume, motions separated in frequency domain WF motions and time domain LF motions, 6 DOFs
- Body Type 3: Small volume, position dependent hydrodynamic coefficients allowed, 3 translational DOFs

Body Type 2 is selected for this model, which requires separation of motions. Body Type 1 involves the simulation of total motion in the time domain, and retardation functions are necessary. As these functions are not available for the model of Safe Scandinavia, Body Type 2 is the preferred body type.

The next point to verify is whether the mooring lines and line types are correctly imported. In terms of defining the mooring line type, the main difference between SIMO and MIMOSA is the calculation of line characteristics. The line characteristics in SIMO can be calculated for several z-levels (depths), whereas they can only be calculated for one z-level in MIMOSA. Another difference rests in the definition of the unit weight for the material in each segment. In MIMOSA, this weight is set as the unit weight in water, whereas it is defined as the unit weight in air in SIMO. A simple hand calculation is performed to verify that the unit weight in water from MIMOSA is correctly

converted to unit weight in air.

A more extensive verification is necessary for the body kinematics, especially due to the fact that only a three DOF analysis, surge, sway and yaw, is performed in MIMOSA and the vessel input file is established based on this analysis. The definition of wind direction is different in SIMO and MIMOSA. Current- and wind force coefficients are studied in SIMO to ensure that they are correctly converted to the local coordinate system provided in SIMO.

The moments of inertia in roll I_{44} and pitch I_{55} needed to be calculated, as they were not included in the MIMOSA model. These values are calculated based on Eq. (5.1) and (5.2) for both roll and pitch, respectively.

$$I_{44} = m \cdot r_{44}^2 \tag{5.1}$$

$$I_{55} = m \cdot r_{55}^2 \tag{5.2}$$

In the above equations r_{44} and r_{55} represent the radius of gyration in roll and pitch, respectively, and is found in Browne (2015). m is the structural mass of the vessel. The moments of inertia, which are calculated based on the given equations, were then included in the mass matrix in SIMO. The added mass in heave A_{33} is defined as 50% of dry mass after guidance from the supervisor, and the added mass in roll A_{44} and pitch A_{55} is set to 50% of I_{44} and I_{55}, respectively. The added mass in surge, sway and yaw is provided from the MIMOSA file.

No hydrostatic stiffness is included in the importation of the model, and therefore this stiffness is calculated and added in heave, roll and pitch. The hydrostatic stiffness in heave is calculated according to the formula presented in Eq. (5.3).

$$T_3 = 2\pi\sqrt{\frac{m + A_{33}}{K_{33}}} \tag{5.3}$$

The eigenperiod in heave is taken from the RAO, which is included in Appendix A.1, and is approximately equal to $19s$. The above equation is then solved for the stiffness K_{33}. This stiffness is implemented into the hydrostatic stiffness matrix in SIMO.

For roll and pitch, the hydrostatic stiffness is calculated from the expression provided in Eq. (5.4).

$$T_i = 2\pi\sqrt{\frac{I_{ii} + A_{ii}}{K_{ii}}},\ i = 4, 5 \tag{5.4}$$

The RAOs in roll and pitch, which are also provided in Appendix A.1, are plotted for periods up to $40s$. The eigenperiod in these DOFs could thus not be found from the RAOs. After a discussion with the supervisor, the hydrostatic stiffness in roll and pitch were selected to ensure an eigenperiod of approximately 40-50s in each of the two DOFs. The eigenperiods are verified through the performance of a decay test in SIMO, which is described in the following sections. As the system already contained a certain amount of stiffness, due to the presence of the mooring lines, the hydrostatic stiffness needed to be smaller than the value that Eq. (5.4) yielded, in the insertion of an eigenperiod of approximately $45s$.

The eigenperiod in each DOF is calculated from the respective restoring curves, found through the performance of a "pull-out" test. The vessel is statically displaced certain offsets and the restoring force at each point is plotted against the offset. The stiffness K_{ii} is then found by dividing the restoring force by the offset at a given point, typically around the offset expected to approximately equal the static offset found from MIMOSA in the project thesis. Eq. (5.4) with $i = 1, .., 6$ is utilized to check the eigenperiod of all DOFs with a stiffness K_{ii} which was from these restoring curves. For the translational motions, the moment of inertia I_{ii} is replaced by the structural mass m. These eigenperiods are then verified through decay tests.

The resulting eigenperiods, or natural periods, are calculated based on the restoring curves in SIMO in all DOFs, and are presented in Table 5.3.

	Surge	Sway	Heave	Roll	Pitch	Yaw
$T_n\ [s]$	52.3	66.0	19.0	49.4	47.4	72.3

Table 5.3: Natural period in each DOF

The decay tests are executed in SIMO by giving the vessel an offset in the desired direction for each DOF, and then running a 2000s dynamic simulation without calculating the static equilibrium. Figure 5.4 presents a decay test in sway for illustrative purposes.

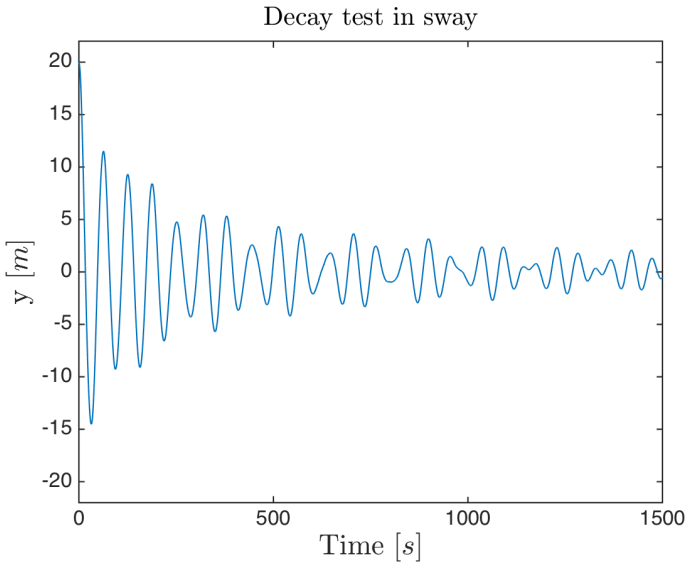

Figure 5.4: Decay test in sway

The linear damping in surge, sway and yaw is excluded from the performance of the decay tests. In heave, roll and pitch, no linear damping is included in the importation of the model from MIMOSA, as the analysis performed in MIMOSA was a three DOF analysis. The decay tests found that the eigenperiods were slightly lower than what was calculated from the restoring curves in surge and sway, but after a discussion with the supervisor, this aspect was assumed to be adequate. Plots of the decay test in each DOF are included in Appendix B.1. The eigenperiod in surge, sway and yaw is also compared to the eigenperiod calculated by the mass and stiffness matrix given as output from the three DOF analysis in MIMOSA. The values calculated from the mass and stiffness matrix in MIMOSA corresponded well with the eigenperiods given in Table 5.3.

The decay tests were also performed to establish the damping level that exist in the model before any linear damping was included. SIMO calculates the current and wind force on the vessel according to relative speed in surge and sway, provided that the excitation is present. The decay test is executed with no environment, which resulted in a quadratic damping force from the current coefficients. The derivation of the quadratic damping force is presented in Eq. (5.5). From the formulation of wind force provided in section 2.2.1, no damping contribution from wind is present with no environment specified.

$$\bar{U} \;=\; 0 \quad \Rightarrow \quad C_{cu}|\bar{U} - \dot{x}|(\bar{U} - \dot{x}) \;=\; -C_{cu}|\dot{x}|\dot{x} \tag{5.5}$$

The observed LF damping contribution from the decay tests in surge and sway emerge from the current forces, i.e. viscous forces on the hull. According to guidance from the supervisor, a total damping level of 40-50% should be obtained in heave, roll and pitch. The total damping in surge, sway and yaw should approximately equal 40% of critical damping. The damping level observed from the decay tests are estimated based on the relationship between the logarithmic decrement and the damping ratio (Steen, 2014). Eq. (5.6) presents the definition of the logarithmic decrement and Eq. (5.7) provides the expression for the damping ratio.

$$\Lambda \;=\; ln(\frac{x_i}{x_{i+1}}) \tag{5.6}$$

$$\xi \;=\; \frac{C}{C_{cr}} \tag{5.7}$$

In Eq. (5.6) Λ represents the logarithmic decrement. x_i and x_{i+1} are two succeeding amplitudes, spaced one natural period T_n apart. In Eq. (5.7) ξ represents the damping ratio that defines the ratio between the actual damping C and the critical damping C_{cr}. Eq. (5.8) provides the relation between the logarithmic decrement and the damping ratio, whereby ω_0 is the natural frequency for the undamped system.

$$\Lambda \;=\; \xi\omega_0 T_n \;=\; 2\pi\frac{\xi}{\sqrt{1-\xi^2}} \tag{5.8}$$

For low damping ratios, typically $\xi < 0.2$, the above expression can be approximated as given in Eq. (5.9) (Steen, 2014).

$$\Lambda \;=\; 2\pi\xi \tag{5.9}$$

Through the observation of the decay tests in each DOF, it is clear that the damping level is relatively low and the simplified expression is used to calculate the damping ratio. The damping ratio in surge and sway is calculated to be lower than 10%. Almost no damping could be observed from the decay tests in heave, roll, pitch and yaw. In order to include correct values in the linear damping matrix, the critical damping, C_{cr} is calculated according to the expression in Eq. (5.10).

$$C_{ii,cr} \;=\; 2M_{ii}\omega_{i,0} \;=\; 2\sqrt{M_{ii}K_{ii}}\;,\; i \;=\; 1,...,6 \tag{5.10}$$

In the above equation, M_{ii} represent structural and added mass for $i = 1,2,3$, and moment of inertia and added mass for $i = 4,5,6$.

As stated previously, the damping observed from the decay test is the quadratic damping forces that arise from the current, and hence the viscous effects that interact with the hull. No wave drift damping is specified for the model. The linear damping matrix should therefore account for the damping that arises from wave drift. As evaluated in section 2.2.3, a large contribution of the total damping arises from direct damping on the mooring lines. In order to account for these additional damping contributions, the damping values included in the linear damping matrix approximately equaled 40% of the critical damping in surge, sway and yaw, and 45% of the critical damping in heave, roll and pitch, as the supervisor advised. The linear damping in surge, sway and yaw included in SIMO are approximately equal to the linear damping included in MIMOSA.

A final verification of correct implementation of the vessel and mooring lines is performed by plotting the restoring forces in four different weather directions. The weather directions corresponds to those directions utilized in the MIMOSA analysis in the project thesis, i.e. 0° , 45° , 180° and 225°, according to the coordinate system in MIMOSA provided in Figure 5.3.a. Figure 5.5.a and 5.5.b present the restoring curves in the global directions 0° and 180° respectively. The restoring curves in the global directions 45° and 225° are included in Appendix B.2.

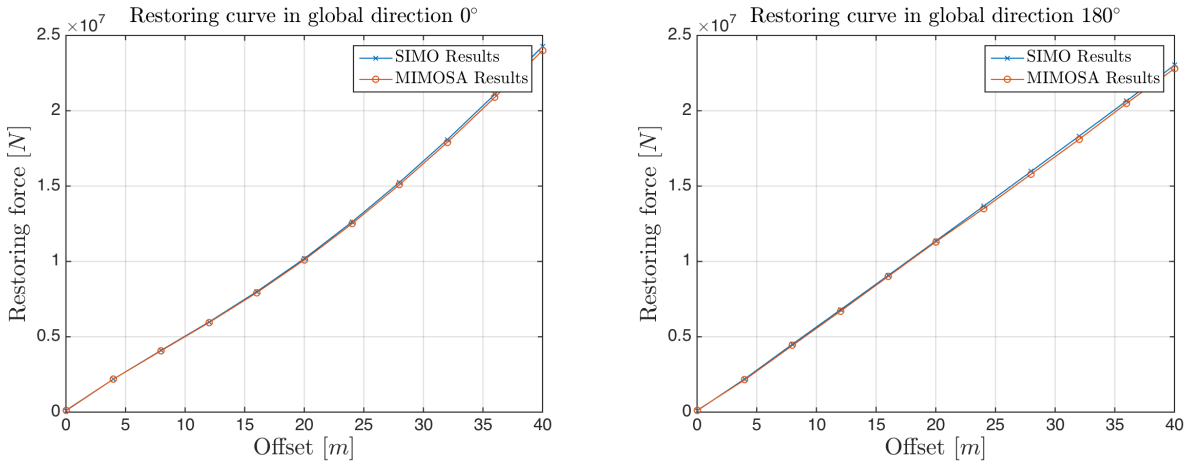

5.5.a Global direction 0°

5.5.b Global direction 180°

Figure 5.5: Restoring curves from SIMO and MIMOSA

Good correspondence between the restoring curves found from SIMO and MIMOSA is observed in Figure 5.5. A slightly non-linear curve is observed in global direction 0°. The steel lines take the heaviest load when the weather acts towards this direction, which results in a system that is more influenced by the nonlinear geometric stiffness. A linear curve is noticed in the global direction 180°. The polyester lines take the heaviest load in this direction, and the restoring force is more influenced by the linear elastic stiffness within the system.

5.2.2 Most Probable Largest Response

To correctly compare the results from SIMO with the ones from MIMOSA, the most probable largest values of the response, vessel motions and line tension, are extracted. The time domain simulation is run with ten different seed numbers, whereby the maximum value of WF, LF and total motion and line tension are extracted from each realization. These maxima, a total of ten for each response parameter, are fitted to a Gumbel distribution with probability level of 0.37. The estimated most probable largest values are given from these Gumbel distributions.

The workflows and post processors utilized for fitting the maxima to the Gumbel distribution is presented in the following. Figure 5.6 represent the superior workflow, where the output is the Gumbel distribution of the maxima of each response. The first box in this workflow refers to the workflow given in Figure 5.7. In this workflow, ten different sea state realizations are run. For each realization, the response calculated by a time domain analysis in SIMO is sent to the post processor, whereby the maximum value from each response time series is extracted. These maximum values, for each desired response from the ten different seed numbers, are merged to one result in the post processor in Figure 5.9. The maxima of each response are then fitted to the Gumbel distribution and is given as output from the workflow and the post processor box in Figure 5.6.

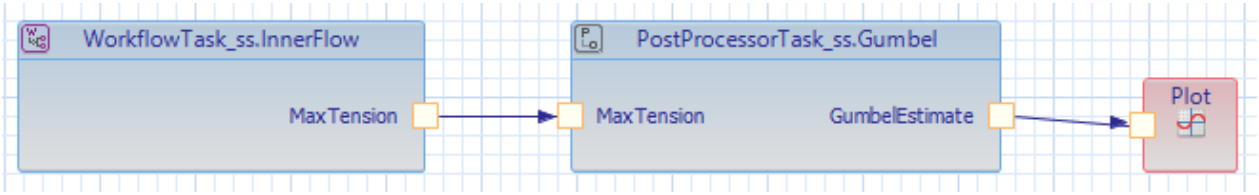

Figure 5.6: Seed variation workflow

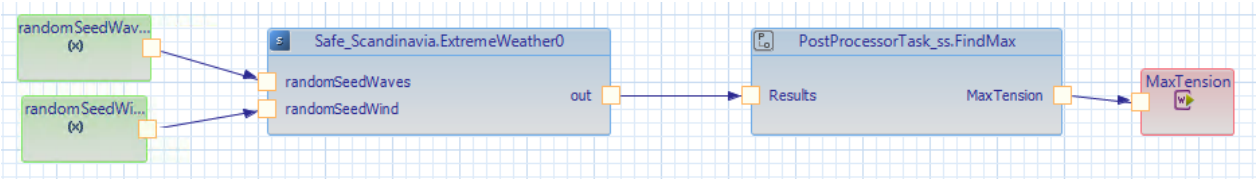

Figure 5.7: Workflow with a condition set running ten different seed number and sea state realizations

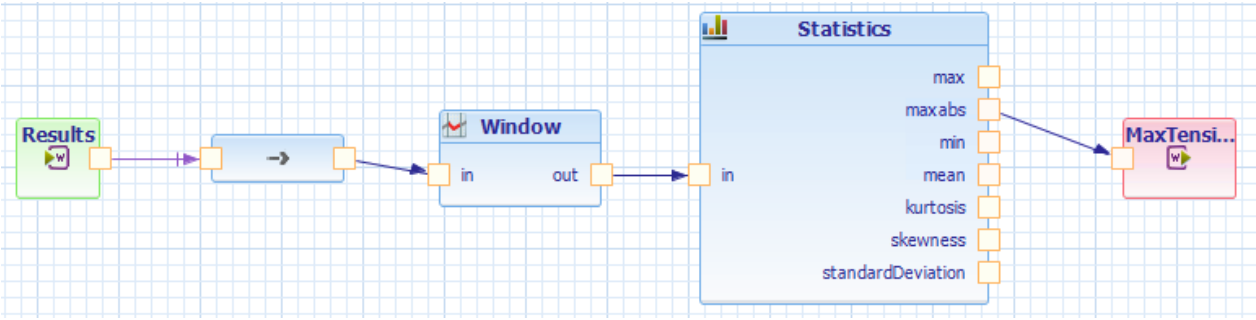

Figure 5.8: Post processor - Extracting maximum values

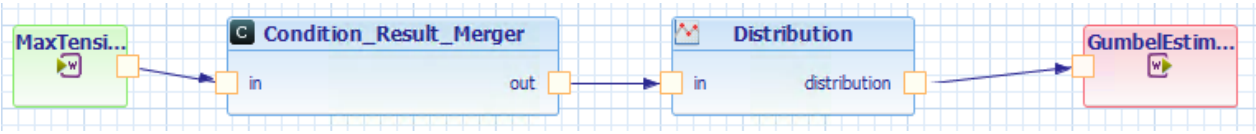

Figure 5.9: Post processor - Gumbel distribution

Figures 5.10.a and 5.10.b illustrate the maxima samples fitted to a Gumbel distribution, for the WF and total response in surge for weather towards 0° only. A noteworthy observation from these figures is the strange point that appears way higher along the y-axis in comparison to the rest of the maxima. This observation was discussed with fellow students, who also experienced this, and Pål Levold, but there is no explanation to why this occurs. It is assumed that this point is incorrect, as this finding was observed in every Gumbel plot. Apart from that point, the other maximum samples indicate an adequate representation of the most probable largest value from the Gumbel distribution.

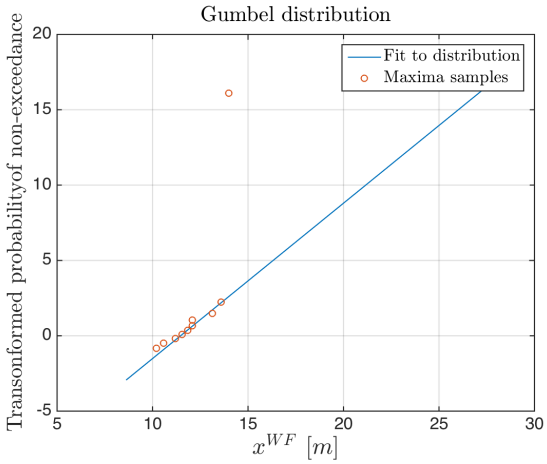

5.10.a WF surge maxima

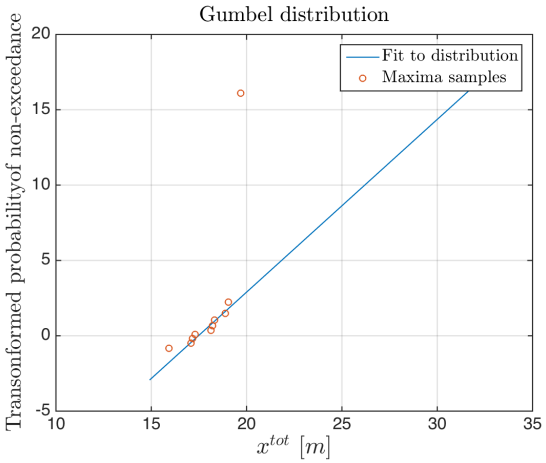

5.10.b Total surge maxima

Figure 5.10: Maxima samples fitted to a line that represents the Gumbel distribution

5.3 Comparison of MIMOSA and SIMO

In this section, the results in terms of vessel response and line tension from the ULS analysis executed in the project thesis are presented in conjunction with the results obtained from an analysis performed in SIMO. A discussion of these results follows in the next section.

5.3.1 Results

A three DOF analysis was executed in MIMOSA. Consequently, the static offset, LF and total motion are only compared in surge, sway and yaw. The WF motions are compared for all DOFs. In the comparison, all the weather directions utilized in the ULS analysis that were performed in the project thesis were considered. The results in this section are presented for weather towards 0° and 180° , whereas the results from 45° and 225° are included in Appendix B.3. The noted weather directions are based on the directions presented in Figure 5.1 provided by the MIMOSA coordinate system. One should keep in mind that when reference is made to for instance 45°, the actual weather direction defined in SIMO is 315°. Global direction 0° and 180° coincides for both coordinate systems. The results are given as offsets, and standard deviations, in the direction in

which the weather acts towards, i.e. for a weather direction of 0° the positive surge motion occurs in positive global x-direction, whereas a weather direction of 180° provides positive surge motion in negative global x-direction.

Table 5.4 lists the static vessel offsets from SIMO and MIMOSA for the two respective weather directions. The difference observed in yaw is mainly a result of the different definitions of rotation direction in SIMO and MIMOSA. A slightly smaller static offset in surge is observed when the weather acts towards 180°, and may arise from the slightly higher restoring force around this offset as depicted in Figure 5.5.

		Surge $[m]$	**Sway** $[m]$	**Yaw** $[°]$
0°	SIMO	4.76	0.01	179.50
	MIMOSA	4.56	0.04	180.53
180°	SIMO	4.14	0.11	180.30
	MIMOSA	4.37	0.03	179.63

Table 5.4: Static offset in global direction 0° and 180°

Tables 5.5 and 5.6 presents the WF vessel response with weather directed towards 0° and 180°, respectively. As expected, the WF response is similar in the two directions, although the windward lines in the global direction 0° are composed of steel, and the windward lines in global direction 180° are polyester. This observation corresponds well to the theory that states that the mooring lines have little or no influence on the WF motions of a moored floater. The WF motions from SIMO and MIMOSA are also quite similar in terms of maximum offset, the most probable largest offset, and standard deviation σ.

Table 5.7 presents the LF response for both weather directions. Larger differences are observed in the comparison of the results from SIMO and MIMOSA than the case for the WF response. A smaller LF response in surge from both SIMO and MIMOSA is noticeable when the weather is directed towards 180°. In this case, the polyester lines are the windward lines, which appears to

	Surge $[m]$		**Sway** $[m]$		**Heave** $[m]$		**Roll** $[^\circ]$		**Pitch** $[^\circ]$		**Yaw** $[^\circ]$	
	max	σ	max	σ	max	σ	max	σ	max	σ	max	σ
SIMO	11.47	3.07	0.14	0.03	12.66	3.37	0.09	0.02	6.45	1.69	0.05	0.01
MIMOSA	11.31	3.01	0.10	0.03	12.24	3.27	0.07	0.02	6.39	1.67	0.03	0.01

Table 5.5: WF vessel response in global direction 0°

	Surge $[m]$		**Sway** $[m]$		**Heave** $[m]$		**Roll** $[^\circ]$		**Pitch** $[^\circ]$		**Yaw** $[^\circ]$	
	max	σ	max	σ	max	σ	max	σ	max	σ	max	σ
SIMO	11.47	3.08	0.09	0.03	12.66	3.38	0.06	0.01	6.45	1.69	0.03	0.01
MIMOSA	11.31	3.01	0.07	0.03	12.24	3.27	0.05	0.01	6.39	1.67	0.02	0.01

Table 5.6: WF vessel response in global direction 180°

create a slightly stiffer system, as the LF response can be limited by the mooring system. As seen from the restoring curves illustrated in Figure 5.5, the stiffness is higher for the 0° curve than for the 180° curve, for offsets between $0m$ and approximately $25m$.

		Surge $[m]$		**Sway** $[m]$		**Yaw** $[^\circ]$	
		max	σ	max	σ	max	σ
0°	SIMO	3.76	1.02	0.21	0.06	1.12	0.19
	MIMOSA	4.71	1.10	0.04	0.01	0.63	0.19
180°	SIMO	3.57	0.98	0.18	0.06	0.83	0.14
	MIMOSA	4.20	0.93	0.06	0.02	0.46	0.14

Table 5.7: LF vessel response in global direction 0° and 180°

Table 5.8 presents the total response, whereby SIMO calculates both maximum offset and standard deviation and MIMOSA provides only the maximum offset. A similar observation with respect to maximum response in the two directions found from the LF response can be seen in the total response, which is a slightly larger surge offset for 0°.

There are both windward and leeward lines for each weather direction. Table 5.9 presents the resulting static and maximum tension in a windward and a leeward line. Line 7 is one of the windward lines when the weather is directed towards 0° and line 1 is one of the leeward lines.

		Surge $[m]$		**Sway** $[m]$		**Yaw** $[^\circ]$	
		max	σ	max	σ	max	σ
0°	SIMO	17.48	3.41	0.23	0.06	1.14	0.19
	MIMOSA	18.06	-	0.16	-	0.64	-
180°	SIMO	17.27	3.62	0.30	0.06	0.84	0.14
	MIMOSA	17.55	-	0.13	-	0.48	-

Table 5.8: Total vessel response in global direction 0° and 180°

With weather towards 180° line 1 becomes one of the windward lines, whereas line 7 is one of the leeward lines.

		Line 1		**Line 7**	
		$\boldsymbol{T_{stat}}$ $[kN]$	$\boldsymbol{T_{max}}$ $[kN]$	$\boldsymbol{T_{stat}}$ $[kN]$	$\boldsymbol{T_{max}}$ $[kN]$
0°	SIMO	573.0	1540.0	1120.0	2590.0
	MIMOSA	504.0	1810.0	1200.0	4260.0
180°	SIMO	1250.0	2930.0	715.0	1370.0
	MIMOSA	1250.0	3090.0	714.0	2600.0

Table 5.9: Line tension in windward and leeward line with weather towards 0° and 180°

Larger deviations between SIMO and MIMOSA, as shown in Table 5.9, are in terms of the maximum tension observed for line 7, which includes steel wire in the middle segment. Line 1 includes a middle segment of polyester. The static tension provided from SIMO and MIMOSA for each line is relatively similar in both weather directions.

5.3.2 Discussion

In consideration of the WF response, good correspondence between SIMO and MIMOSA is observed. This finding is expected as the WF response in SIMO is solved in the frequency domain, with a time series generated by FFT, and MIMOSA is a frequency domain analysis program.

The largest differences in terms of vessel motion between SIMO and MIMOSA is evident in the LF response. One should note that SIMO yields the LF response at global position, and the static offset is used as the starting point for the LF response calculation. The mean of the LF response may slightly deviate from the static offset. The maximum amplitude included in Table 5.7 is directly taken from the time series with the static offset subtracted. This amplitude may be slightly incorrect because the mean and static offset are not completely identical. Another possible reason for the deviation is the fact that the method implemented in MIMOSA tries to account for the LF response being non-Gaussian to estimate maximum LF response, as already explained in section 4.4.1. This factor may overestimate the influence of non-Gaussian effects. The procedure of linearizing the restoring force in MIMOSA should not introduce too large errors as both restoring curves in Figure 5.5 behaves close to linear.

When comparing the LF and WF response from both MIMOSA and SIMO, it is clear that the WF motions dominate the total response. This can also be observed from the response spectrum in surge, presented in Figure 5.11.

By considering the wave drift force coefficient in surge, illustrated in Figure 5.12, it is observed that there are close to no energy from wave drift at wave periods around $18.2s$ which is the peak period for the considered sea state. This means that the LF response is mainly excited by the wind gusts. It is also evident from the RAOs in surge and heave, presented in Figures 5.13 and 5.14, that the maximum response in heave lies around the peak period for the incoming waves, and that the WF surge motion also is excited at this frequency.

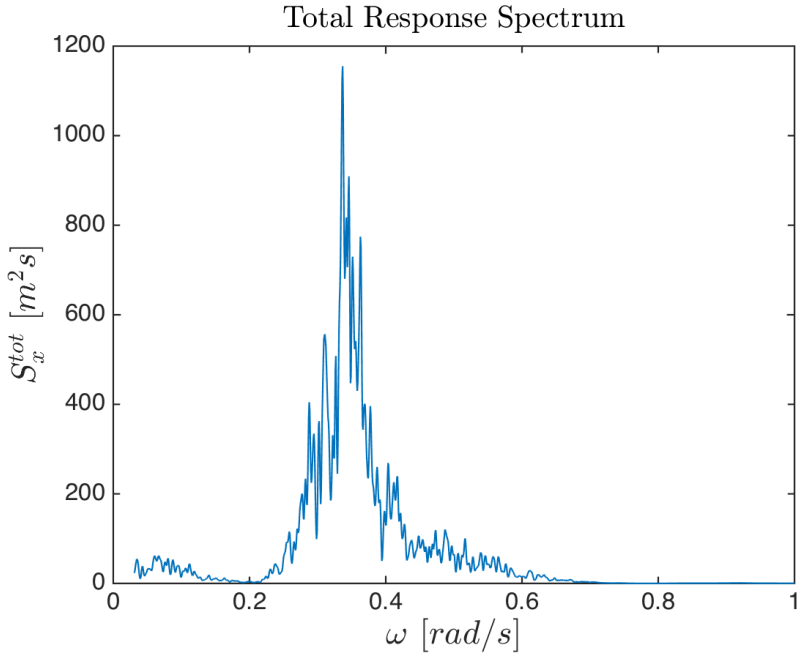

Figure 5.11: Response spectrum in surge for global direction 0°

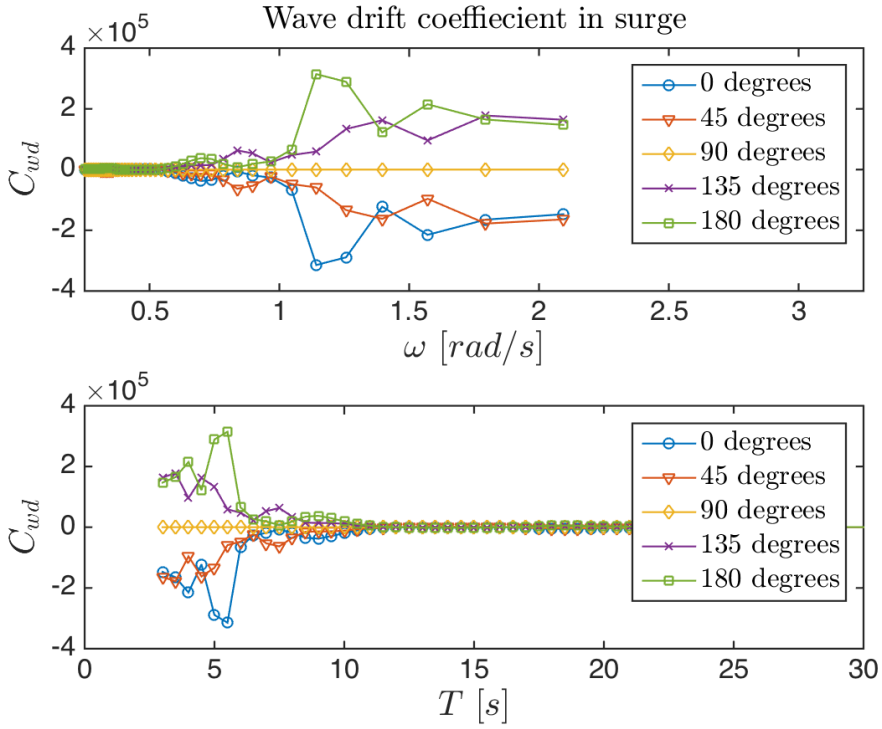

Figure 5.12: Wave drift force coefficient in surge for different weather directions

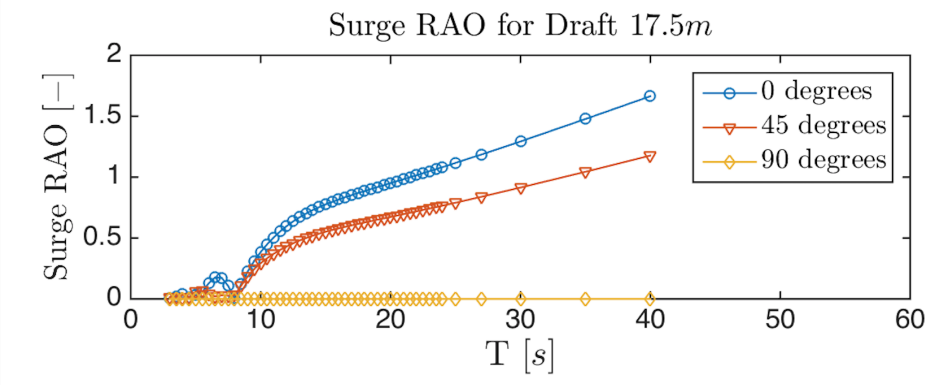

Figure 5.13: RAO in surge

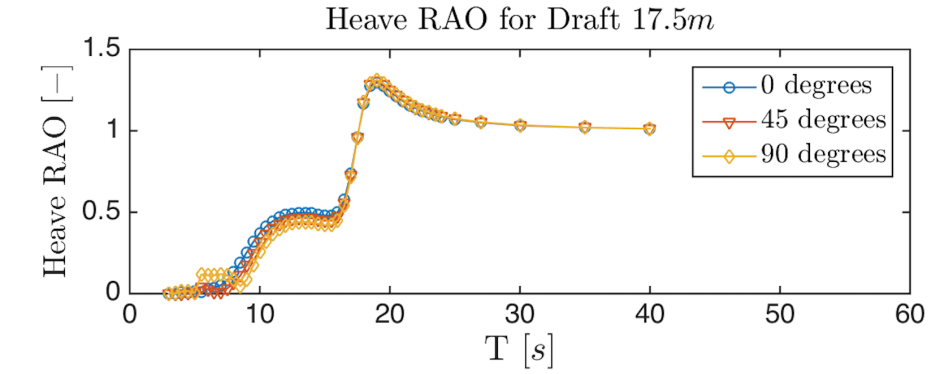

Figure 5.14: RAO in heave

A new simulation is executed with a peak period of 9.0s to study whether the LF response would increase due to the effect from wave drift forces. The corresponding significant wave height is found from the contour plot provided in section 4.3, whereas the wind and current is kept at initial values. The main observation is the reduction in WF response, which results from a less extreme sea state. As observed in Figure 5.15.a, the total response consist of almost equal contributions from WF and LF response. It is made evident, however, from Figure 5.15.b that the LF response has only increased slightly.

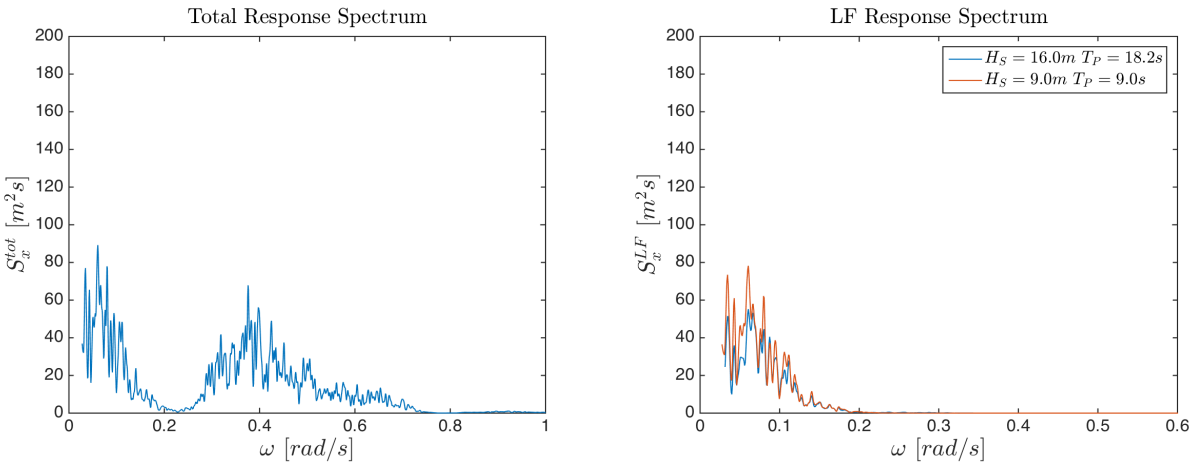

5.15.a Total response spectrum

5.15.b LF response spectrum

Figure 5.15: Total and LF response spectrum with reduced wave conditions

It is expected that the results in terms of tension between MIMOSA and SIMO for the steel lines would deviate, due to the difference in calculation method, i.e. quasi-static versus dynamic computation of tension. A MIMOSA FEM analysis attempts to capture the nonlinear dynamic effects in the mooring lines, such as drag, whereas SIMO uses a quasi-static method to calculate line tension and altogether neglects the dynamic effects. The relatively large deviations observed from Table 5.9 are somewhat unexpected, as drag loads on the mooring lines should typically not have such a great impact on mooring systems in shallow water. Ormberg and Larsen (1998) studied this phenomenon, as mentioned in section 2.3.2.

A quasi-static analysis is performed in MIMOSA to verify if similar line tension as computed by SIMO is obtained. The total vessel offset found from both SIMO and MIMOSA are quite similar, and a quasi-static analysis in MIMOSA should thus yield mooring line tension similar to SIMO. In addition, a new FEM analysis in MIMOSA is performed with drag coefficients that are reduced to 10% of its original values in order to consider to what extent the drag on the mooring lines influences the maximum WF tension in the lines. Table 5.10 presents the resulting line tension from MIMOSA in these two cases, in conjunction with the tension calculated in SIMO and by MIMOSA FEM, for weather towards 0° only.

	$\boldsymbol{T_{stat}}$ $[kN]$	$\boldsymbol{T_{base}}$ $[kN]$	$\boldsymbol{T_{max}^{WF}}$ $[kN]$	$\boldsymbol{T_{max}}$ $[kN]$
SIMO	1120.0	-	-	2590.0
MIMOSA QS	1200.0	1380.0	1230.0	2610.0
MIMOSA FEM	1200.0	1380.0	2880.0	4260.0
MIMOSA FEM RD	1200.0	1380.0	1450.0	2830.0

Table 5.10: Tension in line 7
QS) Quasi-static method
RD) Reduced drag

The maximum tension from SIMO corresponds well to the tension calculated through a quasi-static method in MIMOSA, as expected due to the relatively similar total maximum offset. The FEM in MIMOSA with reduced drag is also quite similar to the tension calculated by SIMO. T_{stat} and T_{base} are equal in all the three analysis performed in MIMOSA, and the main difference between the analyses are T_{max}^{WF}. MIMOSA utilizes a non-Rayleigh based method to calculate this tension, where the effects of non-linear behavior in the dynamic cable model are attempted to be captured (Kaasen et al., 2012). It appears that MIMOSA over-estimates the influence of line dynamics in computation of line tension, and the estimate of drag on the mooring lines is the main reason for the high maximum tension found in the initial FEM analysis in MIMOSA.

In Chapter 7, Case Study 3, the results from a mooring system analysis performed in Riflex is presented. Riflex accounts for dynamic effects in the mooring line, such as drag and inertia. The

tension found in both SIMO, MIMOSA and Riflex are compared to one another. This comparison provides greater insight into whether the estimation of dynamic effects on mooring line tension from MIMOSA is too high, i.e. if MIMOSA overestimates the dynamic tension in the mooring lines.

Chapter 6

Case Study 2: Optimization in SIMA

This chapter focuses on how to establish an optimization problem for a mooring system in SIMA. In general, such an optimization can be utilized for a various of purposes, for instance to minimize the mooring system cost, find the optimum spreading of the mooring lines or to make an under-designed mooring system meet certain criteria. In this thesis, the mooring system is optimized with respect to minimizing the material cost. The objective function, which is minimized, is therefore a cost function, with mooring line dimensions as variables. Its constraints include upper and lower limits on length and diameter, maximum allowable offset and maximum allowable tension in the lines that correspond to specified safety factors.

Section 6.2 assesses a description on how to formulate an optimization problem in the SIMA workbench and how to establish the cost function. The optimization of both a steel system and a polyester system are executed according to the final set-up with different constraints that are presented. Furthermore, this chapter explains and discusses a simple sensitivity study for a given case with respect to the robustness of the optimization procedure, followed by a verification of the optimization results. Lastly, a discussion based on the results, sensitivity study and the verification is included, followed by a section containing experiences from performing a mooring system optimization in SIMA.

6.1 Method

The optimization procedure is formulated in the SIMA workbench and is described in section 6.2. The mooring system analysis for each optimization is executed as a separated analysis in SIMO, i.e. the WF and LF motions are separated. The total motion is found through the summation of the WF and LF motion time series. This total motion is evaluated with respect to the maximum allowable offset. The mooring line tension in SIMO is calculated by a quasi-static method, which means that the tension is provided from the line characteristics. The minimum allowable safety factor in the optimization is based on the maximum tension in the heaviest loaded line.

6.2 Formulation of Optimization Problem in SIMA

The variables to be optimized in this optimization formulation are the diameter and length of each segment. They are referred to at d_1 and l_1, d_2 and l_2 and d_3 and l_3 for the diameter and length of segments one, two and three, respectively. The segments are numbered from the anchor; segment 1 is the bottom chain, segment 2 is the polyester rope or steel wire middle segment and segment 3 is the rig chain, as illustrated in Figure 6.1. These references are consistently used throughout this chapter.

The objective function, which provides the cost for one mooring line and is used in the optimization is expressed in Eq. (6.1) for the polyester system and in Eq. (6.2) for the steel system. In both functions, length and diameter of each segment are given as variables.

$$f_{poly}(d_1, d_2, d_3, l_1, l_2, l_3) = C_{chain}[w_1(d_1) \cdot l_1 + w_3(d_3) \cdot l_3] + C_{poly} \cdot w_2(d_2) \cdot l_2 \tag{6.1}$$

$$f_{steel}(d_1, d_2, d_3, l_1, l_2, l_3) = C_{chain}[w_1(d_1) \cdot l_1 + w_3(d_3) \cdot l_3] + C_{steel} \cdot w_2(d_2) \cdot l_2 \tag{6.2}$$

The corresponding unit weight in air for each segment is represented by w_1, w_2 and w_3. The weight

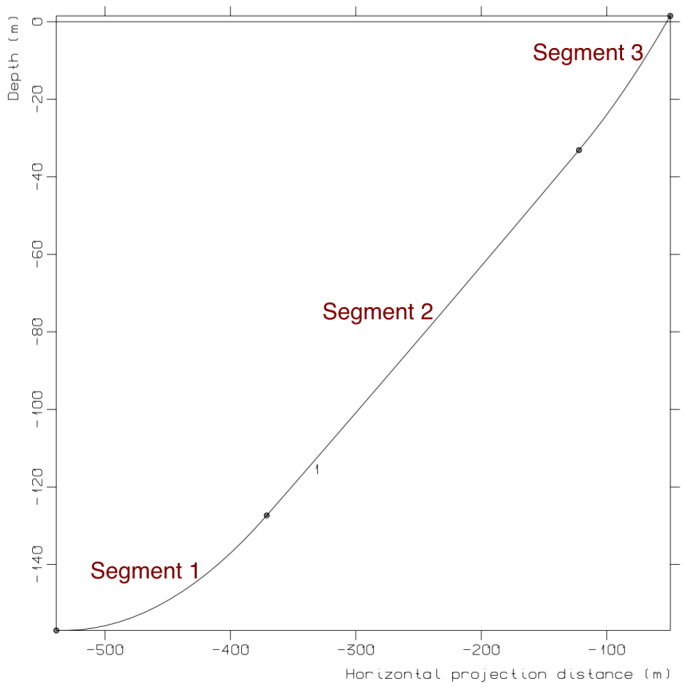

Figure 6.1: Illustration of line segment numbering

of each segment depends on the material, i.e. chain, polyester rope or steel wire. The properties of each material can be found in the catalogs provided by Statoil, who also provides the cost for each material represented in the above equations; $C_{chain} = 2.5kr/N$, $C_{steel} = 5.0kr/N$ and $C_{poly} = 7.0kr/N$. In the property catalogs for chain (Ramnas, 2016), polyester rope (Bridon, 2013b) and steel wire (Bridon, 2013a), the unit weight in air is provided for a wide range of diameters. R4 is the chain class, spiral strand is the steel wire type and superline polyester is the polyester rope type from the catalogs. In order to represent the unit weight as a function of diameter, the two parameters are plotted against one another in Excel. A trend line is fitted to the graph with a corresponding equation. Eq. (6.3), (6.4) and (6.5) provide the resulting expressions. These expressions are directly used in SIMO, in order to ensure that the model input is updated with new values, as the diameter changes throughout each iteration of the optimization.

$$w_{chain} = 196013.61 \cdot d^2 \, [\frac{N}{m}] \tag{6.3}$$

$$w_{poly} = 6568.68 \cdot d^2 \, [\frac{N}{m}] \tag{6.4}$$

$$w_{steel} = 46208.04 \cdot d^2 \, [\frac{N}{m}] \tag{6.5}$$

The breaking strength, MBL, as a function of the diameter for each material, is found according to the same procedure, which yields the expressions in Eq. (6.6), (6.7) and (6.8).

$$MBL_{chain} = 516940.0 \cdot d^{1.72} \, [kN] \tag{6.6}$$

$$MBL_{poly} = 297633.0 \cdot d^{2.06} \, [kN] \tag{6.7}$$

$$MBL_{steel} = 864092.9 \cdot d^{1.97} \, [kN] \tag{6.8}$$

The mooring lines consist of three different segments with different breaking strengths, which are a result of different diameters. The SIMO model of the lines requires one single breaking strength for the entire line. A simple script is created through the built-in minimum function in SIMO, in order to ensure that the lowest of the three MBLs is chosen as the governing breaking strength for the line used in the optimization formulation.

The system is initialized through a prescribed pretension, which allows the anchor to be moved throughout the optimization. As the optimization considered in this thesis is only used for illustrative purposes, this arrangement provides an acceptable solution. In reality there may be restrictions on the anchor placement, for instance, as a result of risers or pipes on the seafloor. If the anchor coordinates are pre-determined, the lines could instead be initialized by these global coordinates, and the total line length would be nearly constant, whereas the segment lengths could be varied relative to each other. Another restriction that may be relevant for mooring systems in shallow water is to require no uplift on the anchor, i.e. no vertical force on the anchor. As this aspect was not easily implemented in SIMO, the underlying assumption for this optimization set up was that the anchor could take forces in both the horizontal and vertical direction.

The pretension in the lines is defined as a percentage of the breaking strength, as expressed in Eq. (6.9).

$$Pretension = p_{factor} \cdot MBL \tag{6.9}$$

After guidance from the supervisor it is necessary to set restrictions on the pretension factor to keep the pretension in the lines between 10% and 25% of MBL; $p_{factor} \in [0.1, 0.25]$ in the above equation. Through this formulation, the optimization was able to vary the pretension, by changing the variable p_{factor}. With this factor as a variable, the optimization procedure consists of seven variables in total: the pretension factor, three diameters and three segment lengths. Each variable is defined with an upper and lower limit, which are specified in section 6.3.

The formulation of an optimization problem in SIMA involves three different building blocks, or "stages". In the following, the set up is described for the polyester system, although the procedure for the steel system is nearly identical. Any differences are explained.

The first block is where the optimization variables are defined, and where their upper and lower bounds are set, together with the optimization parameters. Figure 6.2 presents this stage, which hereby is referred to as stage 1. Figure 6.2.a illustrates the workflow with an optimization node, the large blue box, in SIMA, and Figure 6.2.b is where the value of the starting variables, and their limits, are defined. The optimization parameters which must be defined include the maximum number of iterations and the desired final accuracy.

The desired final accuracy is the convergence parameter, and is strongly dependent on the magnitude of the variables, cost function and the constraints. In order to avoid convergence problems, automatic normalization is on by default. Each optimization variable is normalized as presented in Eq. (6.10), whereby $\tilde{x}$ is the normalized optimization variable, and x_u and x_l are the respective

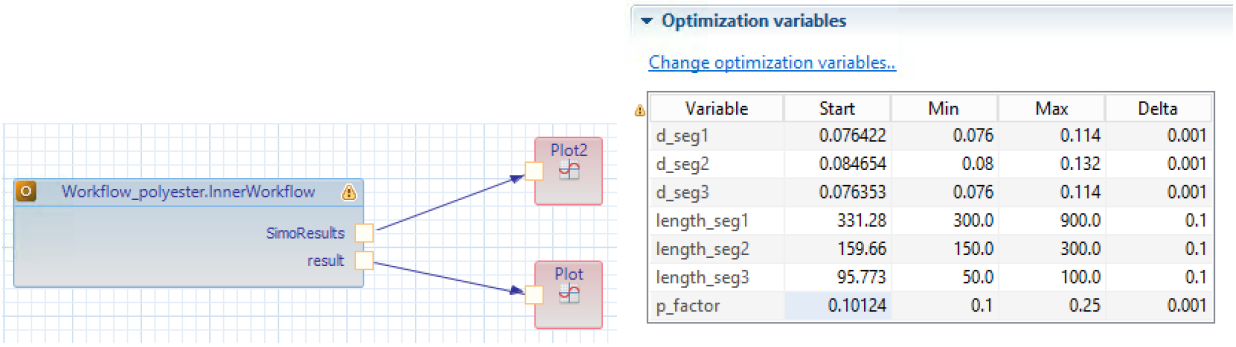

6.2.a Stage 1 6.2.b Input - stage 1

Figure 6.2: Screen shot from SIMA - stage 1 in the optimization set up

upper and lower limits for the variable x.

$$\tilde{x} = \frac{x - x_l}{x_u - x_l} \tag{6.10}$$

The cost function, $f(x)$ is normalized as shown in Eq. (6.11), whereby $\tilde{f}$ is the normalized cost function, x_0 is the initial value of the variable x and ϵ is a small constant.

$$\tilde{f}(x) = \frac{f(x)}{|f(x_0)| + \epsilon} \tag{6.11}$$

Any constraint, $g(x)$, is normalized in the same manner as the cost function; only f is replaced with g.

It is important to notice the *Delta* value for each variable in Figure 6.2.b, as this value is used to calculate the gradients. The gradients are used to search for a minimum point, and the delta value should be specified based on the magnitude of the respective variable. For instance, the delta value for the diameter is significantly smaller than the value for the length variable. The box in Figure 6.2.a, which is named *Plot*, provides the output in terms how the cost function, variables and constraints vary throughout each iteration of the optimization. The box named *Plot2* gives the result from the time domain simulation in SIMO with the final or ”optimum” variables.

The optimization node described in the above workflow refers to another workflow, which is hereby referred to as stage 2. Figure 6.3 presents this workflow.

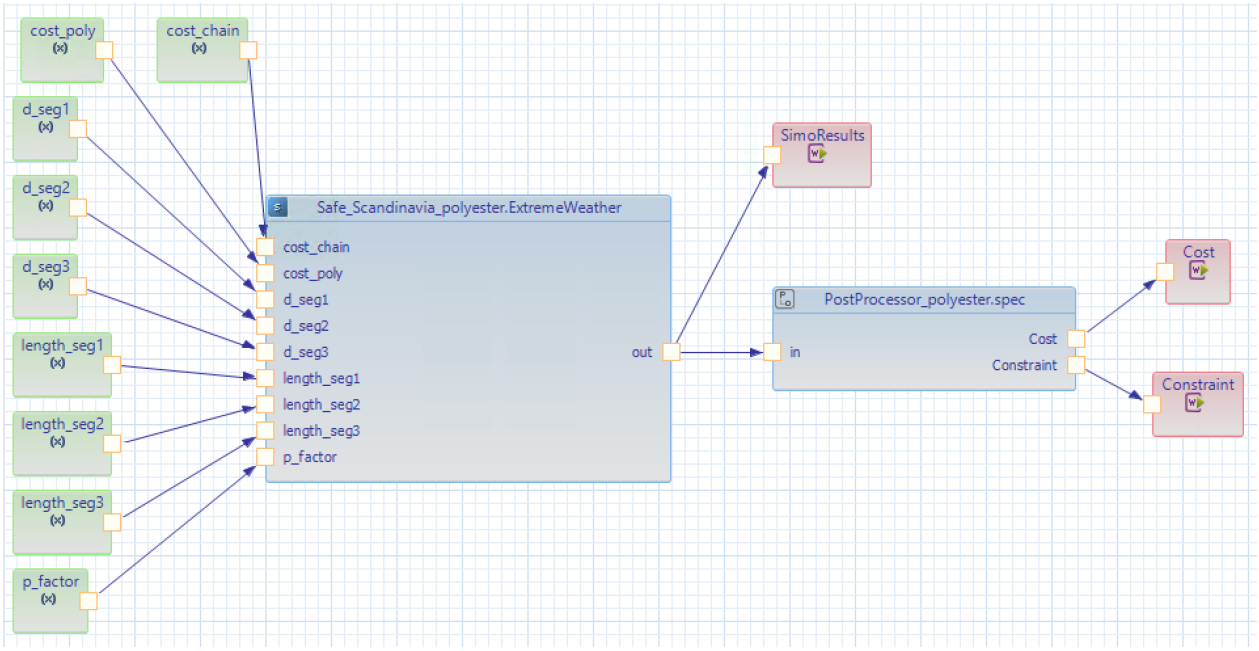

Figure 6.3: Screen shot from SIMA - stage 2 in the optimization set up

In stage 2, an analysis condition is defined in the largest blue box. This condition is defined for a given weather specified in the environment in the SIMO model, and a time domain analysis of the mooring system is executed based on the input variables in conjunction with the SIMO model. The analysis produces time series of the response, such as line tension and WF, LF and total motions which are checked against the constraints. The input to the analysis and this workflow are the variables defined in the green boxes to the left in Figure 6.3, which are specified in stage 1. Thus, the variables given in stage 1 are optimized based on the results from the time domain analysis in stage 2.

In this set up, the variables *cost_poly* (changed to *cost_steel* for the steel system) and *cost_chain* are included to allow the user to directly change these parameters in the workflow. This aspect is strictly not necessary, but it does simplify the process of changing the cost of the material.

The output from stage 2 are the three small, red boxes named *SimoResults*, *Cost* and *Constraint*. To calculate and define the cost and constraints of the optimization, a post processor is needed within this workflow. The results from the SIMO analysis are sent to a post processor known as *PostProcessor_polyester.spec*, as depicted in Figure 6.3. The specifications of the post processor are given in a third workflow, which hereby is referred to as stage 3, and are presented in Figure 6.4.

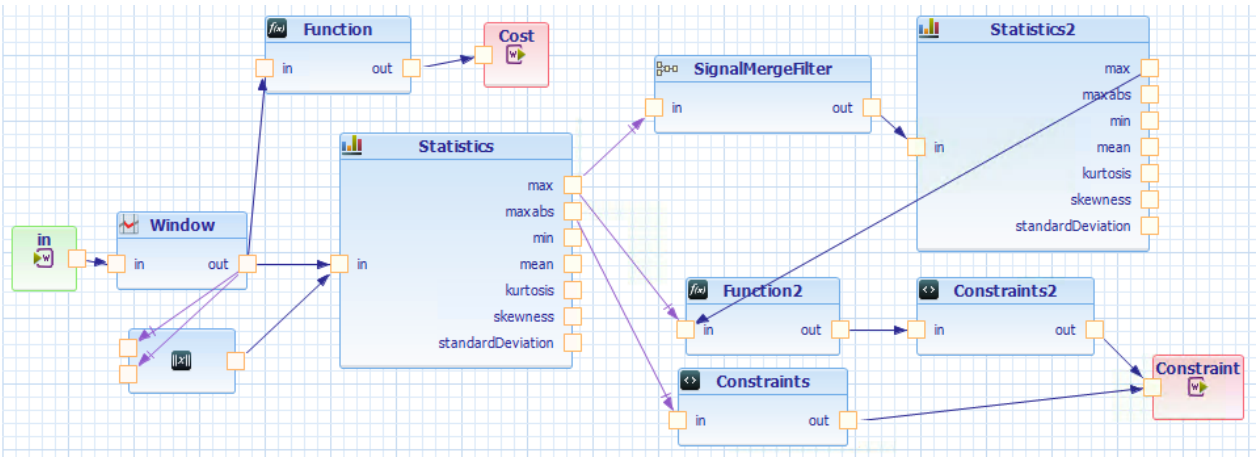

Figure 6.4: Screen shot from SIMA - stage 3 in the optimization set up

The input to the post processor workflow is the results from the SIMO analysis in terms of time series provided from stage 2, represented by the green box in Figure 6.4. The first step in the post processor is to cut out any transient parts of the time series, which is done in the *Window* box. The simulation length of the dynamic analysis is set to 12000s, and the first 1200s are removed to achieve a time series that correspond to a three hour sea state, i.e. 10800s.

The cost function, introduced in Eq. (6.1), is defined within the *Function* box connected to the red *Cost* output box. The variables included in the cost function are selected from a list, and the function is constructed from these variables. The calculated cost is the output from stage 3 to stages 2 and 1.

There are two different constraints implemented in this optimization procedure. One constraint

sets a limit for the maximum total motion, or offset, of the vessel, and the other sets a limit for the maximum tension in any line. The two constraints can mathematically be written as presented in Eq. (6.12) and (6.13).

$$g_1(\boldsymbol{l}, \boldsymbol{d}, p_{factor}) \;=\; \frac{MBL(d)}{T_{max}(\boldsymbol{l}, \boldsymbol{d}, p_{factor})} \;\geq\; sf \tag{6.12}$$

$$g_2(\boldsymbol{l}, \boldsymbol{d}, p_{factor}) \;=\; r_{max}(\boldsymbol{l}, \boldsymbol{d}, p_{factor}) \leq r_{allowable} \tag{6.13}$$

Both the constraint on line tension g_1, Eq. (6.12), and the constraint on offset g_2, Eq. (6.13), depends on the diameter and length of each segment together with the pretension in the line (represented through the variable p_{factor}). MBL depends on the diameter of the segment that provides the lowest of the three breaking strengths. T_{max} is the maximum tension in the line, and varies with changing diameter and length of each segment and with the pretension. For the first constraint to be satisfied, the value of g_1 must be lower than or equal to a pre-defined safety factor sf. This constraint is implemented in the optimization problem through several steps that can be tracked in Figure 6.4. The signal from the *Window* box is first sent through the *Statistics* box in the workflow. The maximum tension in all lines are extracted, and sent to the *SignalMergeFilter* box, whereby the maximum tension from each line is merged to a single signal. This signal is then sent to another *Statistics* box, before the maximum of the merged signal is sent to the *Function2* box. This maximum is the T_{max} value in Eq. (6.12). MBL is defined as a variable in the SIMO model. Its value is calculated in stage 2 and directly sent from the *Statistics* box to the *Function2* box without any modifications. The expression for g_1 is implemented in the *Function2* box, and the calculated value is then sent to the *Constraints2* box. In the *Constraints2* box, the value of sf is specified and the constraint on the calculated value from *Function2* is set as larger than or equal to this sf.

r_{max} in Eq. (6.13) is the magnitude of the maximum horizontal offset that occurs during the three hour sea state simulation. Maximum horizontal offset can occur in any direction in the horizontal plane and it depends on the weather direction considered, with contributions from both surge and sway motion. But, the maximum surge offset and maximum sway offset may not occur simulta-

neously. Finding the maximum offset in any horizontal direction is achieved by sending the time series of total surge and sway motion from the *Window* box through two different connections to the $\|x\|$ box. This box finds the resultant magnitude of two input signals by calculating the norm, and produces a single time series from which the maximum offset in a certain direction can be found. This signal is sent to the *Statistics* box, and its maximum value is sent to the *Constraint* box. In the *Constraints* box the constraint introduced in Eq. (6.13) is implemented, i.e. the maximum offset must be smaller than or equal to a specified value $r_{allowable}$.

In summary, three building blocks are needed to formulate an optimization problem in SIMA. In one block, stage 1, the optimization variables are defined. The next block, stage 2, is a workflow to be optimized with the optimization variables as input. This workflow runs the time domain analysis of the system. The last building block, stage 3, is a post processor with a cost function to be minimized and specific constraints to satisfy.

6.3 Optimization of Mooring Systems

Two different mooring systems were considered in the optimization procedure. One system with 12 lines of a chain-steel wire-chain configuration, termed the steel system, and one system with 12 lines comprised of a chain-polyester rope-chain configuration, referred to as the polyester system. An illustration of the line numbering for both the steel and polyester system is given in Figure 6.5.

Section 4.1 details the properties of the vessel utilized in this optimization. The hydrostatic stiffness matrix and linear damping matrix was derived in section 5.2.1. Section 4.3 describes the environment specified in the optimization, a 100-year design storm.

The optimization procedure described in the preceding section is applied to both the steel and the polyester system. Four different cases are considered for each system, which are listed in Table

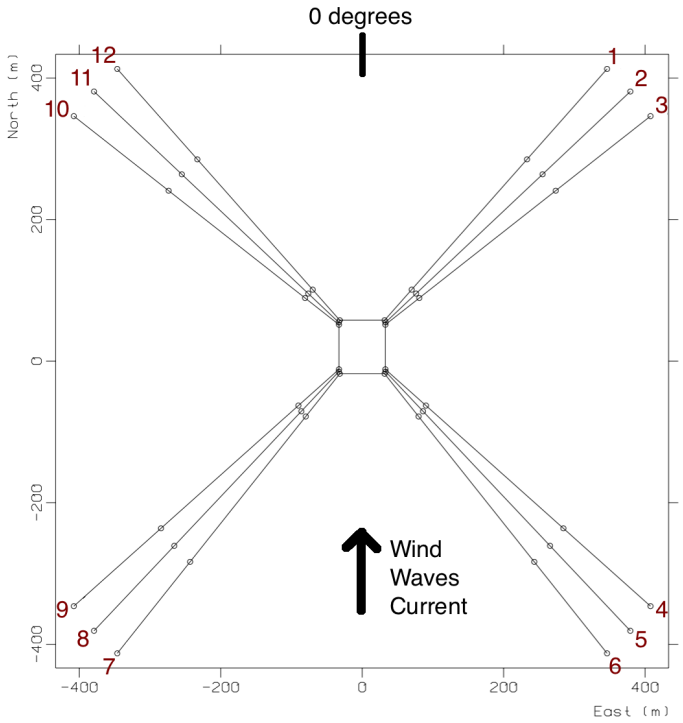

Figure 6.5: Illustration of line numbering

6.1. The weather condition is defined as collinear going towards north, i.e. in global direction 0° as shown in Figure 6.5. This weather direction implies that maximum offset occurs along the positive global x-direction, i.e. in surge, so r_{max} equals x_{max}. A more conservative design would also consider weather directly onto the mooring lines, for instance towards 45°, as this weather direction would result in a higher tension in the heaviest loaded lines. This scenario, however, is not further investigated in this thesis, as this work's main purpose is to study how a general optimization procedure functions.

	Safety factor $sf_{min,allowable}[-]$	**Max offset** $x_{max,allowable}[m]$
Case 1	1.5	20.0
Case 2	1.8	20.0
Case 3	1.5	15.0
Case 4	2.2	20.0

Table 6.1: Cases for the optimization procedure

Case 1 can be considered the base case, and Case 2 and 4 are selected based on regulations set in standards. Case 3 is chosen to evaluate the possibility of setting such a strict constraint on the vessel motion, provided that the maximum WF surge amplitude found in Case Study 1 was $11.47m$ and would not be affected by any change in the mooring system, and furthermore still obtain a safety factor of 1.5. Section 4.2 presents the requirements in terms of clearance to the permanent installation for each optimization case and the corresponding safety factor. In summary, a safety factor of 1.5 is acceptable given that the mobile unit is moved sufficiently far from the permanent installation, and furthermore, that a failure is not likely to lead to catastrophic consequences. A safety factor of 1.8 is applicable for a design in which the mobile unit is detached from the permanent installation, but is still within the vicinity. If the mobile unit is in operational condition, and consequently within the vicinity to the permanent installation, a safety factor of 2.2 should be applied in the design.

For all cases the starting value of the variables, as wll as their upper and lower limits, are listed Table 6.2 for the polyester system and in Table 6.3 for the steel system.

Variable	Unit	Start	Min	Max
Diameter segment 1	$[m]$	0.085	0.076	0.120
Diameter segment 2	$[m]$	0.160	0.126	0.229
Diameter segment 3	$[m]$	0.085	0.076	0.120
Length segment 1	$[m]$	500.0	150.0	600.0
Length segment 2	$[m]$	300.0	200.0	350.0
Length segment 3	$[m]$	90.0	50.0	120.0
Pretension factor	$[-]$	0.13	0.10	0.25

Table 6.2: Optimization variables and bounds for the polyester system

The upper and lower limit on segment lengths are defined to avoid any contact between the polyester or steel wire, segment 2, and the seafloor for the leeward lines. They were roughly estimated by running MIMOSA for a various number of length combinations and offsetting the vessel the al-

Variable	Unit	Start	Min	Max
Diameter segment 1	$[m]$	0.095	0.076	0.114
Diameter segment 2	$[m]$	0.110	0.080	0.132
Diameter segment 3	$[m]$	0.095	0.076	0.114
Length segment 1	$[m]$	700.0	300.0	900.0
Length segment 2	$[m]$	300.0	200.0	350.0
Length segment 3	$[m]$	100.0	50.0	100.0
Pretension factor	$[-]$	0.15	0.10	0.25

Table 6.3: Optimization variables and bounds for the steel system

lowed distance, i.e. $20m$. The leeward lines are, in the case of 0° weather direction, line 1-3 and 10-12. To enable the running of the winch a minimum $50m$ rig chain is required, as explained by the supervisor, and this value is therefore the lower limit for segment 3.

It was somewhat difficult, however, to ensure no steel wire interacting with the seafloor by only controlling the segment length bounds, due to the fact that the weight of the line varies with changes in both diameter and length. An additional constraint g_3 is therefore introduced for the steel system. The constraint involves setting an upper limit on the sum of segment length 1 and 2, as expressed in Eq. (6.14).

$$g_3(l_2, l_3) \; = \; l_2 + l_3 \leq 350m \tag{6.14}$$

When running Case 3 for the steel system, the optimization used over 48 hours before it failed, at which point it reached its maximum number of iterations. After discussing with the supervisor, the constraint on maximum allowable offset was increased to $16.0m$ instead of $15.0m$. The results from section 5.3 indicate that the vessel has a most probable maximum WF surge motion of 11.47 m for the given sea state. It may therefore be too strict to set a requirement of maximum allowable offset equal to $15.0m$ for the steel system, as the WF motions of the vessel cannot be regulated by the mooring system. One possibility would be to to increase the maximum number of iterations,

and to allow the simulation to run for several days. Due to the need for running other optimization procedures, this aspect is not prioritized.

6.3.1 Results - Polyester System

Table 6.4 presents the final configuration with respect to material dimensions for all four cases.

Variable	Unit	Case 1	Case 2	Case 3	Case 4
Diameter segment 1	$[m]$	0.076	0.076	0.077	0.110
Diameter segment 2	$[m]$	0.130	0.126	0.151	0.137
Diameter segment 3	$[m]$	0.076	0.076	0.077	0.076
Length segment 1	$[m]$	172.16	204.23	150.91	195.02
Length segment 2	$[m]$	265.09	350.0	340.18	334.98
Length segment 3	$[m]$	80.60	61.00	88.07	72.20
Pretension factor	$[-]$	0.10	0.10	0.10	0.10

Table 6.4: Final line configuration after optimization - polyester system

The different line configurations in each case resulted in different costs, pretensions and breaking strengths listed in Table 6.5. The resulting safety factor and maximum offset x_{max} are also presented in the same table.

It is noteworthy that the lowest possible breaking strength for the chain segments is $6143.40kN$, which corresponds to a diameter of $0.076m$. Accordingly, any lower MBL implies that the governing breaking strength for the line is established by the polyester segment and its diameter.

As made evident in Table 6.5, in cases 1, 2 and 4, the maximum offset is well below the allowable offset of $20m$. Therefore, the governing constraint was the minimum allowable safety factor, i.e. this constraint needed to first be met. In Case 3, both constraints affected the final mooring line

	Unit	Case 1	Case 2	Case 3	Case 4
Total line length	$[m]$	517.85	615.23	579.16	602.2
Cost per line	$[MNOK]$	0.91	1.00	1.03	1.63
MBL	$[kN]$	5046.50	4724.70	6242.80	5562.80
Pretension	$[kN]$	504.65	472.74	624.28	556.28
Safety factor	$[-]$	1.48	1.77	1.49	2.20
Max offset	$[m]$	15.81	16.68	15.01	17.38

Table 6.5: Results for each optimization case - polyester system

configuration. The highest pretension is also observed in Case 3. As p_{factor} is 0.1 in all cases this result stems directly from the largest segment 2 diameter observed in Table 6.4, which yields the highest MBL. A higher pretension limits the static offset of the system, and consequently limits the total offset.

Figure 6.6 graphically represents the cost difference among all the cases. The dotted lines are an extrapolation of the costs obtained at the final iteration for each case.

From both Table 6.5 and Figure 6.6 it is evident that Case 1 produces the system with the lowest cost. This result is expected as Case 1 is exposed to the softest constraints. The most expensive system is the one obtained from Case 4, which has the strictest constraint on the safety factor. As the safety factor was the governing constraint when an offset of $20m$ was allowed, this finding is also expected. Such an increase in minimum allowable safety factor appears to strongly influence the mooring system cost.

The segment lengths are relatively equal for Case 2 and 4, in terms of total chain length as well as the polyester length. The main relative difference is found in the cross-section parameters; larger segment diameters are observed for Case 4. These diameters lead to a higher MBL of the line, and consequently, a higher cost. There is a very slight difference between Case 2 and 3 in terms of cost, which implies that a small increase in minimum allowable safety factor has the same influence on

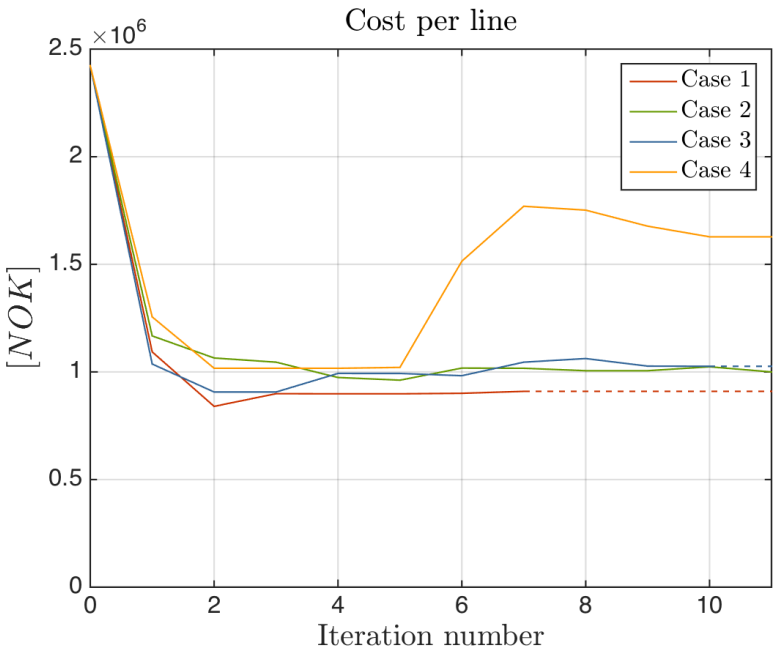

Figure 6.6: Cost variation for each optimization case - polyester system

hardware cost as a small reduction of maximum allowable offset.

The stiffness of the polyester system is mainly provided by the elastic elongation of the lines, but will also contain contributions from geometric stiffness. The geometric stiffness is most important when the bottom chain is lifted from the seabed, which results in change in line weight. The elastic stiffness for the polyester segment is described as $\frac{EA}{L}$, whereby E represent the E-modulus, A represent the cross-section area and L represent the length. When comparing the results from Case 2, 3 and 4 in Table 6.4 it is noticed that the lengths of segment 2 are quite similar, but the diameter is larger for Case 3, thus resulting in a higher elastic stiffness.

In terms of segment lengths, segment diameters, cost, pretension, safety factor and maximum offset, the results for Case 1 during each iteration are presented graphically in the following diagrams. The cost and pretension variation throughout the optimization is illustrated in Figure 6.7.

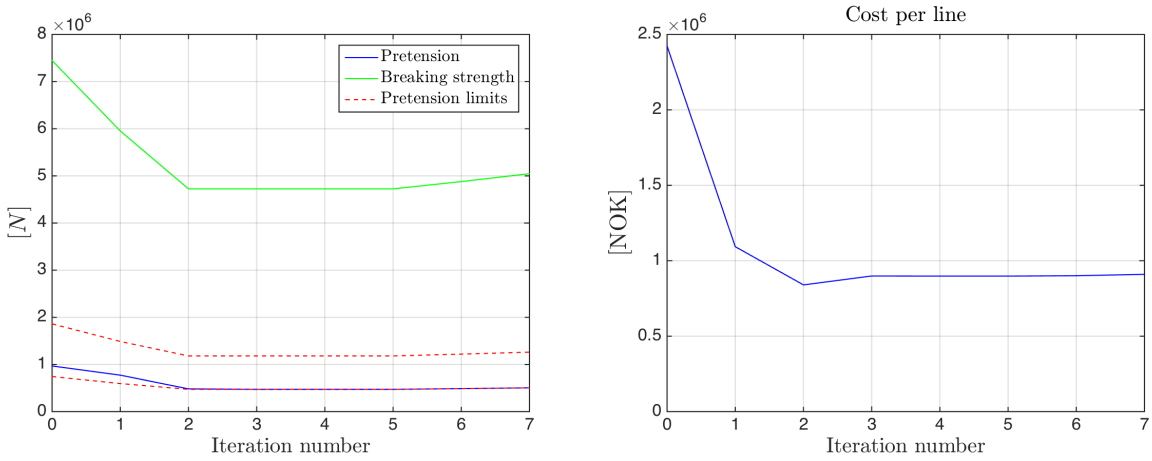

6.7.a Pretension as a function of MBL

6.7.b Cost function

Figure 6.7: Pretension and cost variation for Case 1 - polyester system

In Figure 6.7.a, the dotted lines represent the upper and lower limit of the pretension. It is apparent that the pretension already seeks its minimum value at the second iteration, and that both the pretension itself and its limits depend on the breaking strength.

The variation in segment lengths and diameters are illustrated in Figure 6.8 and 6.9 respectively. The red dotted lines in each figure represent the upper and lower limit on each segment variable.

Figure 6.10 illustrates the variation in safety factor and maximum offset. The red dotted line in Figure 6.10.a represents the minimum allowable safety factor, and the red dotted line in Figure 6.10.b represents the maximum allowable offset.

The most significant change in all parameters occur before iteration number three. The lowest calculated safety factor observed in Figure 6.10.a is at the first iteration, in which the lowest maximum offset also is observed, whereas the pretension factor is higher than 0.1. At iteration number three, the diameters of each segment has reached the minimum values, and the lowest MBL is observed in conjunction with the lowest pretension. Only minor changes are observed after iteration number three; from iteration number five to seven the diameter of segment 2 increases slightly

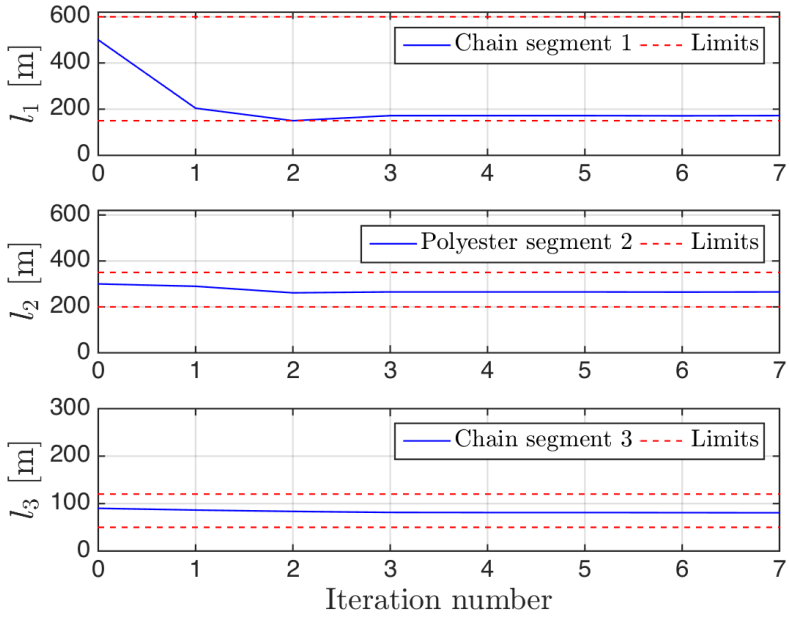

Figure 6.8: Length variation for Case 1 - polyester

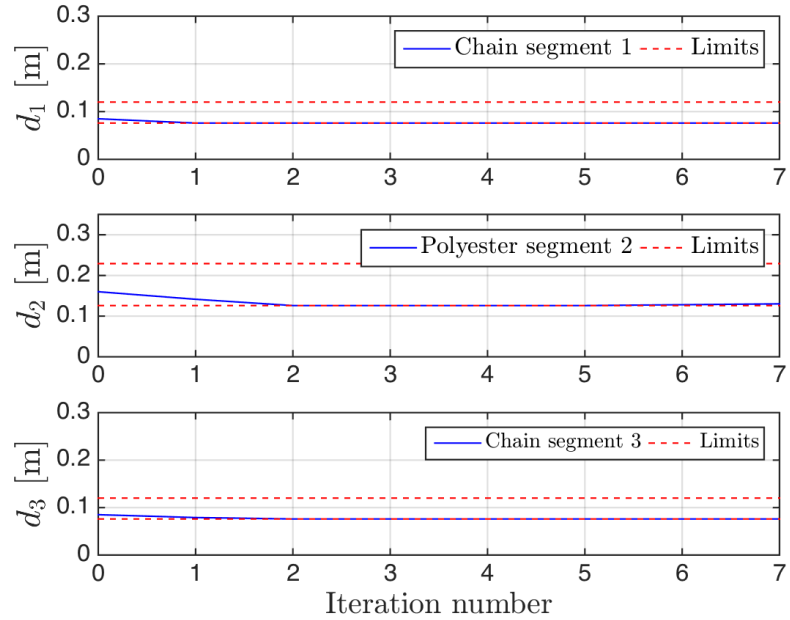

Figure 6.9: Diameter variation for Case 1 - polyester system

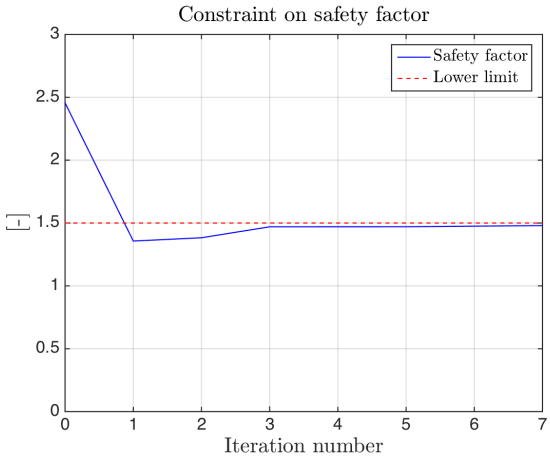

6.10.a Safety factor

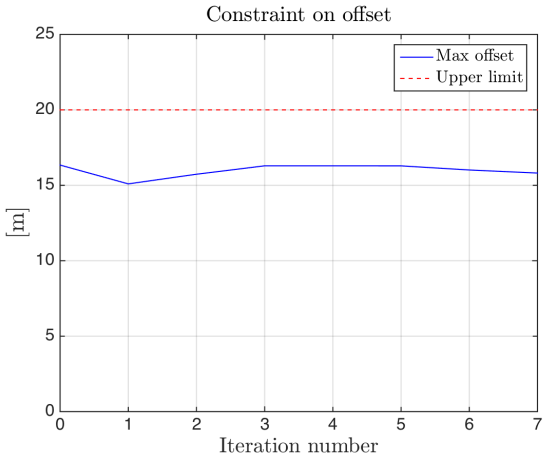

6.10.b Maximum offset

Figure 6.10: Variation in constraint functions for Case 1 - polyester system

and thus increases the MBL of the line which results in a slight increase in safety factor. As the MBL increases, the pretension also increases and the maximum offset observed from iteration five to seven in Figure 6.10.b has decreased. As shown in Figure 6.10.b, the offset never approaches the maximum allowable value during the iterations. This constraint thus never has an effect on the optimization.

A total of seven iterations were needed on order for the optimization to achieve satisfactory convergence. During the first two iterations the diameter of each segment seeks its minimum value. Chain is the most expensive material in this system as a result of its weight. It is therefore somewhat logical that the longest chain segment, segment 1, seeks a value close to as minimum as possible.

Graphical illustration of variation in pretension, cost, segment lengths, segment diameters and constraint functions for Cases 2, 3 and 4 is included in Appendix C.1.

6.3.2 Results - Steel System

With respect to material dimensions, the final line configuration for all four cases is presented in Table 6.6.

Variable	Unit	Case 1	Case 2	Case 3	Case 4
Diameter segment 1	$[m]$	0.076	0.076	0.076	0.084
Diameter segment 2	$[m]$	0.085	0.086	0.083	0.086
Diameter segment 3	$[m]$	0.076	0.083	0.076	0.078
Length segment 1	$[m]$	352.66	346.24	581.43	368.61
Length segment 2	$[m]$	150.00	265.97	216.12	235.68
Length segment 3	$[m]$	83.97	77.66	53.38	80.96
Pretension factor	$[-]$	0.104	0.100	0.206	0.100

Table 6.6: Final line configuration after optimization - steel system

Table 6.7 lists the resulting total length, cost, pretension and breaking strength for the line configuration in each case.

	Unit	Case 1	Case 2	Case 3	Case 4
Total line length	$[m]$	586.63	689.87	850.93	685.25
Cost per line	$[MNOK]$	1.57	1.85	2.24	2.04
MBL	$[kN]$	6143.40	6143.40	5967.90	6358.60
Pretension	$[kN]$	638.9	614.34	1231.50	635.86
Safety factor	$[-]$	1.48	1.84	1.44	2.20
Max offset	$[m]$	20.24	19.41	15.99	19.48

Table 6.7: Results for each optimization case - steel system

From the results in Table 6.7, it is clear that both constraints influence the final mooring line configuration in all cases. The offset in Cases 1, 2 and 4 is close to $20m$, which is the maximum allowed. In the same cases, the pretension factor, and pretension, is near the minimum value allowed, i.e.

10% of the breaking strength. Twice as large pretension can be observed in Case 3, whereby the maximum allowable offset is reduced to $16m$. As mentioned in the previous section, a higher pretension limits both the static offset and the offset caused by LF motions, and hence limit the total offset. A higher pretension in Case 3 is therefore expected. In the same case the length of segment 1, and consequently the total line length, is significantly larger than the total length observed for the other cases. When the line is lifted off the seabed, this increase in length significantly increases the weight of the suspended line, and the point of attack moves further away from the vessel. A larger restoring moment is consequently created, which increases the stiffness of the system in comparison to the other cases, as depicted in Figure 6.11.

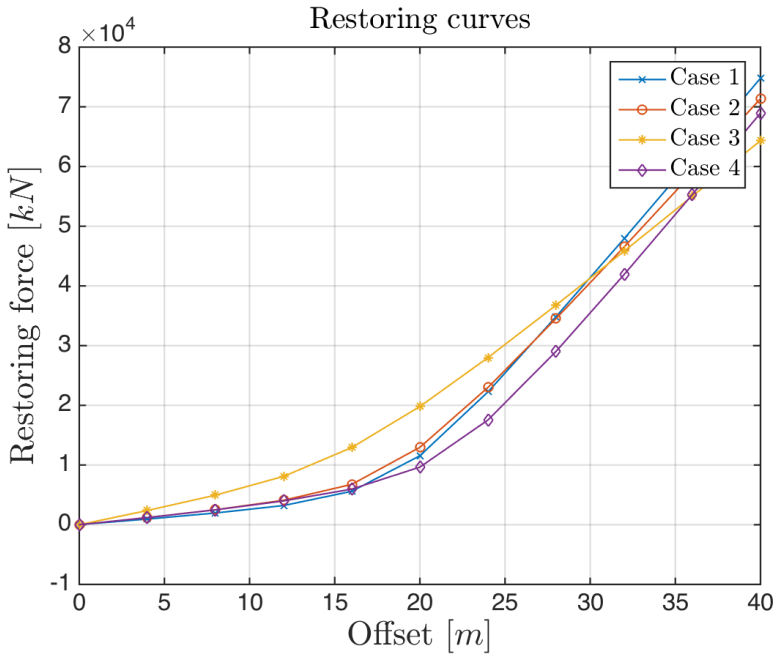

Figure 6.11: Restoring curves for each optimization case - steel system

The segment diameters in Cases 1, 2 and 3 do not vary significantly, which results in quite similar MBL. The breaking strength of the line, however, is somewhat higher in Case 4, where the segment diameters slightly increase. In terms of segment lengths, the results from Cases 2 and 4 are quite similar. The main difference between the two cases is the slight increase in segment diameters in Case 4. This increase produces a higher MBL, which again results in a higher safety factor, pro-

vided that the maximum tension in the lines are near equal.

When comparing the results in terms of cost, it is clear that the system with the softest constraints, Case 1, produces the lowest hardware cost. A graphical illustration of the cost variation in each optimization case is presented in Figure 6.12. The dashed line in the figure represents an extrapolation of the cost calculated at the last iteration in each case.

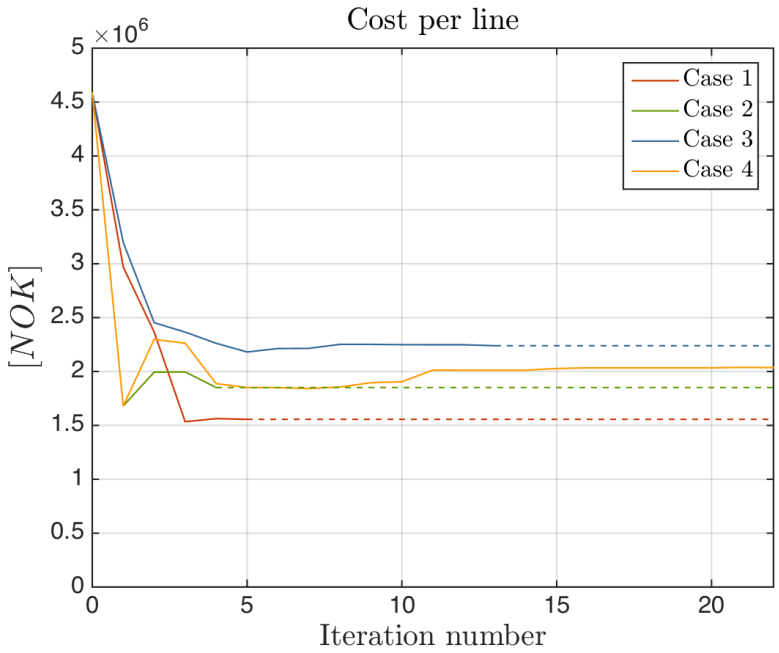

Figure 6.12: Cost variation for each optimization case - steel system

From both Figure 6.12 and Table 6.7 it is evident that the most expensive system results from Case 3, in which the allowable offset was reduced from $20m$ to $16m$. This alteration implies that the most dominating impact on hardware cost for the steel system, in terms of safety factor and maximum allowable offset, is to set stricter restrictions on the vessel motion.

Figure 6.13 graphically presents the pretension, as a function of MBL, and the cost variation at each iteration step. In Figure 6.13.a, the dotted lines represent the upper and lower limit for the pretension. As the pretension, and its limits, depend on the breaking strength, both vary with

varying MBL values.

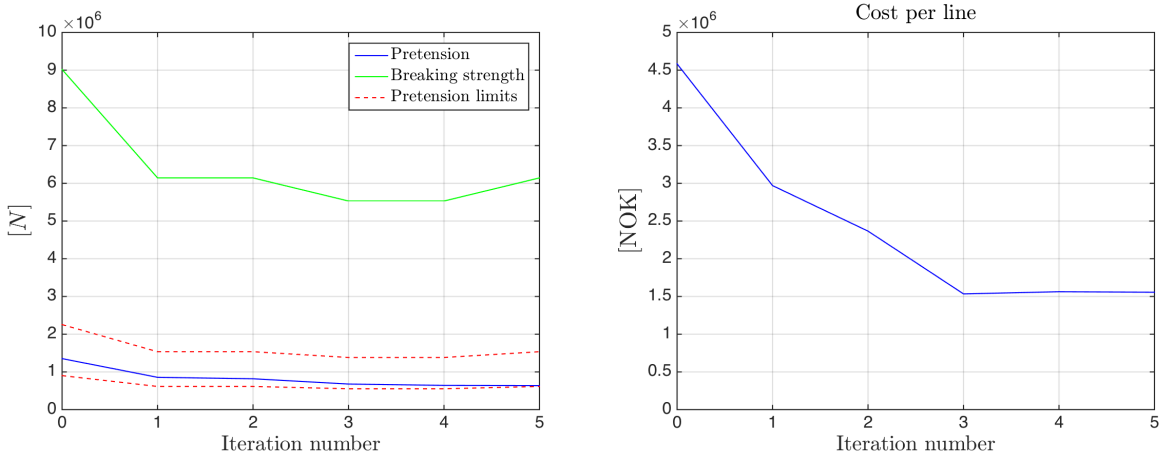

6.13.a Pretension as a function of MBL

6.13.b Cost function

Figure 6.13: Pretension and cost variation for Case 1 - steel system

Figures 6.8 and 6.9 illustrate the variation in segment lengths and diameters, respectively. The red dotted lines in each figure represent the upper and lower limit of each segment variable.

The material cost is specified in section 6.1 and is presented as price per unit weight. The cost per unit weight for chain is half the cost per unit weight for the steel wire. In the insertion of the values for chain and steel wire diameter from Case 1 into the expression for weight per unit length, as in Eq. (6.3) and (6.5), the weight per unit length for steel wire is less than half the weight per unit length for chain. This finding implies that with diameters resulting from Case 1, one would expect that the segment consisting of steel wire should have a length that approaches the maximum allowable value. The length of chain segments would then decrease, as chain appears slightly more expensive than steel wire. As the optimization depends on the constraints together with the cost function, the final segment lengths seem to be quite influenced by the constraints.

Figure 6.16 illustrates the variation in safety factor and maximum offset. The dashed red line in Figure 6.16.a represents the minimum allowable safety factor, and the dashed red line in Figure

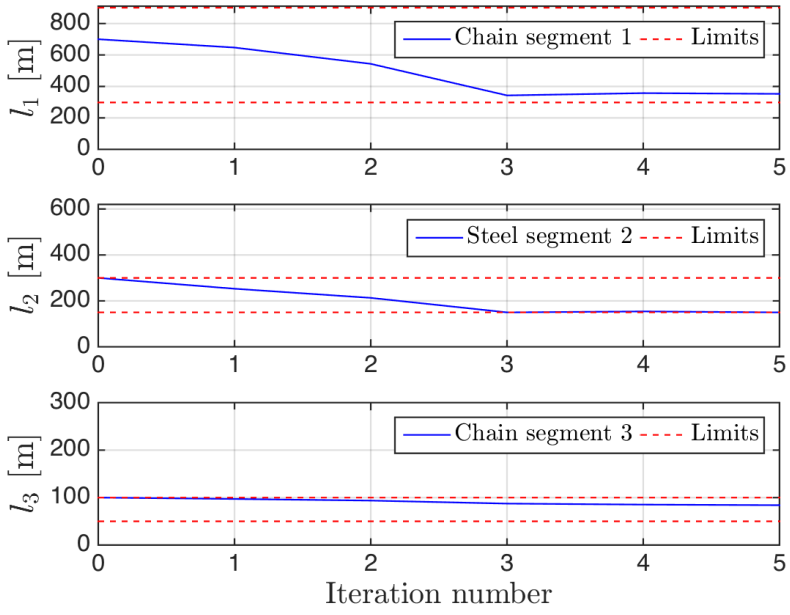

Figure 6.14: Length variation for Case 1 - steel system

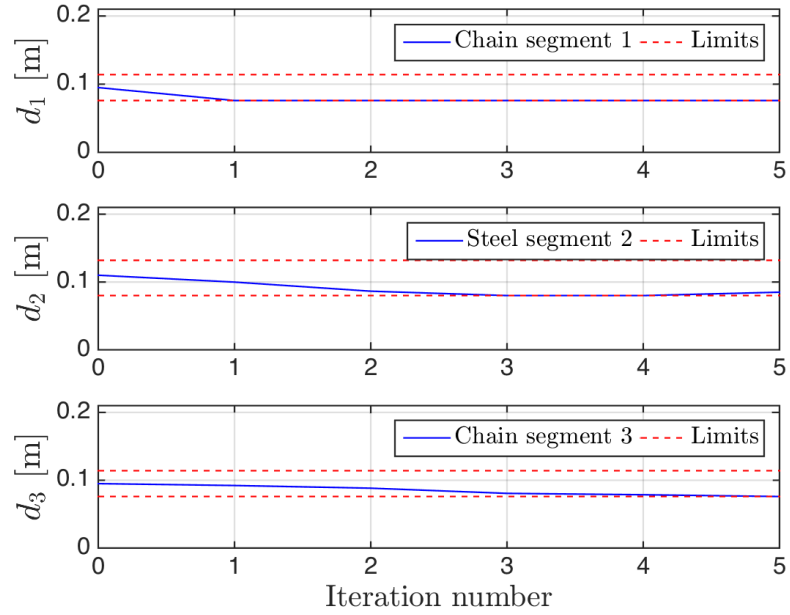

Figure 6.15: Diameter variation for Case 1 - steel system

6.16.b represents the maximum allowable offset.

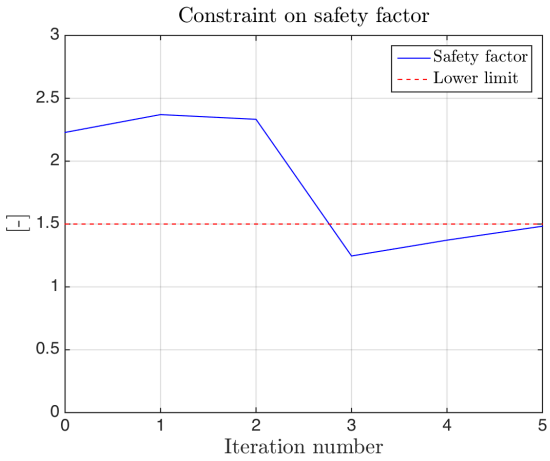

6.16.a Safety factor

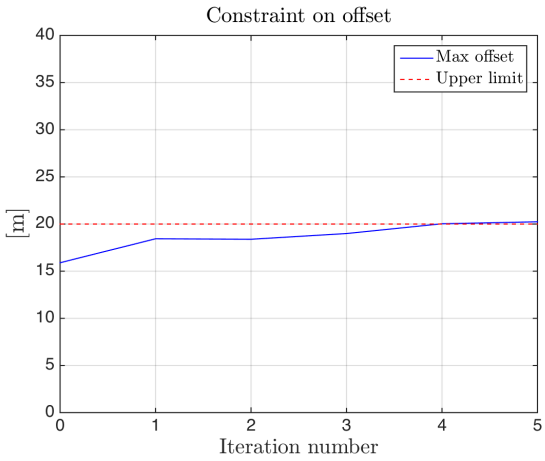

6.16.b Maximum offset

Figure 6.16: Variation in constraint functions for Case 1 - steel system

Unlike the offset in Case 1 for the polyester system, the offset of the steel system is quite similar to the maximum allowable value as observed in Figure 6.16.b. Hence, both the constraint on safety factor and on maximum offset influence the final line configuration.

From the plots of all variables, it is clear that the most significant changes occur before iteration number three. A small increase in safety factor is observed between iteration number three and four, whereby the pretension decreases. The constraint on safety factor is not met before iteration number five, were the MBL has increased due to increase in diameter of segment 2. Also, the diameter of segment 1 reaches its minimum value at iteration number five which again reduces the total line length and thus the tension in the line.

A graphical illustration of variation in pretension, cost, segment lengths and diameters and constraint functions for Case 2, 3 and 4 are given in Appendix C.1.

6.3.3 Sensitivity Study

In order to investigate the robustness and the sensitivity, with respect to small changes of the optimization procedure, the following cases were considered:

1. Change in environment for both the steel and polyester system
2. Evaluate global minimum for both the steel and polyester system
3. Increase the polyester cost with 50%

The two first sensitivities are performed for the base case, Case 1, for both the steel and polyester system, as introduced in section 6.3. The third sensitivity is only performed for the polyester base case.

Sensitivity 1 - Change in Environment

In Sensitivity 1, the environment is changed by increasing the significant wave height with $10cm$. Such a small increase should not make a great impact on the cost of the system. The cost before and after the environmental change for each base case is presented graphically in Figure 6.17. The red line represents the variation for $H_S = 16.1m$, whereas the blue line represents $H_S = 16.0m$. In all plots the dashed line represent the value obtained at the final iteration for the respective parameter.

Table 6.8 also numerically details the final cost before and after the change in environment, in conjunction with the difference in percentage.

	Cost $[MNOK]$ $H_S = 16.0m$	**Cost** $[MNOK]$ $H_S = 16.1m$	**Difference** $[\%]$
Polyester system	0.91	0.96	5.21
Steel system	1.56	1.83	14.75

Table 6.8: Sensitivity 1 - Difference in cost

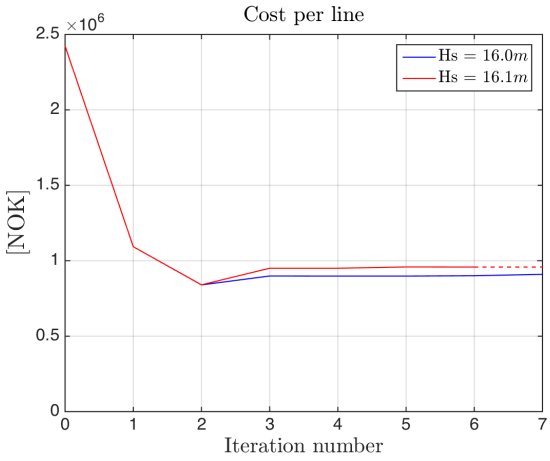

6.17.a Polyester system

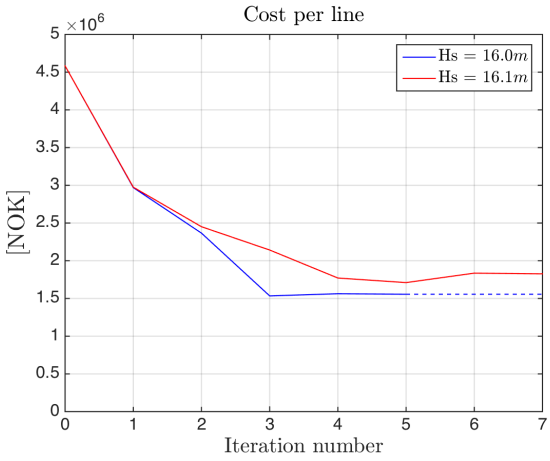

6.17.b Steel system

Figure 6.17: Sensitivity 1 - Plot of cost function for $H_S = 16.0m$ and $H_S = 16.1m$

As made evident in Table 6.8, the steel system appears to be more sensitive with respect to environmental changes in comparison to the polyester system. To evaluate which parameters lead to the increase in the cost for the steel system, Figure 6.18 presents a plot of both diameter and segment length variation during the two optimization cases.

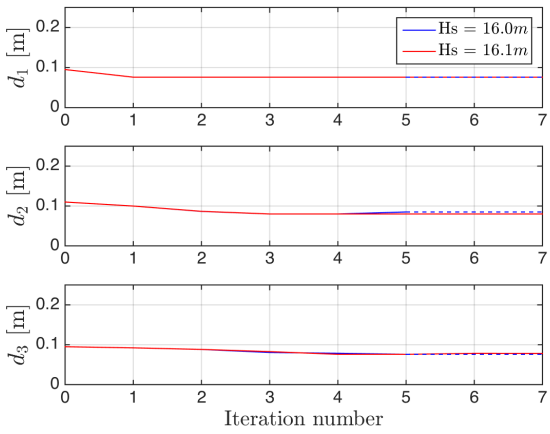

6.18.a Segment diamteter variation

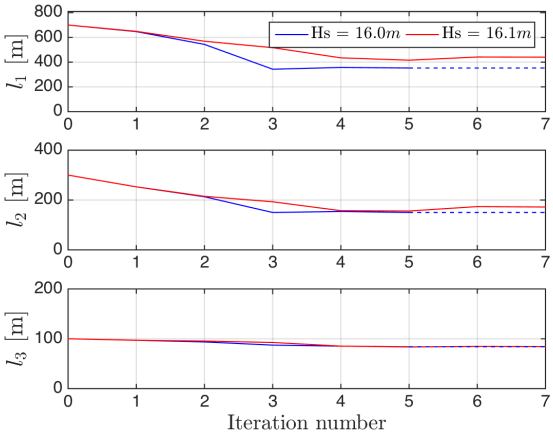

6.18.b Segment length variation

Figure 6.18: Sensitivity 1 - Segment length and diameter variation for the steel system

As demonstrated in Figure 6.18.b, the length of segment 1 for $H_S = 16.1m$ has the largest devia-

tion in comparison to $H_S = 16.0m$. This deviation explains the difference in final cost, as the cost function varies significantly with increased chain length, due to the high weight per unit length. From Figure 6.18.a a minor, almost insignificant, change in the diameter of segment 2 is noticeable, while the diameter of segment 1 and 3 are the same for the two cases. This result indicates that the breaking strength of the line is almost identical before and after the change in significant wave height.

Through changes in the significant wave height, the constraints are slightly altered. The tension in the lines may increase which leads to small changes in the line configuration to achieve a satisfactory safety factor. As stated above, however, the segment diameters and hence the MBL for the steel system are nearly identical for $H_S = 16.0m$ and $H_S = 16.1m$. In order to meet the safety factor constraint, the tension in the lines could not have changed significantly. The increase in line length may therefore be a result of a change in vessel motions. As established in section 5.3, the main excitation on the system is the WF forces, as the wave drift coefficients has very little energy at the specified peak period of the waves. A small increase in significant wave height may therefore have an influence on the total vessel motions. Still, such a small change in wave height should not result in such noteworthy changes in the mooring system configuration, and hence the cost, as seems to be the case for the steel system. The optimization algorithm in SIMA appears to be overly sensitive, as an increase the significant wave height by less than 1% results in almost 15% increased cost.

Figure 6.19 presents a graphical representation of both variation in maximum offset and pretension for the steel system.

The pretension of the system with changed significant wave height has increased in comparison to the original case, as observed in Figure 6.19.a. The maximum offset presented in Figure 6.19.a is consequently lower for this system. It was somewhat strange that the maximum offset was reduced to approximately $17.5m$ as the results from section 6.3.2 implies that the offset of the steel system lies around the maximum allowable offset. A higher pretension increases the tension in the lines. A

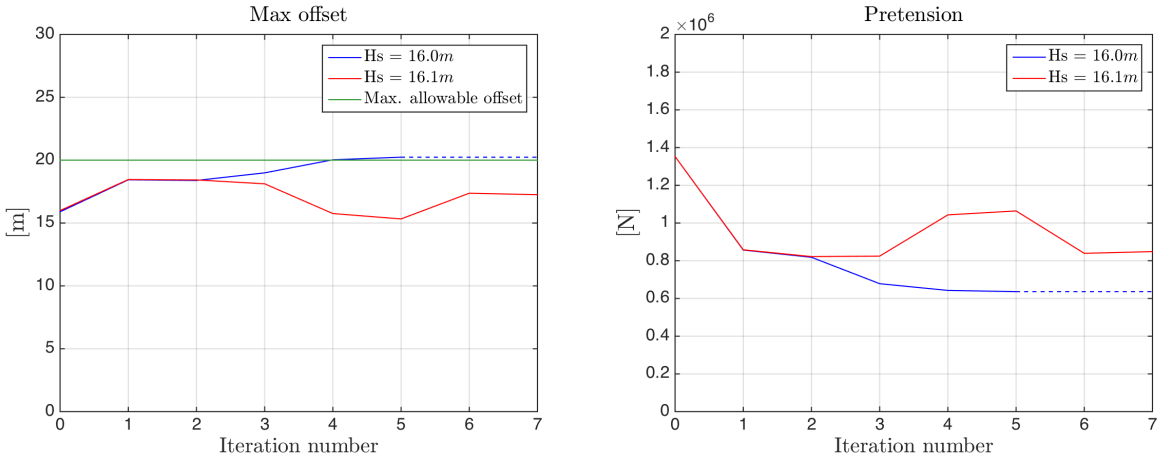

6.19.a Segment diamteter variation

6.19.b Segment length variation

Figure 6.19: Sensitivity 1 - Variation in maximum offset and pretension for the steel system

larger offset, however, also implies a higher tension in the lines as the tension provided from SIMO is directly taken from the line characteristics. There is no simple or intuitive explanation of why this phenomenon occurs, but any change in cost function may result in a different search direction. Any further explanations are not provided in this thesis, as it requires a thorough understanding of the underlying mathematics of the optimization algorithm and is outside the scope of this thesis.

A graphical representation of diameter and segment length variations, together with the variation in pretension, maximum offset and safety factor for the polyester system are included in Appendix C.2. The largest difference is found in the length of segment 3, which is the rig chain.

Sensitivity 2 - Global Minimum Evaluation

The next sensitivity case involved the evaluation of the global minimum of the cost function. Since the cost function is a function of the diameter squared and the length, it was expected that its value obtained after the first optimization run would be the global minimum. In order to assess this prediction, several runs were executed with different starting values. The input for the first run was the same as for the base case, Case 1, with relatively high starting values. The input for the next run is then the optimized variables obtained in the previous run, and so forth. For the polyester system,

a total of 33 iterations, and three runs, were needed to obtain convergence. The convergence was assumed when the next run was finished after one iteration. In order to verify that this value was indeed the minimum, a similar procedure was carried out with starting values for the first run as the lower limit of each variable. Figure 6.20 presents the resulting cost variation for the polyester system. The blue line in the plot contains starting values equal to the values given in section 6.3 in Table 6.2, and the red line has starting values equal to the lower limit of the variables, which are also listed in Table 6.2. The dashed line in each plot represent the final value of the respective variable or parameter at the last iteration.

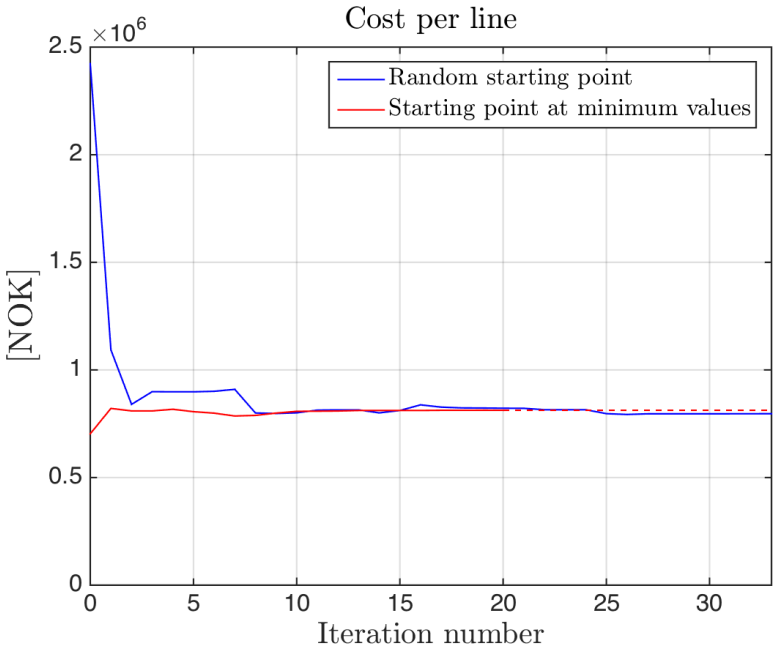

Figure 6.20: Cost variation for global minimum convergence - polyester system

As observed in the Figure 6.20, fewer iterations were needed to obtain convergence when starting at the lower limit value for the variables for the polyester system. The cost function also approached the minimum value more quickly from this starting point.

The same procedure described for the polyester system is also applied to the steel system. The resulting cost variation is presented in Figure 6.21, whereby the blue line represents the starting values from Table 6.3, and the red line has starting values equal to the lower limit values listed in

the same table.

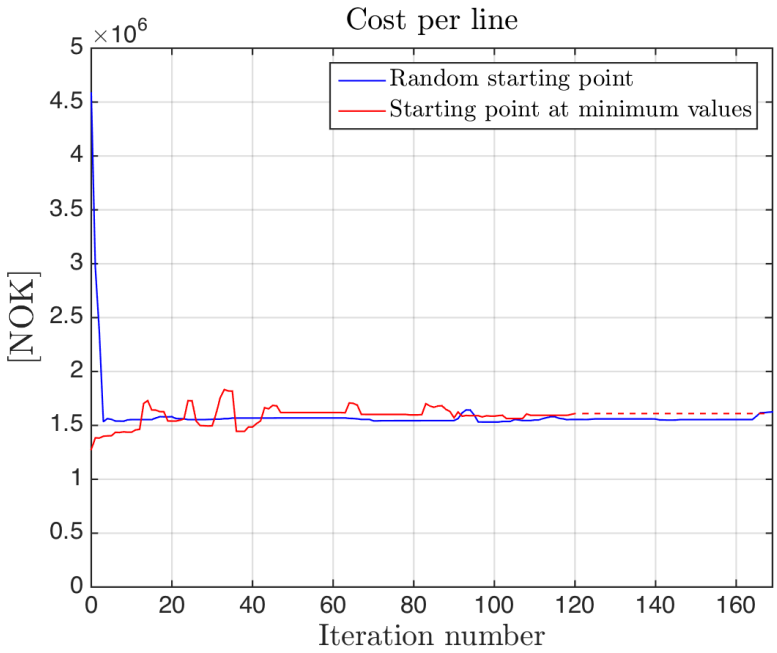

Figure 6.21: Cost variation for global minimum convergence - steel system

From the figures, it can be observed that the steel system requires a significantly higher number of iterations than the polyester system in order to achieve convergence. Eight runs from each starting point, and a total of 169 iterations for the blue line, were required to achieve the results presented in the figure. Due to the time demanding task of running the steel optimization, convergence in this sense is achieved when the cost approaches the same value from each starting point. The blue line does not vary considerably after the first 20 iterations, except for some minor peaks, while larger deviations around the minimum value can be observed for the red line.

Figures 6.22.a and 6.22.b present plots of variation in optimization variables for the steel system, and Figures 6.23.a and 6.23.b present plots for the polyester system, in order to inspect what happens to the variables during the iterations. Only minor changes in segment diameters for both steel and polyester system can be observed in Figure 6.22.a and 6.23.a, respectively.

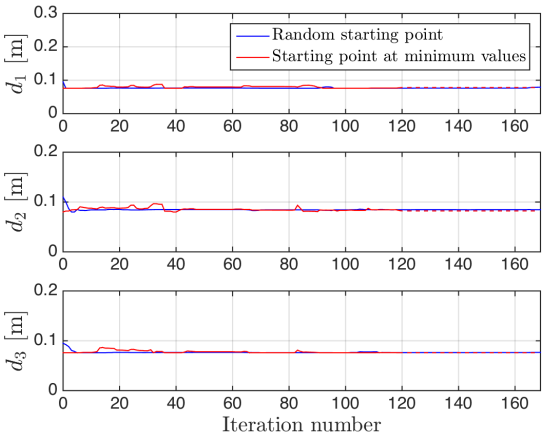

6.22.a Segment diamteter variation

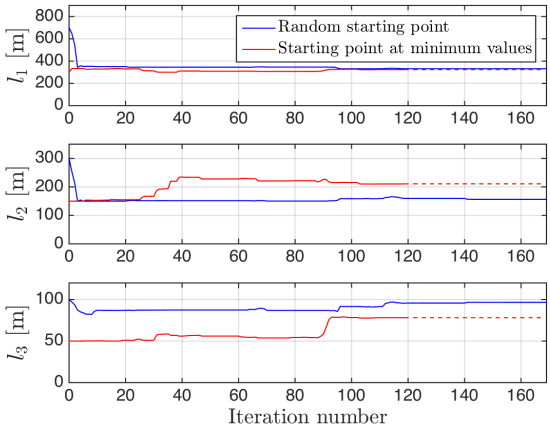

6.22.b Segment length variation

Figure 6.22: Sensitivity 2 - diameter and segment length variations for the steel system

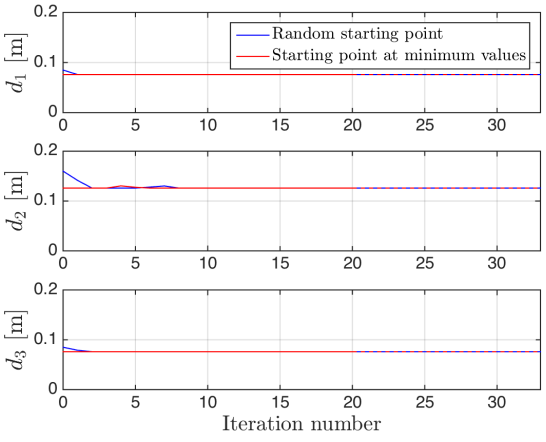

6.23.a Segment diamteter variation

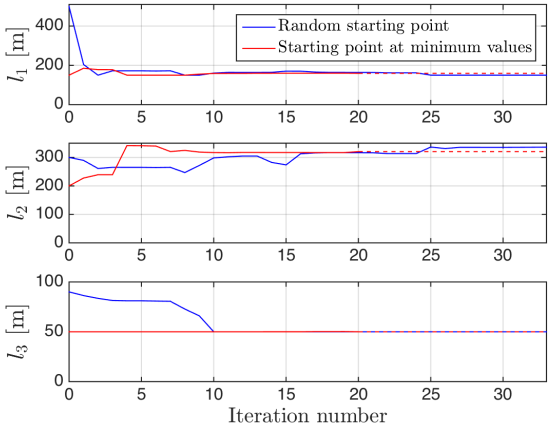

6.23.b Segment length variation

Figure 6.23: Sensitivity 2 - diameter and segment length variations for the polyester system

The same trend found in Figure 6.21 is recognized in Figure 6.22. There are only minor changes in the blue line after iteration number 20. A small increase in segment length 3 around iteration number 100, as demonstrated in Figure 6.22.b. As segment length 3 increases, segment length 1 decreases. However, in consideration of segment lengths 2 and 3, a difference is evident between the red line with a starting point in the minimum values in comparison to the blue line. An interesting observation is although these lines differ in terms of segment length, the cost only indicates smaller variations. For instance, at iteration number 80 the cost is almost equal for the two lines, but the line configuration in terms of segment lengths is quite different. This variation may indicate that a different combination of segment lengths produce approximately the same cost, i.e. the cost function may have similar minimum points with different relative segment lengths.

No easy explanation can be provided for why the steel system optimization requires a significantly larger number of iterations than the polyester system. By the same reasoning as above, several combinations of segment length can result in almost equal cost, and any small changes in segment length only affect the cost slightly, making it harder for the optimization routine to ”decide” on an optimum line configuration.

The segment length variation for the polyester system, as presented in Figure 6.23.b, is also exposed to variations. It is noteworthy that the number of iterations for the polyester system is almost only one sixth of the iterations needed for the steel system. The most pronounced changes appear in the first run, which ended at iteration seven for the blue line, and is observed in segment length 1 and 2. The length of segment 2 slowly increases as the length of segment 1 and 3 begins to approach the minimum values.

The difference in cost between the mooring configuration obtained in the base case, Case 1 from section 6.3, and the configuration given by global minimum convergence is given in Table 6.9. Both the polyester and steel system are represented in the table.

As specified in Table 6.9, there are some deviations between the cost obtained after one optimiza-

	Cost $[MNOK]$ Base case	**Cost** $[MNOK]$ Global minimum	**Difference** $[\%]$
Polyester system	0.91	0.80	12.09
Steel system	1.56	1.63	4.29

Table 6.9: Sensitivity 2 - Difference in cost

tion procedure compared to the final cost after several optimization runs. Section 6.5 discusses theories related to this phenomena.

Sensitivity 3 - Increase in Polyester Cost

The last sensitivity studied is the influence of increasing cost for one material. The polyester system is chosen for this purpose, and is increased with 50%; $C_{poly} = 10.5kr/N$. Table 6.10 presents the difference in cost for the base case and the case with increased cost.

	Cost $[MNOK]$ $C_{poly} = 7.0kr/N$	**Cost** $[MNOK]$ $C_{poly} = 10.5kr/N$	**Difference** $[\%]$
Polyester system	0.91	0.96	5.21

Table 6.10: Sensitivity 3 - Difference in cost

The cost variation for the two cases is also presented graphically in Figure 6.24.

From the figure, it can be observed, that the cost has increased with increasing polyester cost. It would also be interesting to see how the line dimensions are influenced by this increase in cost. Figure 6.25.a and 6.25.b provide the diameter and length variation of each segment.

From these diagrams above, it is interesting how the length of segment 2 has increased in comparison to the original system with lower polyester cost. This result is somewhat unexpected, although one should be aware that the optimization formulation minimizes the total cost without ”knowledge” of what material is more or less expensive. An explanation may be that the increase

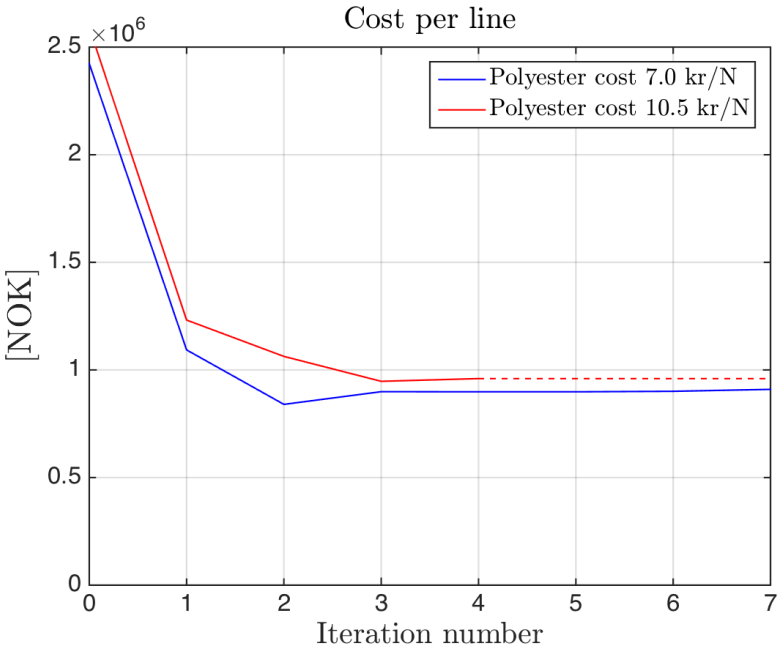

Figure 6.24: Sensitivity 3 - Cost variation for polyester system

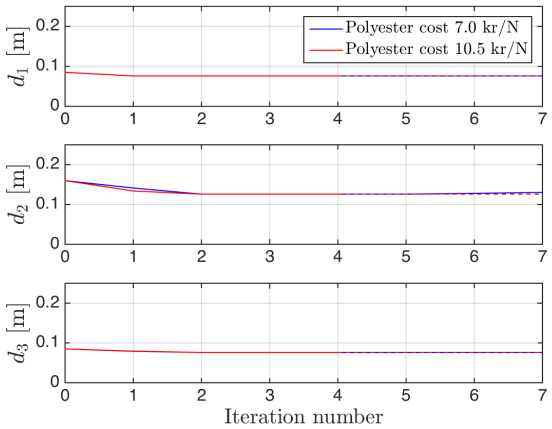

6.25.a Segment diamteter variation

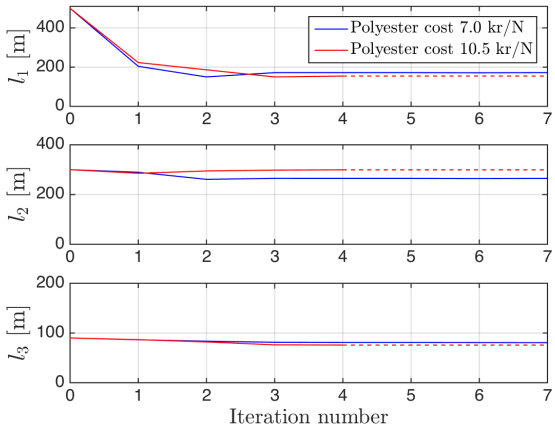

6.25.b Segment length variation

Figure 6.25: Sensitivity 3 - diameter and segment length variations for the polyester system

in polyester cost is almost insignificant in the minimization of the total cost, and the differences observed in the segment lengths are random. It could also be coincidental that the mooring line configuration changed when increasing the polyester cost, i.e. that this change in cost function affected the search direction of the algorithm. A difference of 5% presented in Table 6.10 is, however, less than half of the difference observed in the global minimum convergence sensitivity study. Also, as explored in Sensitivity 2, the mooring system configuration may change by running several optimization runs, whereby the input values for the next run are obtained from the previous run. There is, however, the possibility of this configuration not being the most optimal, and by running several sequential runs a different mooring configuration may be obtained.

Plots of the maximum offset and safety factor variation are provided in Appendix C.2. From these plots, it can be seen that the resulting maximum offset is close to the same for each case, and both meet the requirement of a safety factor of 1.5.

6.4 Verification of Optimization Results

An important fact to consider is that this optimization formulation only considers a time domain simulation with one single seed number. Several realizations with different seed numbers are in theory necessary when working with time series in order to obtain reliable statistics. In each of the four cases, the optimized system, for both the steel and polyester system, is verified by running time domain simulations with ten different seed numbers. The method described in section 5.2.2 is utilized to extract the most probable largest values of line tension, WF motion, LF motion and total motion. The results, with respect to motions and line tension for Case 1, with constraints $sf \geq 1.5$ and $x_{allowable} \leq 20.0m$, for both steel and polyester system, are presented in Table 6.11 and 6.12. Only the surge motion of the vessel is presented as a result of the weather acting in positive global x-direction, and the horizontal motion occurring mainly in surge. Results from the seed variation for optimization Cases 2, 3 and 4 for both the polyester and steel systems are included in Appendix C.3.

	$\bar{\boldsymbol{x}}$ $[m]$	$\boldsymbol{x^{WF}}$ $[m]$		$\boldsymbol{x^{LF}}$ $[m]$		$\boldsymbol{x^{tot}}$ $[m]$	
		max	σ	max	σ	max	σ
Steel	9.80	11.46	3.07	4.04	1.39	20.25	3.47
Polyester	6.10	11.47	3.07	3.03	1.23	16.39	3.55

Table 6.11: Case 1 - most probable max and standard deviation of surge motion

	$\boldsymbol{MBL}$	$\boldsymbol{T_{stat}}$	$\boldsymbol{T_{max}}$	$\boldsymbol{sf}$
Steel	6140.0	989.0	4250.0	1.35
Polyester	5050.0	947.0	3740.0	1.44

Table 6.12: Case 1 - Tension in heaviest loaded line, line 7

From Table 6.11 it can be observed that the motion in the steel system is larger than in the polyester system. The stiffness of the steel system is mainly governed by the geometric stiffness, i.e. the change in line geometry from initial position. As explained in section 2.2.2, when the steel line is being lifted off the seabed, the weight of the suspended line increases. The point of attack of the weight will thus move further away from the vessel than in initial position. The restoring force for a system governed by geometric stiffness increases non-linearly with increasing offset. When most of the bottom chain is lifted off the seabed, the restoring force will act linearly due to the effect of elastic stiffness in the steel wire. The stiffness of the polyester system is influenced by both geometric and elastic stiffness, but the geometric stiffness will mainly affect the restoring force when the vessel is offset only a few meters. After that, the stiffness increases and behave linearly due to the elongation of the polyester line. These effects are observed from the restoring curves in Figure 6.26.

As evident in the figure, for offsets between $0m$ and $5m$ the restoring force is relatively small for the both polyester and steel system. It is not easily observed from the plot, but the restoring force for the polyester system is slightly nonlinear in the same interval. The geometric stiffness influences the restoring force at relatively small offsets for the polyester system, as the line is lifted off the seabed and the weight of the suspended line increases together with a change in the line shape.

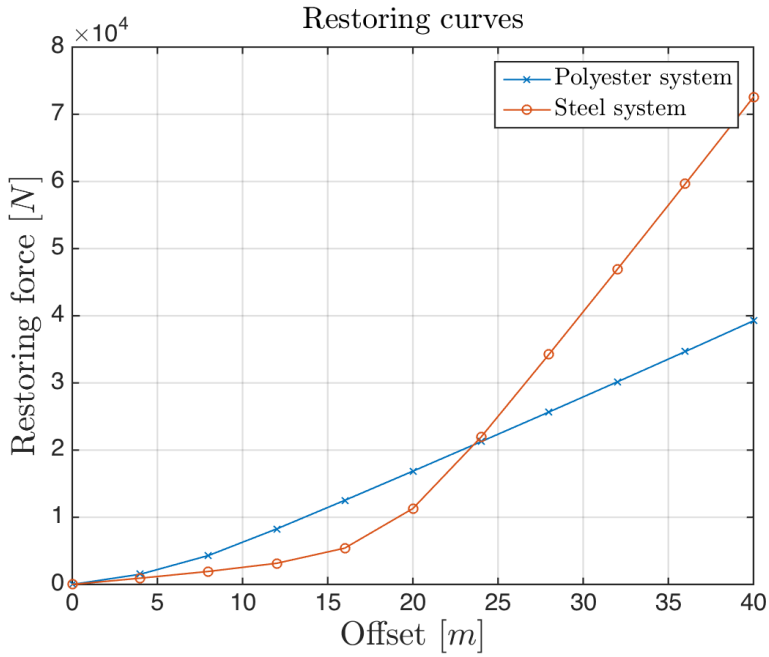

Figure 6.26: Restoring curves for Case 1 for both polyester and steel system

To identify an interesting observation from Table 6.11, the maximum total offset appears somewhat low, for both steel and polyester system, in comparison to the sum of static and maximum WF offset. This aspect possibly indicates that the WF and LF motion are out of phase, and may cancel one other out to a certain extent. The same trend is found in all four cases. In order to investigate this scenario, time series for one realization, and only Case 1 for both the polyester and steel system, were studied. The time series for WF motion is based on a local coordinate system, and therefore the signal is multiplied to -1 to convert it to the global coordinate system. The time series for LF and total motion are provided in the global coordinate system, with the static offset as a starting point. Then, an exploration of the hypothesis $\bar{x} + x^{WF} \geq \bar{x} + x^{WF} + x^{LF}$ follows. By subtracting the static offset from both the LF motion and total motion time series, this hypothesis may be further studied. A window from the time series, for both the polyester and steel system, in which the maximum total motion occurred, are imported into MATLAB, and these plots are shown in Figure 6.27 and 6.28. One should note that the static offset has been subtracted from the LF and total motion in this figure, and the WF is computed in the local coordinate system and thus

oscillates with zero mean at the static offset.

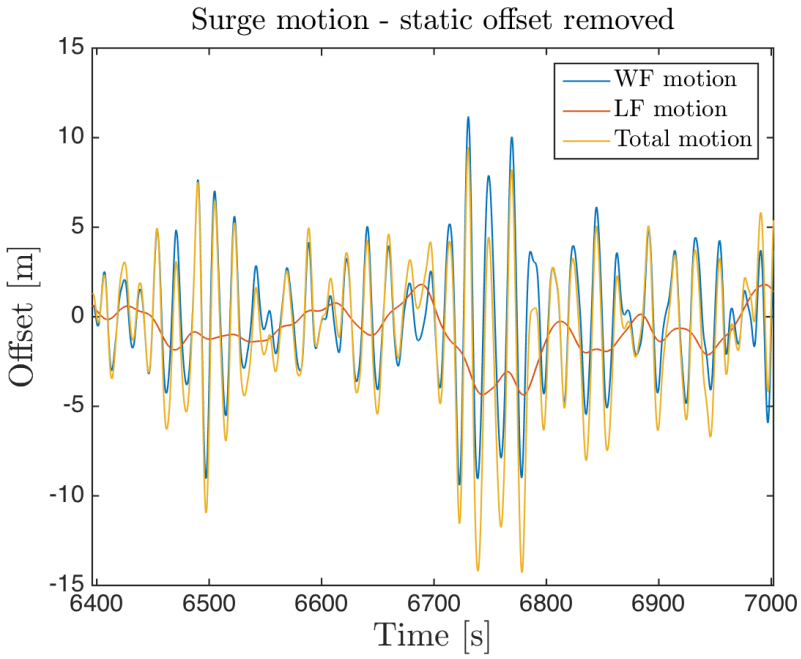

Figure 6.27: Window from surge motion time series for the polyester system

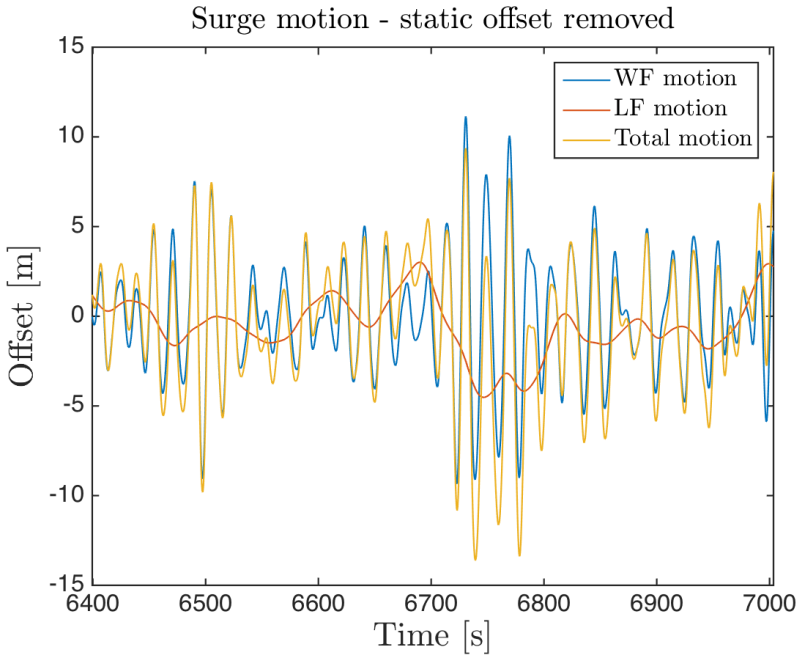

Figure 6.28: Window from surge motion time series for the steel system

The maximum WF and total motion occurs in the time span 6700-6800s. As observed from the figure, the LF motion is negative at the time instants at which the WF motion experiences its maximum. This aspect strengthens the hypothesis defined above, i.e. that the LF response limits the WF maximum response and the total dynamic maximum response is lower than expected.

The mean of both the LF and the total motion time series is lower than the static offset, which indicates that the process is exposed to a negative skewness in surge. The mean tension in the lines is also higher than the static tension,which results in a stiffness higher than experienced at the static offset, and the total response in positive x-direction is thus limited. This phenomenon is explored further in Chapter 7.

From Table 6.12 it is noticed that the safety factor is below 1.5, which was the constraint set in the optimization for this case. From Table 6.11 it is also observed that the maximum total offset in surge is higher than calculated at the final iteration of the optimization. Both these observations indicate that the seed number used in the time domain simulations produce a somewhat ”kind” sea state.

6.5 Discussion

From the sections that presented the results for polyester and steel system, several observations can be made. Firstly, in a comparison of each of the four optimization cases for polyester and steel together, a polyester system tends to be the most cost efficient. This is illustrated in Figure 6.29. The most expensive polyester system resulted from requiring a minimum safety factor of 2.2, whereas limiting the maximum offset to 16m resulted in the most expensive steel system. This finding indicates that to obtain a smaller offset is easier for the polyester system. The stiffness is governed by elastic stiffness, the restoring curves behaves relatively linearly and the restoring force are typically higher than for a steel system for offsets of interest. Figure 6.26 also reflected this result. When considering the results from the verification in section 6.4, it is clear that the static

and LF response for the steel system are larger than for the polyester system. When limiting the steel system's maximum offset to $16m$, the total line length increases significantly, which results in a stiffer system. This is illustrated in Figure 6.11.

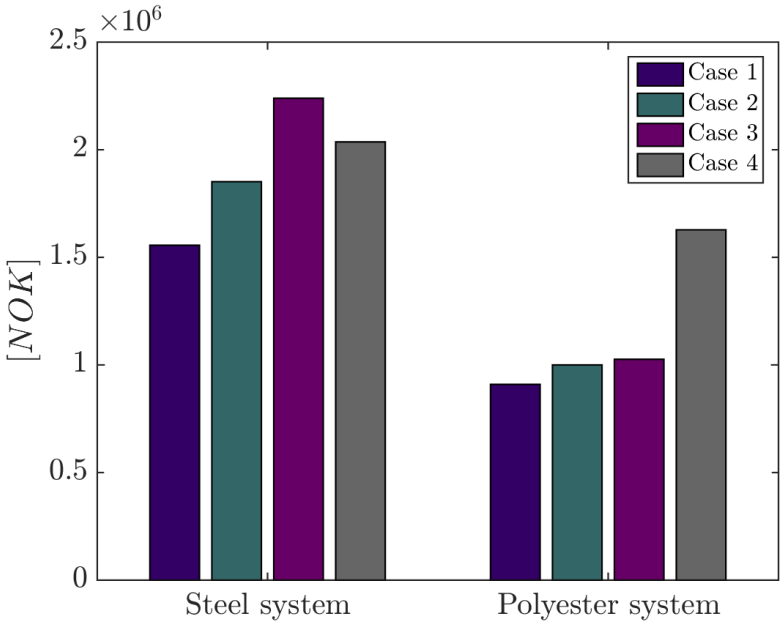

Figure 6.29: Cost for each optimization case - both polyester and steel system

Based on the fact that polyester systems are more cost efficient, in addition to being both less expensive and easier to install than steel systems, one may ask why steel wires are still widely used in mooring systems. The main drawback of polyester lines is their low abrasion resistance (Larsen, 2015). For offshore vessels that operate in areas, for instance, with significant trawling activities, the risk of mechanical interaction between the mooring lines and trawls must be taken into consideration. Any mechanical interaction between a mooring line and another subsea installation, riser or pipeline must be considered in order to avoid a line failure due to abrasion. Steel wire has superior qualities in comparison to the polyester rope with respect to abrasion resistance. Additionally, companies that operate offshore vessels may have additional requirements with respect to the acceptability of polyester ropes. For instance, as explained by the supervisor, Statoil has additional requirements to support vessels that operate next to a permanent platform. The lines taking the heaviest load, when the weather is directed such to give the support vessel an offset towards the

permanent structure, has to be made from steel.

For the three polyester optimization cases with an allowable maximum offset of $20m$, the analysis found that the maximum offset was significantly lower than the allowable offset. The pretension factor therefore seeking its minimum value is expected, as this factor may result in a lower maximum line tension, which is directly used in the governing safety factor constraint.

The computation method utilized in SIMO to calculate the line tension constitutes an important consideration to be kept in mind for this optimization. As already mentioned, tension found quasi-statically neglects the influence of important dynamic effects on the line tension. For the polyester system, with relatively linear characteristics, a quasi-static method may be acceptable, as the suspended line is taut and light, and is not significantly influenced by dynamic effects. On the other hand, for the steel system, a quasi-static approach might underestimate the tension in the mooring lines. This phenomenon is observed in Case Study 1 in section 5.3. The difference the in time domain calculation of mooring line tension, i.e. quasi-static versus dynamic, is assessed in Case Study 3 in Chapter 7.

In the consideration of the different sensitivity studies, some unexpected outcomes are noticed. Firstly, a small and almost insignificant change in a significant wave height resulted in an almost 15% increase in the cost for the steel system. Preferably, such a small change in the environment should not influence the optimization to that extent. This issue was discussed with Vegard Aksnes, but no apparent reason was unveiled. The mathematics in the optimization algorithm is quite complex, for example, in terms of gradient search directions, and a more in-depth study of the algorithm would be necessary to further explore this phenomenon.

Secondly, the global minimum sensitivity study indicated that the best possible outcome in terms of lowest cost may not be achieved by only running one optimization procedure. After a discussion with Vegard Aksnes, no easy explanation could be provided for this phenomenon. It seemed some-

what illogical that the insertion of the optimized variables from one optimization run as starting values for the next run would produce another mooring system configuration, and hence, a lower cost. An important issue was then raised about why the initial optimization had stopped in the first place, as a lower cost was clearly possible to achieve. It was discussed whether the value for the parameter called desired final accuracy, which is the convergence criterion for the optimization, could be the reason. By running Case 1, a simple check is performed for the polyester system with a desired final accuracy equal to 0.001 as opposed to 0.01. The simulation needed an increased number of iterations to achieve convergence, but the cost is still higher than what was found from the global minimum convergence. A theory discussed with Vegard was whether the relative change in cost, from initial to the cost at convergence, influenced the optimization. This hypothesis could neither be confirmed nor disproved. An indication of the relative change in cost affecting the final cost is that the first optimization run used significantly fewer iterations than the proceeding runs, in which the initial cost is already near the minimum value. It seemed as though the closer the initial cost was to the global minimum, the more iterations were needed to achieve convergence, especially for the steel system.

In consideration of the global minimum convergence study, it became clear that different configurations of the steel lines would produce approximately equal costs. This fact implies that there is no absolute minimum for the cost function with only one line configuration for the steel system. The same tendency was also observed for the polyester system, but a more limited minimum area appeared present. The global minimum convergence for the polyester system indicates a clear tendency to increase the polyester segment length in comparison to the chain segment lengths, which was expected, as polyester is clearly cheaper than chain.

During every optimization, the anchor was allowed to relocate. If specific requirements were present with respect to the anchor coordinates, the optimization could be performed with pre- determined global anchor coordinates. In order to enable a change in pretension during the optimization, a static analysis could then be included in the workflow and the static tension in the mooring lines

could be constrained to 10-25% of MBL.

In this optimization formulation the spread of the mooring lines was kept fixed. The relative angle between the mooring lines within one cluster could be introduced as additional variables in the mooring configuration. This aspect was not explored any further as the computation for the optimization would increase with increasing number of variables, and the main object of this optimization is to compare the cost difference between a polyester and steel system.

The verification of the results, included in section 6.4, emphasized the importance of running a time domain simulation with at least ten different realizations. The trend found that in all four optimization cases, for both steel and polyester system, the simulation in the optimization was run with a seed number that resulted in a relatively ”kind” sea state. For each case, the safety factor found from running ten different simulations, with extracted maximum values fitted to the Gumbel distribution, was lower than the safety factors computed in the optimization. It would have been possible to run a condition set inside the optimization instead of one single condition to ensure more correct values for the maximum line tension. But, requiring ten or more simulations at each iteration step to correctly extract the maximum values would require significantly more computation time. This endeavor, however, was not prioritized in this study.

6.6 Experiences with Optimization in SIMA

There were some obstacles encountered when formulating the optimization problem. Firstly, SIMO is not specialized for mooring system analysis in the same way as MIMOSA. It was not possible to visually observe where each segment started and ended, which is possible when plotting in MIMOSA.Moreover, there was no output on the suspended length of the line, i.e. the length which hangs freely in the water. As it was impossible to refer to a starting or ending point of a segment, it was not possible to set restrictions on whether the polyester, or steel wire, segment could interact with the seabed. An explored approach was to consider the mooring line as a triangle. Based on the

length of segment 2 and 3, in conjunction with the top end angle from vertical, the vertical distance $z_{segment2}$ between the fairlead and the bottom end of segment 2 could then be calculated. An introduced constraint could require that $157m$, the water depth, subtracted the vertical distance $z_{segment2}$ should be larger than zero. As the steel lines have a pronounced catenary shape, the simplification to estimate the line as a triangle was quite inaccurate. This idea was therefore rejected.

For shallow water it is common to require no vertical force on the anchor, as the most common anchors used in shallow water mooring only take horizontal forces. In the optimization in SIMO, it was not possible to set such a constraint on the line, namely to require zero vertical force at the line end. Another explored approach concerned whether it was possible to require that a portion of the mooring line should rest on the seabed. This requirement could not be implemented in the optimization problem in any simple way. One possible solution could be to run several analyses in MIMOSA, with different plausible variations of length and diameter of the segments, and then to estimate a global anchor position that would uphold the requirement of no uplift on the anchor. As mentioned, MIMOSA calculates the suspended line length. The optimization in SIMO would then be based on initializing the lines by global anchor coordinates, and the anchor would be restrained to this position, while the diameters and segment lengths would vary relative to one another. This process, however, would have been a very time-consuming task.

Some problems were encountered with the static This aspect was especially an issue when the limit of maximum offset was $16m$. For the cases where the maximum allowable offset was set to $20m$, the optimization finished without any errors, but the number of iterations and the simulation length was reduced the lower steel diameter limit increased. When including an additional constraint in the optimization of the steel system, the computation time further increased. The program calculates both the constraint and cost gradients by dividing the respective function on each of the variables at each iteration step. In this optimization procedure, a total of seven variables were introduced, which led to seven different gradient calculations for each constraint and cost function. For this reason, it is clear that the computation time increases with an increasing number of constraints.

The theory manual for the optimization is very mathematical and not always easy to understand. The parameter named ”Desired final accuracy” was especially difficult to comprehend. The way that this parameter affects the resulting cost and mooring line configuration was discussed with Vegard Aksnes, but no obvious explanation was unveiled. It was especially discussed with respect to the observations from the global minimum convergence, where new solutions were found by running sequential optimization runs. By in-depth studying of the NLPQL algorithm and the mathematics behind it, one can possibly correctly interpret this parameter.

The formulation of the optimization problem in SIMA was relatively simple once it became clear how to correctly include the different constraints. The optimization tutorial available in SIMA was quite helpful in the start phases of formulating the optimization problem.

Chapter 7

Case Study 3: Comparative Study

In this chapter the results in terms of vessel motion and line tension from SIMO, MIMOSA and Riflex are presented and compared.

7.1 Method

As explained in section 4.4.2, SIMO calculates the line tension quasi-static, which means that important dynamic effects such as drag and inertia forces on the lines are neglected. In MIMOSA, the vessel motions are calculated in the frequency domain and the user is able to specify whether to calculate the tension quasi-static or through finite element analysis. Riflex calculates the tension using a finite element model in the time domain. In this comparison analysis motions from SIMO were applied to the top end of the line in SIMO as forced motions.

In MIMOSA, the mooring system configuration and vessel description can be read from a separate file. The same files can be read by SIMO, and the vessel properties and mooring system configuration can be modeled from these files. In Riflex the mooring lines are modeled by finite elements, i.e. made up from nodes and elements, which can be modeled directly in the SIMA interface, or be converted from a SIMO model. In this case, line 7 is converted from a SIMO model to a Riflex task. The line is then connected through a supernode to a fictive vessel. The vessel itself is not modeled, but referred to as a box with motions. The vessel motions are imported from a SIMO simulation. This concept is explained in section 2.3.2, and is referred to as an uncoupled time domain analysis.

The systems considered in this comparative study are those obtained in section 6.3.3, which are found by global minimum convergence. Both the polyester and steel mooring system are evaluated. The restrictions on these systems are specified in the optimization as a maximum allowable offset of 20.0m and a minimum safety factor on line tension of 1.5.

Table 7.1 lists the configuration of both the polyester and the steel lines, whereby all lines in the respective system are identical, and Figures 7.1.a and 7.1.b illustrate a vertical projection of the two mooring systems.

	$\boldsymbol{d_1}$ $[m]$	$\boldsymbol{d_2}$ $[m]$	$\boldsymbol{d_3}$ $[m]$	$\boldsymbol{l_1}$ $[m]$	$\boldsymbol{l_2}$ $[m]$	$\boldsymbol{l_3}$ $[m]$	$\boldsymbol{MBL}$ $[kN]$	$\boldsymbol{Pretension}$ $[kN]$
Polyester	0.076	0.126	0.076	150.0	336.1	50.0	4724.7	472.5
Steel	0.079	0.085	0.077	330.9	156.3	87.4	6188.2	644.4

Table 7.1: Mooring line composition of mooring systems obtained by global minimun convergence

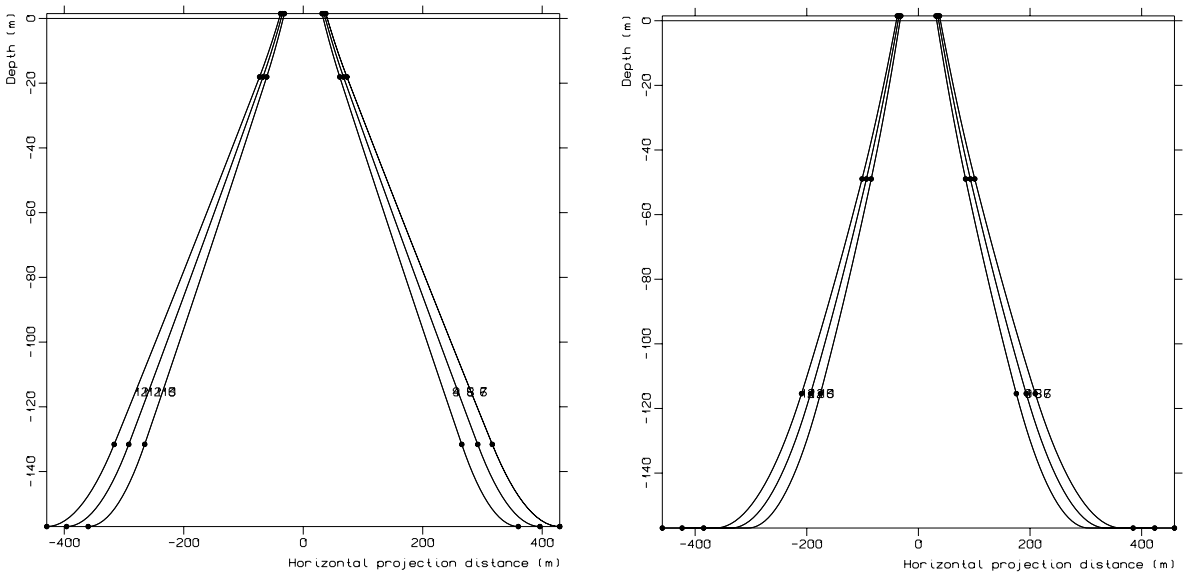

7.1.a Polyester system

7.1.b Steel system

Figure 7.1: Vertical projection of mooring systems

For both the steel and polyester system, one single line is modeled and analyzed in Riflex; line 7. The attachment point to the vessel is defined through a supernode, fairlead 7, with coordinates listed in Table 7.2. The coordinates is defined with respect to the global coordinate system used in SIMO, which is provided in Section 5.2.1 in Figure 5.3, with the origin of the coordinate system coinciding with the vessel origin.

	$\boldsymbol{x}$ $[m]$	$\boldsymbol{y}$ $[m]$	$\boldsymbol{z}$ $[m]$
Fairlead supernode	-37.8	31.7	1.5

Table 7.2: Coordinates fairlead 7

The modeling of the steel and polyester line is presented in Figures 7.2 and 7.5, respectively. The static configuration of line 7, where the weight of the line is taken into account, is presented in Figures 7.3 and 7.6 for the steel and polyester system respectively.

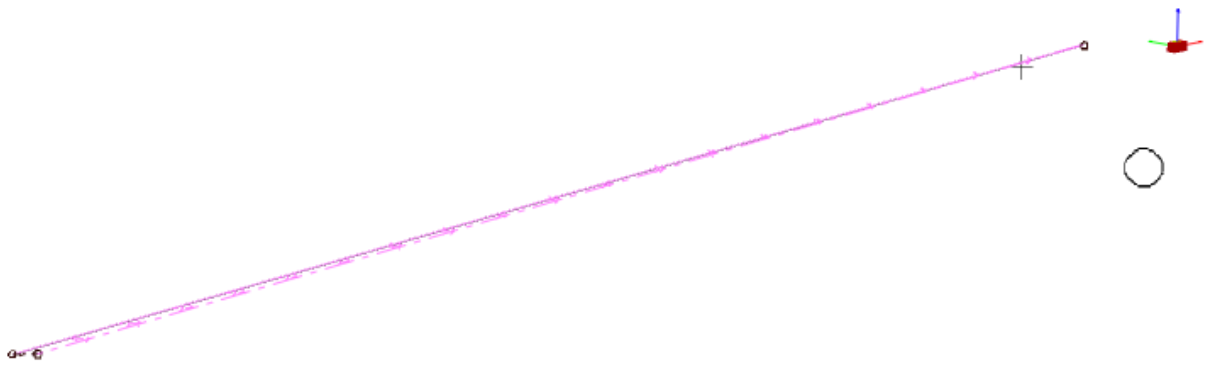

Figure 7.2: FEM model of line 7 for the steel system

The small box with the coordinate system is the origin of the semi, enhanced in Figure 7.4. The red arrow represent global x-direction, the green arrow represent global y-direction and the blue arrow represent the global z-direction.

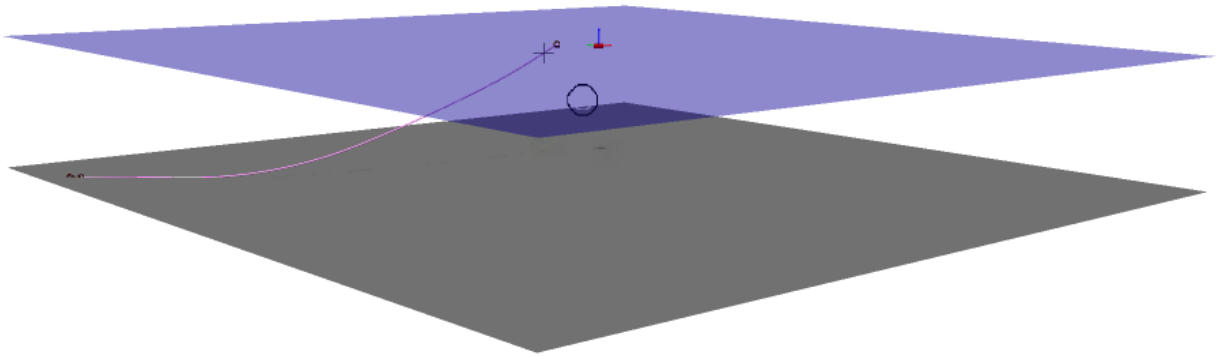

Figure 7.3: Static line configuration of line 7 for the steel system

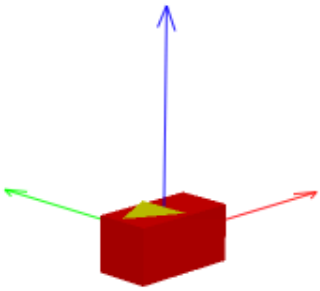

Figure 7.4: Global coordinate system in Riflex and SIMO

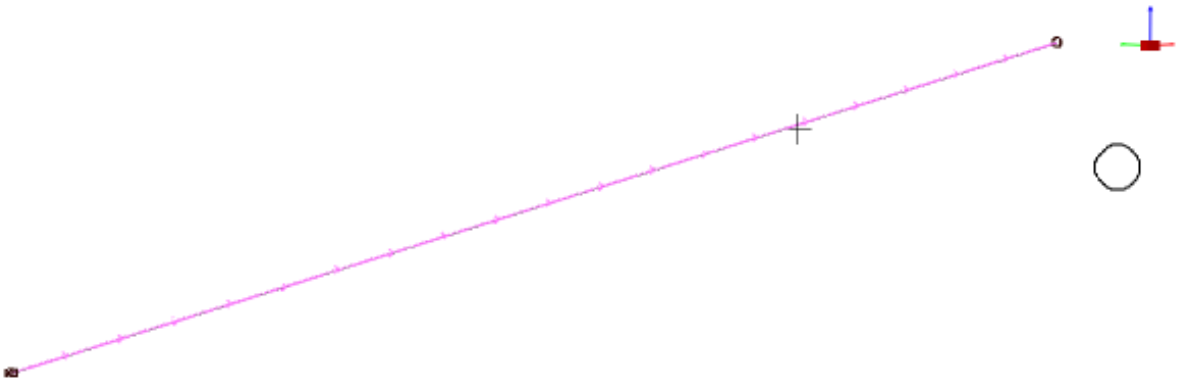

Figure 7.5: FEM model of line 7 for the polyester system

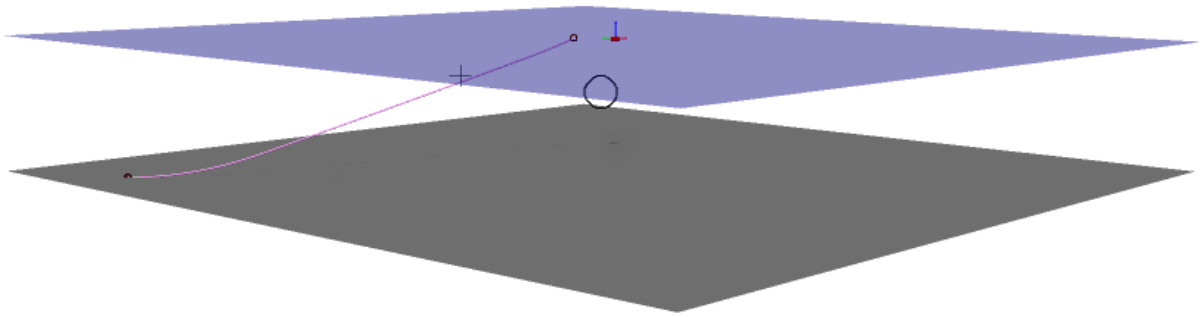

Figure 7.6: Static line configuration of 7 for the polyester system

7.2 Results

The time series of motion and line tension are based on a 12000s simulation, in which the first 1200s are omitted to avoid any transient results. The results from SIMO and Riflex are given for three different seed numbers in order to confirm that observations made in the results from one seed number correspond to those from the two other seed numbers. The notation #1-3 in the following four tables refer to runs with different seed numbers. The same seed numbers are utilized in both the SIMO and Riflex analysis. The notation ”-” in the tables implies that these values are not calculated in the respective analysis tool.

Tables 7.3 and 7.4 present the resulting motions, or offsets, in surge x and heave z for the polyester and steel system, respectively.

The sway motion is not included since the horizontal translation occurs mainly along the x-axis, i.e. in surge. In both tables x_{mean} and z_{mean} are directly found from the generated time series, whereas $\bar{x}$ is the static offset. Static offset implies the offset caused by static wind, wave and current forces, and is only calculated in SIMO and MIMOSA. One should be aware when studying these results that SIMO calculates the motions at the vessel origin, whereas the motions from Riflex are simulated at fairlead 7, due to the modeling of the mooring line. The motions calculated by MIMOSA

	$\bar{\boldsymbol{x}}\ [m]$	$\boldsymbol{x_{mean}}\ [m]$	$\boldsymbol{x^{tot}}\ [m]$		$\boldsymbol{z_{mean}}\ [m]$	$\boldsymbol{z^{tot}}\ [m]$	
			σ	max		σ	max
SIMO #1	5.35	4.78	3.53	15.57	0.34	3.56	13.08
SIMO #2	5.35	4.74	3.62	17.12	0.34	3.67	14.56
SIMO #3	5.35	4.80	3.43	14.65	0.34	3.44	13.12
Riflex #1	-	5.14	3.59	16.34	-2.47	3.54	11.56
Riflex #2	-	5.11	3.67	17.59	-2.46	3.65	10.51
Riflex #3	-	5.16	3.49	15.23	-2.46	3.44	8.88
MIMOSA a)	4.89	-	-	17.93	-	3.27	12.24*
MIMOSA b)	4.89	-	-	18.04	-	3.09	11.60*

Table 7.3: Polyester system - offsets and standard deviation in surge and heave
a) Motions calculated at vessel origin
b) Motions calculated at fairlead 7
*) Only WF motion

are given at a) the vessel origin and b) the coordinates of fairlead 7.

	$\bar{\boldsymbol{x}}\ [m]$	$\boldsymbol{x_{mean}}\ [m]$	$\boldsymbol{x^{tot}}\ [m]$		$\boldsymbol{z_{mean}}\ [m]$	$\boldsymbol{z^{tot}}\ [m]$	
			σ	max		σ	max
SIMO #1	9.49	9.01	3.43	20.01	-0.01	3.47	12.75
SIMO #2	9.49	9.03	3.57	20.84	-0.01	3.59	14.30
SIMO #3	9.49	9.07	3.37	19.06	-0.01	3.40	12.92
Riflex #1	-	9.43	3.53	20.81	-2.97	3.37	11.08
Riflex #2	-	9.38	3.63	21.66	-2.96	3.47	9.52
Riflex #3	-	9.43	3.45	19.94	-2.97	3.27	8.13
MIMOSA a)	9.56	-	-	23.84	-	3.27	12.24*
MIMOSA b)	9.56	-	-	23.98	-	3.09	11.60*

Table 7.4: Steel system - offsets and standard deviation in surge and heave
a) Motions calculated at vessel origin
b) Motions calculated at fairlead 7
*) Only WF motion

It should be noted that the maximum total heave offset $\boldsymbol{z^{tot}_{max}}$ from SIMO and Riflex is taken di-

rectly from the time series with a mean specified in the table. The same value from MIMOSA is the amplitude given based on the vessel WF motions. As z_{mean} from SIMO is close to zero, the values from SIMO and MIMOSA may be directly compared. In a comparison of the results from Riflex and MIMOSA, the magnitude of the mean value z_{mean} from Riflex should be added to the total offset z_{max}^{tot} to correctly compare the amplitudes. As the motions provided from SIMO is taken at the vessel origin, these values should be compared to the MIMOSA a) results. The motions from Riflex are taken at fairlead 7 and should therefore be compared to the motions given in MIMOSA b).

Firstly, there is a noteworthy observation in the relatively large differences in mean heave motion from SIMO and Riflex. The difference may be explained based on the difference in location in which the motions are simulated. As previously stated, Riflex provides the results at fairlead 7, whereas SIMO calculates the motions at the vessel origin. Consequently, the heave motion from Riflex is to a higher degree influenced by coupling effects, for instance the coupling between heave and pitch, than the heave motion from SIMO. The equation to calculate the motion at any point on the vessel is given in Eq. (2.1) in section 2.1. To study this phenomena further, a new mooring line, of the steel system only, is modeled in Riflex. The coordinates of fairlead 7 are changed to the origin of the vessel and the global coordinates of the anchor are accordingly modified. Figure 7.7 presents a window of the generated time series of heave motion with both initial and modified coordinates of fairlead 7 in both SIMO and Riflex, for the steel system.

The deviation in mean offset observed in Figure 7.7.a may arise from the static forces. The static wind, wave and current forces causes a static rotation about the y-axis, i.e. a static pitch moment, resulting in a negative static offset along the z-axis of fairlead 7. By changing the coordinates of the fairlead, this mean offset was thus removed. As depicted in Figure 7.7.b, the heave motion from SIMO and Riflex is identical, which is expected when applying the motions calculated in SIMO as forced motions of the fictive vessel in Riflex.

As evident from the results in 7.3 and 7.4, a small deviation in surge motion is also present. A

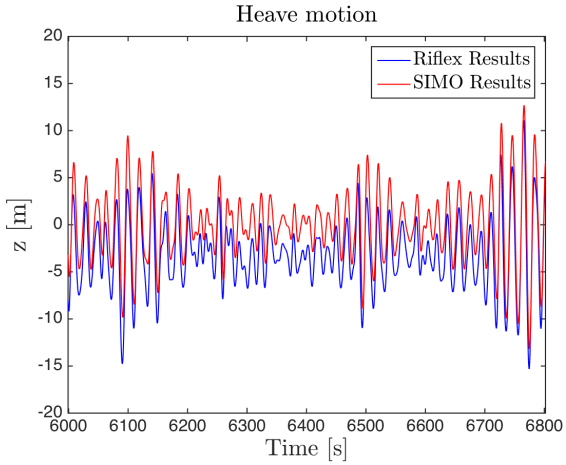

7.7.a Fairlead 7 at inital coordinates

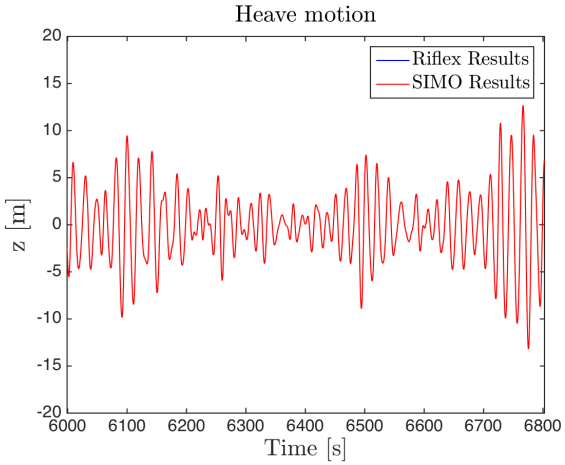

7.7.b Fairlead 7 at vessel origin

Figure 7.7: Comparison of heave motion simulated in Riflex and SIMO for seed #1 - steel system

comparison of the resulting surge motion from Riflex and SIMO with both the initial and modified coordinates of fairlead 7 is illustrated in Figure 7.8.

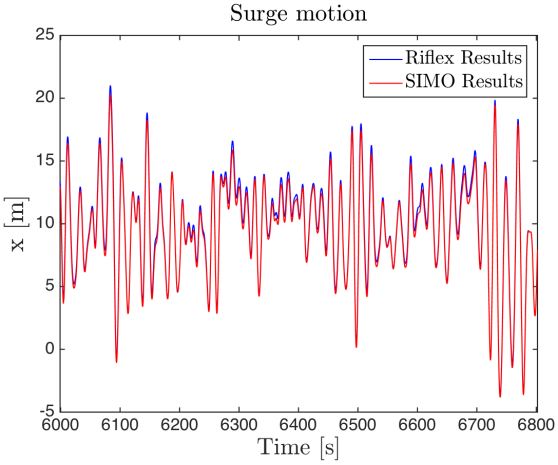

7.8.a Fairlead 7 at inital coordinates

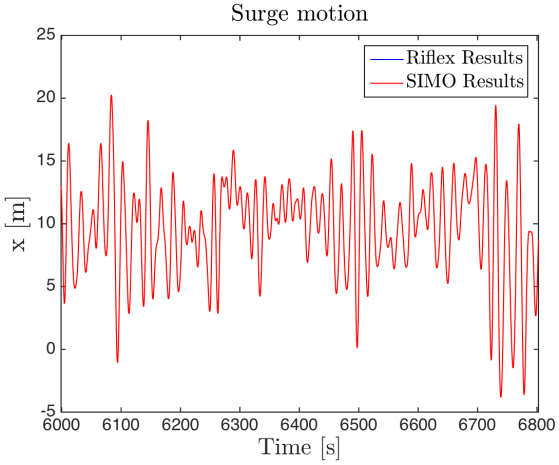

7.8.b Fairlead 7 at vessel origin

Figure 7.8: Comparison of surge motion simulated in Riflex and SIMO for seed #1 - steel system

The same trend observed for the heave motion is apparent in both Figures 7.8.a and 7.8.b. The deviation, however, is much smaller, which may indicate a significantly smaller effect of coupled motions in surge at fairlead 7.

From Tables 7.3 and 7.4, it is clear that different seed numbers produce different results relative to one another. In terms of standard deviation $\sigma_{x^{tot}}$ and maximum value x^{tot}_{max} of the horizontal motion, seed #3 yields the lowest results, whereas seed #2 yields the highest values of the three. This trend can be observed for the results obtained from SIMO and Riflex, for both the polyester and steel system. There are relatively small deviations between the mean horizontal offsets x_{mean} for different seed numbers in both tables. The same trends are noticed for the heave motion and its standard deviation in the SIMO results. The small difference in maximum heave offset from SIMO between Tables 7.3 and 7.4 mainly results from the minor difference in mean heave offset.

In consideration of the heave motion results from Riflex, the mean varies almost does not vary, and the standard deviation follows the trend whereby the lowest value is observed for seed #3 and the highest for seed # 2. The same pattern, however, cannot be observed in the maximum values z^{max}_{tot}. This finding is discussed further in the proceeding section.

The resulting line tension in mooring line 7 for polyester and steel system is presented in Table 7.5 and Table 7.6, respectively. The breaking strength for the polyester system is $4724.7kN$, and the safety factor specified in Table 7.5 is calculated based on this value. The calculated safety factor for the steel system, listed in Table 7.6, is calculated based on a breaking strength of $6188.2kN$.

The tension in line 7 for the polyester system, provided in Table 7.5, indicates that the tension computed by SIMO correspond well to the tension calculated in Riflex. There is a slight difference in both the mean tension T_{mean} and the maximum tension T_{max} which is further studied in section 7.3. The tension calculated quasi-statically by MIMOSA corresponds to the tension calculated from Riflex at seed #2, and is near the one computed by SIMO for the same seed. It is, however, higher than the tension from both SIMO and Riflex for the other seed numbers. The tension calculated by FEM in MIMOSA is even higher. The next section discusses possible explanations for this finding.

	$\boldsymbol{T_{stat}}$ $[kN]$	$\boldsymbol{T_{mean}}$ $[kN]$	$\boldsymbol{T_{max}}$ $[kN]$	$\boldsymbol{sf}$ $[-]$
SIMO #1	910.0	951.0	3152.0	1.50
SIMO #2	910.0	952.2	3510.0	1.35
SIMO #3	910.0	945.6	3149.0	1.50
Riflex #1	-	919.1	3178.0	1.49
Riflex #2	-	921.1	3541.0	1.33
Riflex #3	-	912.4	3182.0	1.49
MIMOSA Q-S	944.1	-	3545.3	1.33
MIMOSA FEM	944.1	-	3739.3	1.26

Table 7.5: Polyester system - Tension in heaviest loaded line; line 7

	$\boldsymbol{T_{stat}}$ $[kN]$	$\boldsymbol{T_{mean}}$ $[kN]$	$\boldsymbol{T_{max}}$ $[kN]$	$\boldsymbol{sf}$ $[-]$
SIMO #1	995.8	1032.0	4129.0	1.50
SIMO #2	995.8	1034.0	4548.0	1.36
SIMO #3	995.8	1031.0	3653.0	1.69
Riflex #1	-	1031.0	5214.0	1.19
Riflex #2	-	1033.0	5975.0	1.04
Riflex #3	-	1022.0	4965.0	1.25
MIMOSA Q-S	1061.8	-	6821.0	0.91
MIMOSA FEM	1061.8	-	8290.6	0.75

Table 7.6: Steel system - Tension in heaviest loaded line; line 7

Table 7.6 presents the results in terms of tension in line 7 for the steel system. The results from SIMO and Riflex differ to a significantly greater extent than what observed for the polyester system. A higher maximum tension T_{max} is computed by Riflex, whereas the mean tension T_{mean} has smaller differences. The same observation made for the polyester system is noticed in the steel system, i.e. the maximum tension calculated by FEM in MIMOSA yields the highest line tension of all methods. This tension is about twice the magnitude of the tension found from the SIMO computation and about 24% larger than the tension calculated in Riflex. The proceeding section also assesses this difference.

7.3 Discussion

In consideration of the surge and heave motion of the vessel from SIMO and Riflex, the previous section established that a difference arose from the motions being simulated at different positions on the vessel. When fairlead 7 was localized at the vessel origin, the motions from SIMO and Riflex became identical.

For both the polyester and the steel system, a higher horizontal maximum offset was found from the MIMOSA analysis. A similar phenomenon was encountered in Case Study 2 in section 6.4, whereby the results from the optimization were verified by running several time domain realizations. The total motion was lower than expected when the static, WF and LF response from SIMO were separately considered. As the mooring systems considered in this comparative analysis are almost identical to the steel and polyester system evaluated in the mentioned verification, the underlying arguments will be the same. The investigated hypothesis was that the LF and WF motions are, to a certain extent, out of phase. By plotting the time history for the same seed number, referred to here as seed #1, it was observed that when the maximum WF motion occurs, the LF response was negative. This finding is illustrated in section 6.4 in Figure 6.27. This aspect then resulted in a lower total maximum response than expected. One would expect that if the second order wave

drift force had a strong influence on the LF response, the maximum WF and LF would occur at the same time instant as the two time series are generated from the same wave realization. As explained in Case Study 1 in section 5.3, the main contribution to the LF response is the slowly varying wind excitation, and the maximum LF and WF motion may not occur at the same time. The total response spectrum for both polyester and steel system is presented in Figure 7.9.

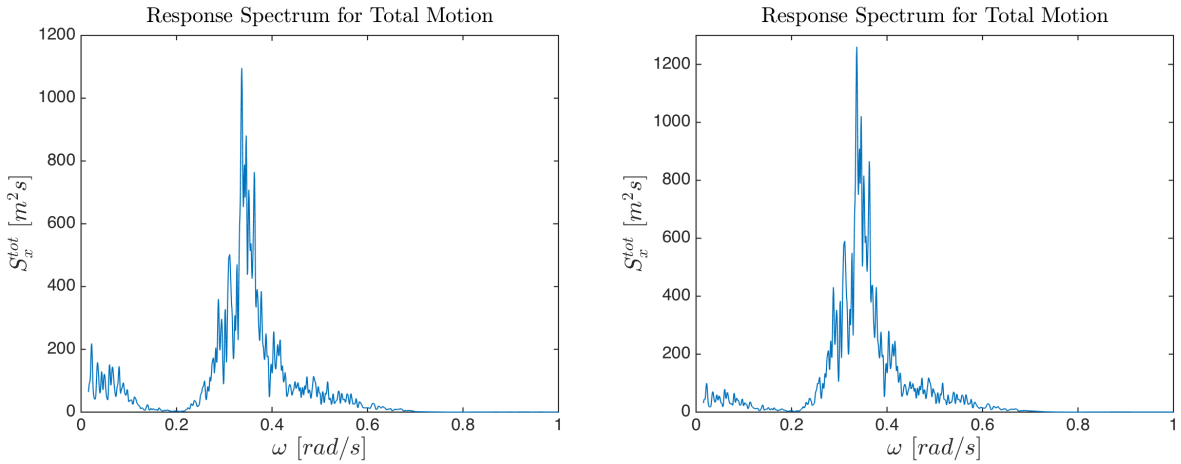

7.9.a Response spectrum - steel system

7.9.b Response spectrum - polyester system

Figure 7.9: Total response spectra

It is noticed from both spectra that the WF response is the governing response in both systems. By comparing Figures 7.9.a and 7.9.b a larger LF response is depicted for the steel system than for the polyester system. When considering the restoring curves for both polyester and steel system, in Figure 7.10.a and 7.10.b respectively, the polyester system appears stiffer within the offset range of interest; up to approximately $20m$. The LF response is thus limited, while the WF response is quite similar for both cases as this response is not generally influenced by the mooring system.

As stated previously, MIMOSA uses the combination rule given in Eq. (7.1) to estimate the maximum vessel response.

$$x_{max}^{tot} = max \begin{cases} \bar{x} + x_{max}^{LF} + x_{sign}^{WF} \\ \bar{x} + x_{max}^{WF} + x_{sign}^{LF} \end{cases} \tag{7.1}$$

This estimation does not account for the correlation between the LF and WF response which leads the estimate to be relatively conservative. To simplify this claim, MIMOSA does not account for the possibility of having a negative LF response at the time when the maximum WF response occurs. Additionally, the method used in MIMOSA to calculate the linearized stiffness and damping matrix is expected to introduce some conservatism in the LF response (Kaasen et al., 2012), and then consequently the total response. From Case Study 1, the most probable largest offset found by MIMOSA corresponded well with the one from SIMO. The restoring curve was almost linear for the steel lines, and the procedure of linearizing the stiffness may not introduce too large errors. As the restoring curve for the steel system considered in this chapter is very nonlinear, the errors from linearizing the stiffness may be too inaccurate. In addition, a frequency domain analysis do not discriminate between a symmetric or slightly skewed response (Fylling, 1980). For both the polyester and the steel system a lower mean offset is found from the time series compared to the static offset. This indicates a negatively skewed process, which is also found when considering the skewness coefficient provided as output from a post-processor in SIMO. According to Leira (2014), a negatively skewed response will result in lower positive extreme values compared to a symmetric response. The maximum offset in positive x-direction will thus be reduced as a result of the negative skewness of the response, while the motion amplitudes are larger in negative global x-direction.

The difference in static offset in surge between SIMO and MIMOSA observed in Tables 7.3 and 7.4 may result from the difference in static tension found in Tables 7.5 and 7.6. The difference in static tension is approximately equal for both the steel and the polyester system, but the difference in static offset is larger for the polyester system. Figure 7.10 presents the restoring curve for both the polyester and steel system to investigate this difference.

As evident from Figure 7.10.a, the restoring curve for polyester is steeper than the restoring curve

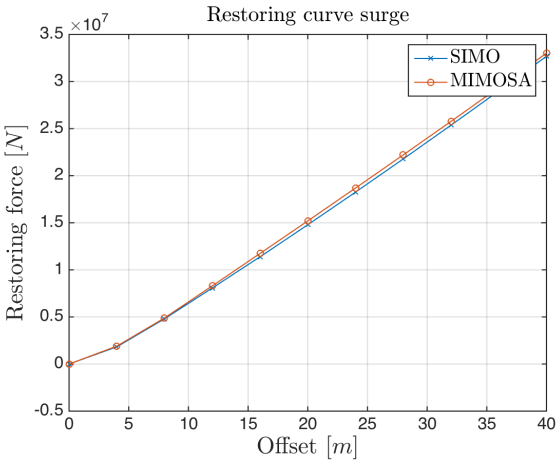

7.10.a Polyester system

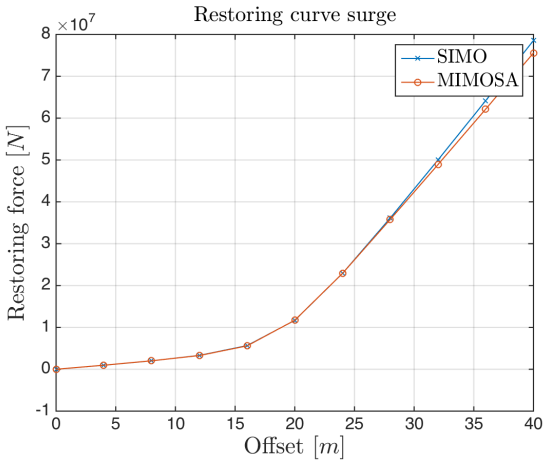

7.10.b Steel system

Figure 7.10: Restoring curves

for steel from Figure 7.10.b for offsets below approximately $20m$. Thus, a small difference in static tension may lead to a larger difference in offset for the polyester system, in comparison to how a small difference in tension affects the static offset for the steel system. The restoring force in the steel system increases only slightly for offsets up to $10m$.

The heave motions simulated at the initial coordinates of fairlead 7 in Riflex do not show the same trend with respect to magnitude variation for each seed number in comparison to heave motions from SIMO. The heave response should mainly be excited by the WF excitation, and consequently be approximately Gaussian distributed. For a Gaussian process the expression $x_{max}^{WF} = \sigma_{x^{WF}}\sqrt{2ln(N)}$ should be valid. For a three hour sea state simulation this expression becomes approximately $x_{max}^{WF} \approx 3.8\sigma_{x^{WF}}$. By dividing the maximum amplitude in heave, the difference between the maximum value and the mean offset, by the standard deviation for each seed number from Table 7.4, the results provided in Eq. (7.2), (7.3) and (7.4) are reached.

$$Seed\ \#1: \frac{z_{max}}{\sigma_z} \simeq 4.17 \tag{7.2}$$

$$Seed\ \#2: \frac{z_{max}}{\sigma_z} \simeq 3.60 \tag{7.3}$$

$$Seed\ \#3: \ \frac{z_{max}}{\sigma_z} \ \simeq \ 3.39 \tag{7.4}$$

From the above expressions, it can be observed that the values are within an acceptable range around the expected value ≈3.8 for a Gaussian process. The deviations may be due to the variability in each time domain simulation; the extracted maximum values from each time domain realization appear slightly above or below the most probable largest value. From Leira (2014) another parameter defining whether a process is Gaussian distributed is the skewness coefficient. The skewness coefficient provides an indication of the asymmetry in the response. This value should be zero for a Gaussian process. The skewness coefficient estimated from the statistics of the heave motion time series, which is found from the post-processor in SIMO, is approximately zero. This aspect strengthens the argument of a Gaussian distributed heave response. The symmetry could also be observed directly from the time series presented in Figure 7.7.

The heave motion in MIMOSA is calculated directly from the RAOs of the vessel without considering the mooring lines, as they do not significantly influence the WF response. In SIMO and Riflex, the heave motion is simulated with different sea state realizations. This discrepancy may lead to the deviations in maximum offset observed in Tables 7.3 and 7.4. In addition, the heave motion at fairlead 7 found from Riflex indicates a strong dependence on the pitch motion. This heave motion is thus influenced by different realizations of the heave motion itself as well as the pitch motion. This contribution may explain the somewhat strange variation in maximum heave offset provided from Riflex.

The tension in line 7 for the polyester system given in Table 7.5 indicates a slightly lower mean from Riflex for the polyester system, and a slightly higher maximum value, in comparison to the results from SIMO. This difference may be explained by the effect of inertia and drag on the lines. To compare the tension from SIMO and Riflex, a window of the time history for seed #1 is presented in Figure 7.11.

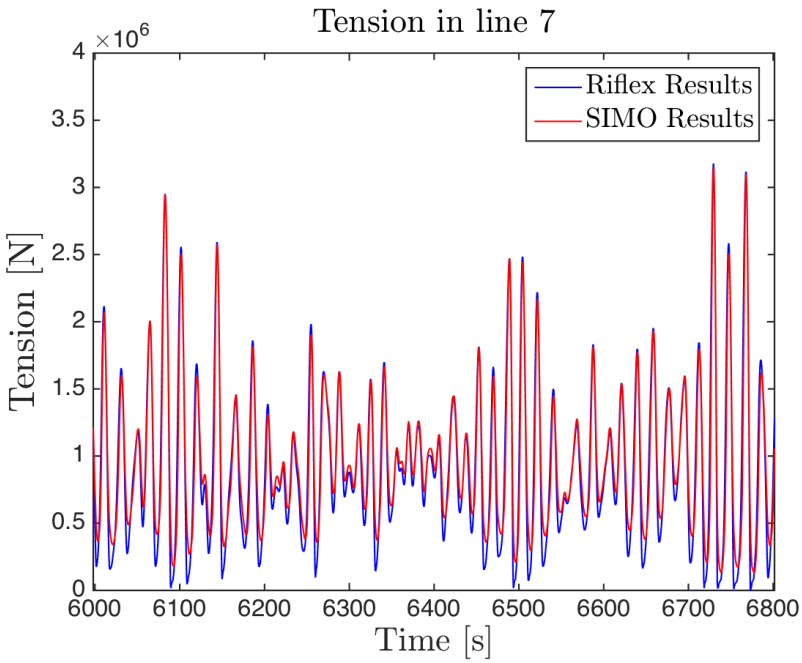

Figure 7.11: Window from the time history of the tension in line 7 - polyester system

From the figure above it can be observed that the peaks, the maximum values, are of approximately equal magnitude with only some minor deviations. The deviation in minimum values are thus larger, which leads to the difference in mean tension observed from Table 7.5. The minimum values calculated by Riflex is very close to zero. This may be due to the inertia of the line. There is a part of the suspended line that consists of chain segments, and the tension from Riflex is calculated at the upper element in the upper chain segment. When the vessel shifts from a positive to a negative acceleration the inertia in the line caused by the presence of the chain may result in nearly zero tension in the line.

The maximum tension found by quasi-static calculation in SIMO correspond well to the dynamic tension calculated in Riflex. The verification of optimization results in section 6.4 implied that the seed number used in the optimization, same as seed #1 here, provided a relatively ”kind” sea state. By running ten different sea state realizations, the maximum tension resulted in a safety factor slightly below 1.5. Keeping this in mind, the maximum tension found from seed #2 may be the most realistic extreme value. T_{max} for seed #2 from SIMO and Riflex correspond well to the

estimated maximum from a quasi-static MIMOSA analysis. The small deviation is probably due to the difference in maximum offset. The maximum tension provided by a FEM analysis in MIMOSA is slightly higher, most likely due to the correction implemented when calculating the extreme WF tension in MIMOSA attempting to capture nonlinear dynamic effects in the mooring line, which might be inaccurate.

Significantly larger deviations between the maximum line tension computed by SIMO and Riflex are noticed for the steel system in comparison to the polyester system. Figure 7.12 presents a graphical illustration of the line tension from SIMO and Riflex for the steel system.

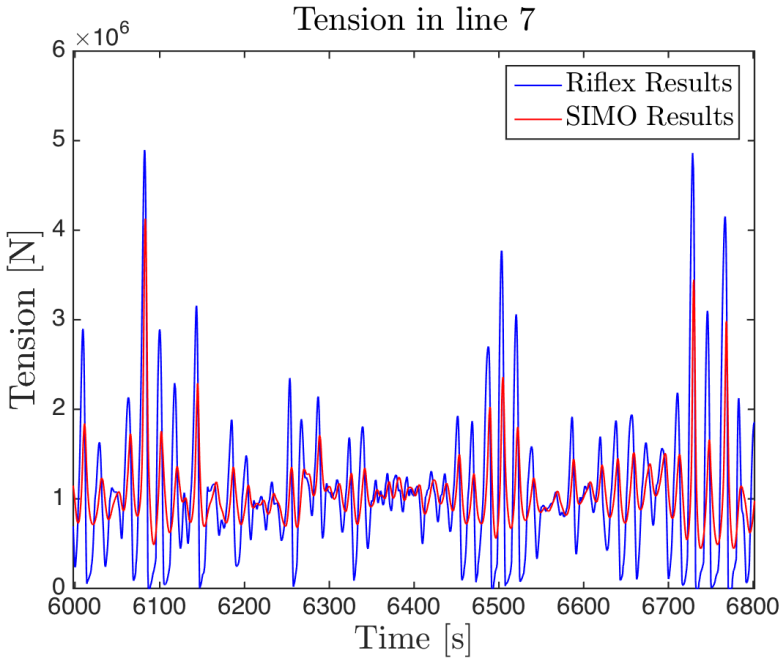

Figure 7.12: Window from the time history of the tension in line 7 - steel system

Both larger positive and negative amplitudes are noticed in line tension computed by Riflex, which results in a relatively similar mean tension as found from SIMO. The quasi-static method for computing line tension in SIMO is based directly on the non-linear line characteristics and is therefore only a function of top end position; $T(x, z)$, whereas the dynamic tension calculated in Riflex depends on top end position, velocity and acceleration; $T(x, z, \dot{x}, \dot{z}, \ddot{x}, \ddot{z})$. As the steel line is much

heavier than the polyester system, the dynamic effects on the system resulting from top end velocity and acceleration, drag and inertia, will be more pronounced for this system. The inertia in the line will strongly affect the line tension when the vessel shifts from positive to negative acceleration, or the other way around. This inertia makes the mooring lines react somewhat slower and gives rise to the large amplitudes observed from the figure.

In the results from Case Study 1, which are provided in section 5.3, a quasi-static method to calculate the line tension in MIMOSA resulted in line tension that corresponded well to the tension calculated in SIMO. This result is not the case for the steel system with this mooring system configuration. The difference in T_{max} for the steel system between MIMOSA Q-S and SIMO arises probably from the large deviation in maximum offset, which is tried explained previously by considering the combination rule utilized in MIMOSA to estimate the maximum offset together with the inaccuracy of linearizing a pronounced nonlinear restoring curve. The maximum tension computed in the MIMOSA FEM analysis is approximately twice the magnitude of the maximum tension calculated in SIMO, and roughly 35% larger than the results from Riflex. This large deviation may partially result from the difference in maximum vessel offset between the programs and partially from the correction factor in MIMOSA attempting to capture the nonlinear behavior of the dynamic cable. The actual response of a moored vessel, and the line tension, is typically better represented in a time domain analysis as all non-linearities are directly accounted for in the simulation. The linearization of damping and restoring terms in MIMOSA introduces simplifications and some inaccuracies. Based on the results in terms of both most probable largest vessel motion and line tension, it appears that MIMOSA overestimates the nonlinear dynamic effects in the mooring system, and the modified method trying to capture the nonlinear dynamics provides too large loads, for this steel system.

It is of interest to determine whether the dynamic amplification factor varies with different seed numbers. The dynamic amplification factor DAF is calculated based in the expression given in Eq. (7.5), and the resulting DAF for the three different seed numbers is listed in Table 7.7.

$$DAF = \frac{T_{max_{Riflex}}}{T_{max_{SIMO}}} [-] \tag{7.5}$$

	Polyester system			Steel system		
	Seed #1	Seed #2	Seed #3	Seed #1	Seed #2	Seed #3
DAF	1.01	1.01	1.01	1.26	1.31	1.36

Table 7.7: DAF for both steel and polyester system

From 7.7 it is clear that the dynamic effects are more pronounced in the steel system. Based on these results, a quasi-static method for calculating mooring line tension seems adequate for polyester systems, where the lines are light and relatively taut, operating in shallow water. For the steel systems, however, the tension should preferably be computed with effects from the line dynamics included, as the dynamic amplification factor for the steel system lies around 1.3. One should also keep in mind that the nonlinear dynamic time domain analyses performed in this chapter, and in this thesis, is based on the decoupled approach and without any current acting directly on the mooring lines. The effects from the mooring line dynamics on the vessel response and the drag from current on the lines are thus not included. The linear damping arising from the presence of mooring lines is included in a simplified manner in the linear damping matrix specified in the vessel properties. As explored in Ormberg and Larsen (1998), a decoupled approach may prove sufficient for mooring systems at relatively shallow water depths, as the dynamic effects from drag becomes more important with increasing water depth.

Chapter 8

Conclusion and Recommendations for Further Work

8.1 Conclusions

The main work performed in this thesis has been to formulate an optimization problem in SIMA, explore the robustness of this optimization and a verification of the optimization by running both time and frequency domain analyses. Additionally, the implementation of Safe Scandinavia from a MIMOSA model to a SIMO model required thorough verification.

To formulate an optimization procedure in the SIMA workbench proved to be a useful step in the initial design phases of a mooring system, but should preferably be used as a first estimate of the design and further design checks should be performed. Some drawbacks with respect to the utilization of SIMO to execute a time domain simulation of the response in the optimization procedure were encountered. These drawbacks include the lack of ability to require no vertical force on the anchor and not being able to refer to neither the starting nor the ending point of each line segment. This resulted in approximate bounds on the length of the middle mooring line segments to avoid interaction between either polyester rope or steel wire and the seabed. This was mainly the issue for the leeward lines, and the optimization would have been easier to formulate is the user was able to refer to each starting and ending point of the line segments, and thus set direct constraints on these points with respect to seabed interaction. The assumption of allowing both vertical and horizontal forces on the anchor may not be valid for shallow water moorings, but was assumed

adequate for the illustrative purpose of how an optimization formulation can be implemented for a mooring system in SIMA.

Several observations are evident from the optimization performed in this thesis. Firstly, it became clear that a polyester system is the most cost efficient in terms of material cost in comparison to a full steel system. The main drawback in the utilization of a polyester lines is the low abrasion resistance, especially in areas with possibilities of mechanical interaction between the mooring lines and other materials. As the optimization is based on a nonlinear time domain analysis in SIMO, whereby the tension in the lines is calculated quasi-statically, the steel lines may be under-designed with respect to maximum allowable tension in the line. Thus, the obtained hardware cost for the steel system may be underestimated.

Secondly, the sensitivity study of the optimization indicated that the formulation tended to be overly sensitive with respect to small environmental changes. With a ten centimeters increase in the significant wave height, the cost for the steel system increased with 15 percent, which seemed unreasonable. Additionally, the line configuration and cost that results after one optimization run was not the most optimum, as a lower cost and different line configuration was achieved by running several optimization procedures after one other, whereby the starting point for the next run was the results obtained after the previous optimization run. Still, the difference between running only one optimization and running several subsequent runs was approximately 12% for the polyester system and 5% for the steel system. The optimization should be utilized only in the initial stages of a mooring system design, and this difference may become less important as other verifications are still needed before the mooring system design is finalized.

Ten different sea state realizations for each optimization case were simulated to verify the optimization results. The most probable largest offsets and tension were found by a fit of the individual maxima from each run to a Gumbel distribution. For all optimization cases, the maximum offset and line tension from the single time domain simulation was lower than the most probable largest

values provided by the Gumbel distribution. The importance of running more than ten sea state realizations is evident, as only one realization with one specific seed number may produce a somewhat ”kind” sea state.

Finally, a comparative study was executed to investigate the differences that arise from a quasi-static method for computing mooring line tension, in comparison to a dynamic method. Additionally, the results from a nonlinear time domain simulation of the vessel response was compared to a frequency domain simulation in which the system was linearized and the nonlinear effects were accounted for through the introduction of certain correction factors. The dynamic effects related to the velocity and acceleration, drag and inertia, of the line influenced the steel lines to a significant higher degree in comparison to the polyester lines. As the polyester lines are relatively taut and light, the dynamic effects from drag and inertia had nearly no influence on the resulting mooring line tension, and a quasi-static calculation method seemed to provide an adequate representation of the tension in the lines. The comparative study highlighted the importance of a dynamic computation of tension in the steel lines. The line tension that resulted from Riflex, which is based on a FEM, was approximately 24% higher than the tension found quasi-statically from SIMO. The response provided from the time domain simulation also deviated from the response found from the frequency domain simulation. As the steel lines produce a nonlinear restoring curve, in conjunction with the relatively high weight of the line and a pronounced catenary shape, the preferred analysis method is a nonlinear time domain analysis, in which the dynamic effects are accounted for in the computation of line tension. The general tendency observed in this thesis was that MIMOSA overestimates the influence of nonlinear dynamic effects on the mooring lines tension, in conjunction with not discriminating between a symmetric or skewed response, but utilizes a correction factor to account for the non-Gaussian response.

8.2 Recommendations for Further Work

Recommendations for future work follows:

- Formulate an optimization problem in SIMA with a condition set within the workflow to enable running a time domain analysis with several sea state realizations at each iteration. This would produce more correct extreme values, most probable largest values, from which the constraint functions are calculated.
- Utilize Riflex in the optimization procedure for calculation of line tension, which appeared to be especially important for a full catenary steel system. This aspect results in a dynamic computation of line tension, and an increase in maximum line tension.
- Explore the possibilities of utilizing a Riflex model of the mooring lines, whereby each node can be referred to and hence be constrained in the optimization formulation. By enable reference to, for instance, the bottom node of segment 2, a possible formulation of no seabed interaction for this node could be studied and maybe introduced as a constraint in the optimization problem. In addition, no vertical force on the anchor could be set as restriction by constraining the anchor node. As Riflex utilizes a FEM analysis, this would require a significant amount of computational time and power. As the optimization is typically utilized in the initial phases of a mooring design, the benefits from the introduction of the above mentioned constraints may become insignificant.
- Run a coupled time domain analysis of the model to consider the effects of interaction between mooring lines and vessel response, and compare the results to the decoupled approach.
- Include current acting directly on the mooring lines to verify if this does not influence a mooring system in shallow water significantly, as found from previous work.

Bibliography

Aksnes, V. and Levold, P. (2013). Multi-program optimization tool. Report.

API (2005). Design and analysis of stationkeeping systems for floating structures. *API Reccomended Practice 2SK*.

Bridon (2013a). Structural systems - bridon spiral strand. Material catalog.

Bridon (2013b). Superline polyester. Material catalog.

Brown, D. T. (2005). Chapter 8 - mooring systems. In Chakrabarti, S. K., editor, *Handbook of Offshore Engineering*, pages 663 – 708. Elsevier, London.

Browne, V. (2015). Mooring analysis for safe scandinavia. Global Maritime.

DNV (2013). Position mooring. *Offshore Standard DNV-OS-E301*.

Eik, K. J. and Nygaard, E. (2004). Heidrun metocean design basis. Statoil Internal.

Faltinsen, O. (1993). *Sea Loads on Ships and Offshore Structures*. Cambridge Ocean Technology Series. Cambridge University Press.

Fontaine, E., Kilner, A., Carra, C., Washington, D., Ma, K., Phadke, A., Laskowski, D., and Kusinski, G. (2014). Industry survey of past failures, pre-emptive replacements and reported degradations for mooring systems of floating production units. In *Offshore Technology Conference*, Texas.

Fylling, I. J. (1980). Analysis of anchoring systems. In *Offshore Marine Operations*, Fagernes. Norwegian Society of Chartered Engineers.

Fylling, I. J. (2003). Optimization of mooring and riser system for deep water floating production systems including fatigue life requirements. In Zhang, J. and Mercier, R., editors, *Deepwater Mooring Systems*, pages 286–299. American Society of Civil Engineers.

Huse, E. (1991). New developments in prediction of mooring system damping. In *Offshore Technology Conference*, pages 291–298, Richardson, TX. The Conference.

ISO (2013). Part 7: Stationkeeping systems for floating offshore structures and mobile offshore units. *International Standard ISO 19901-7*.

Johanning, L., Smith, G. H., and Wolfram, J. (2007). Measurements of static and dynamic mooring line damping and their importance for floating {WEC} devices. *Ocean Engineering*, 34(14–15):1918 – 1934.

Kaasen, K. E., Lie, H., and Moe, K. (2012). *MIMOSA User's Documentation*. MARINTEK, 6.3 - 06 edition.

Larsen, C. M. (2014). *Marin Dynamikk*. Kompendieforlaget.

Larsen, K. (2015). Mooring and station keeping of floating structures [lecture notes]. Retrieved from NTNU's website.

Leira, B. J. (2014). *Stochastic Theory of Sealoads*. Akademika Forlag.

Low, Y. and Langley, R. (2008). A hybrid time/frequency domain approach for efficient coupled analysis of vessel/mooring/riser dynamics. *Ocean Engineering*, 35(5–6):433 – 446.

Ma, K., Duggal, A., Smedley, P., L'Hostis, D., and Shu, H. (2013). A historical review on integrity issues of permanent mooring systems. In *Offshore Technology Conference*, Texas.

MARINTEK (2013). *SIMO - Theory Manual Version 4.0*. MARINTEK, 3 edition.

MARINTEK (2015). *Riflex Theory Manual*. MARINTEK.

Nocedal, J. and Wright, S. J. (2006). *Numerical Optimization*. Springer New York.

Ormberg, H., Fylling, I. J., Larsen, K., and Sødahl, N. (1997). Coupled analysis of vessel motions and mooring and riser system dynamics. In *OMEA 1997*, pages 91–100. American Society of Mechanical Engineers.

Ormberg, H. and Larsen, K. (1998). Coupled analysis of floater motion and mooring dynamics for a turret-moored ship. *Applied Ocean Research*, 20(1–2):55 – 67. Offshore Technology in Focus.

Prosafe (2016a). Picture of safe scandinavia. Webpage. Retrieved April 8, 2016, from `http://www.prosafe.com/safe-scandinavia/category142.html`.

Prosafe (2016b). Safe scandinavia. Webpage. Retrieved May 16, 2016, from `http://www.prosafe.com/getfile.php/Rig%20sheets%20and%20fleet%20list/Safe%20Scandinavia.pdf`.

Ramnas (2016). Ramnas bruk product catalogue. Ramnas Bruk AB website. Retrieved June 7, 2016, from `http://ramnas.com/wp-content/uploads/2012/11/Ramnas-Technical-Broschure.pdf`.

Schittkowski, K. (1986). Nlpql: A fortran subroutine solving constrained nonlinear programming problems. *Annals of Operations Research*, pages 485–500.

Shafieefar, M. and Rezvani, A. (2007). Mooring optimization of floating platforms using a genetic algorithm. *Ocean Engineering*, 34(10):1413 – 1421.

Sjøfartsdirektoratet (2011). Forskrift om posisjonerings- og ankringssystemer på flyttbare innretninger. Webpage. Retrieved May 30, 2016, from `https://lovdata.no/dokument/SF/forskrift/2009-07-10-998`.

Steen, S. (2014). Experimental methods in marine hydrodynamics. Lecture notes.

Triantafyllou, M. S. (1999). Cable dynamics for offshore applications. In Herbich, J. B., editor, *Developments in Offshore Engineering - Wave Phenomena and Offshore Topics*, pages 257–283. Elsevier.

Wang, L. (2010). Coupled analysis of deepwater floating systems. [Power point presentation].

Yang, X.-S. (2011). *Computational Optimization, Methods and Algorithms*, chapter Optimization Algorithms, pages 13–31. Springer Berlin Heidelberg, Berlin, Heidelberg.

Zhang, S.-x., Tang, Y.-g., and Liu, X.-j. (2012). Experimental investigation of nonlinear dynamic tension in mooring lines. *Journal of Marine Science and Technology*, 17(2):181–186.

Appendix A

Vessel Description

A.1 RAO Plots

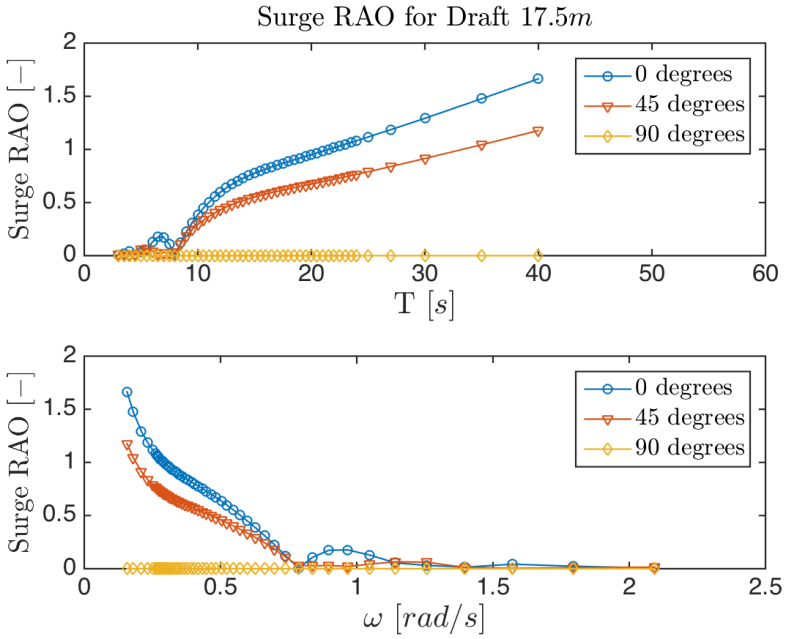

RAO in surge plotted against period and frequency, respectively

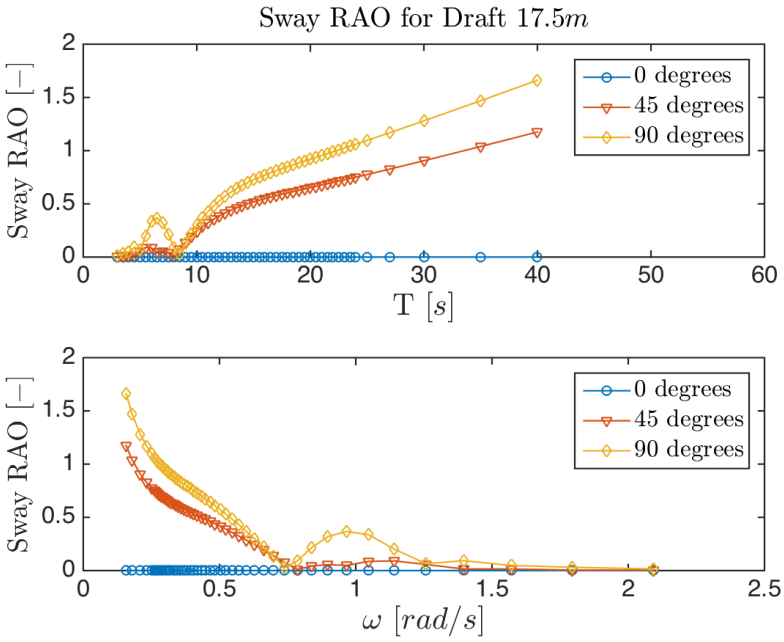

RAO in sway plotted against period and frequency, respectively

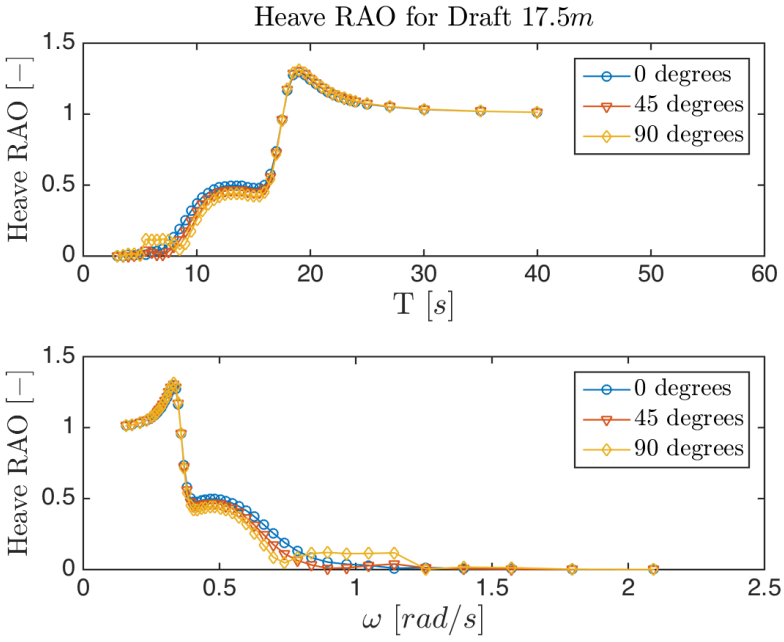

RAO in heave plotted against period and frequency, respectively

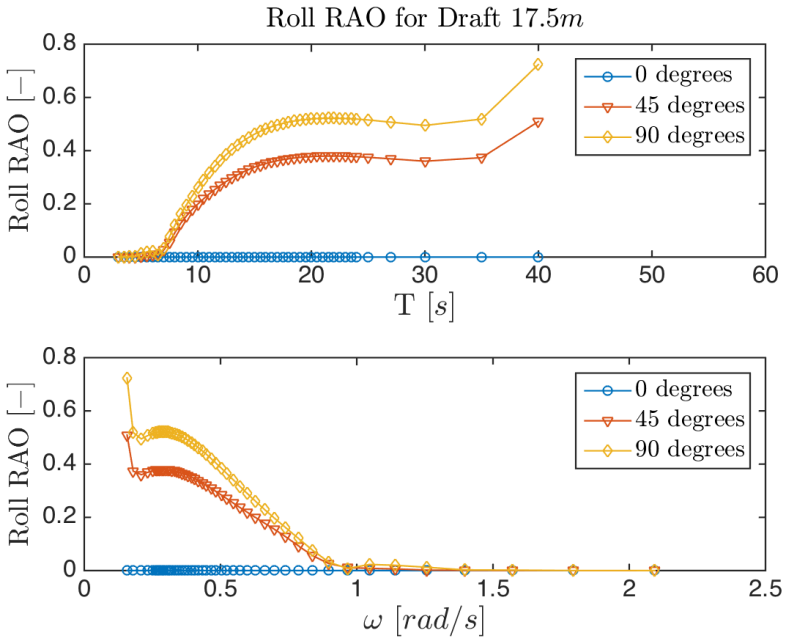

RAO in roll plotted against period and frequency, respectively

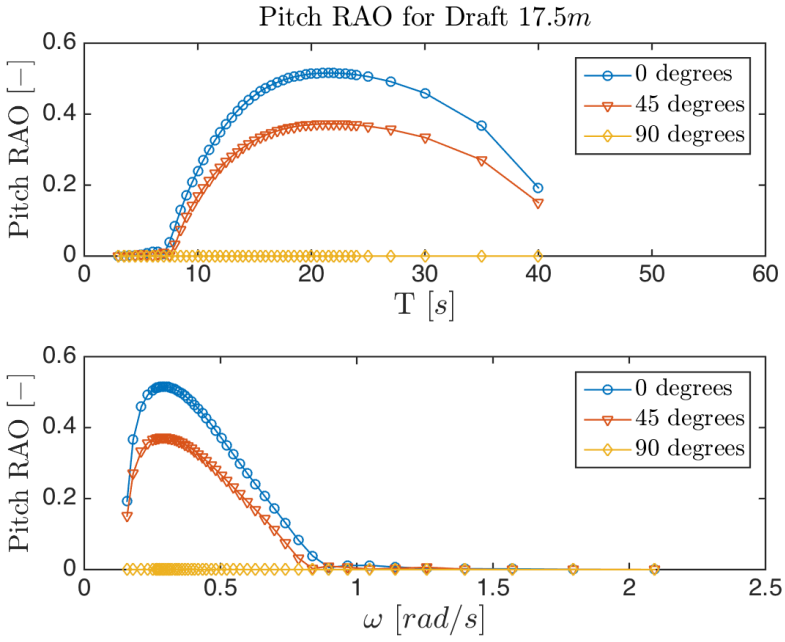

RAO in pitch plotted against period and frequency, respectively

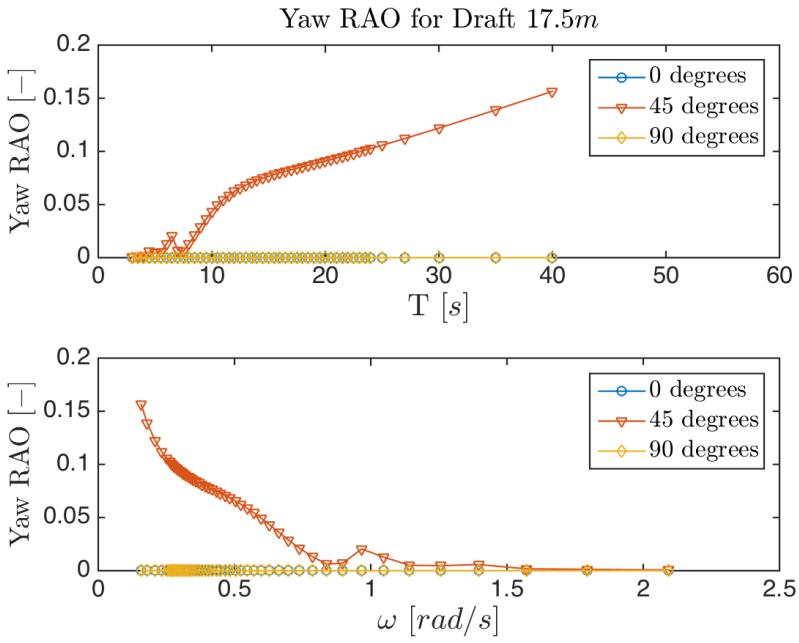

RAO in yaw plotted against period and frequency, respectively

A.2 Wave Drift Coefficients

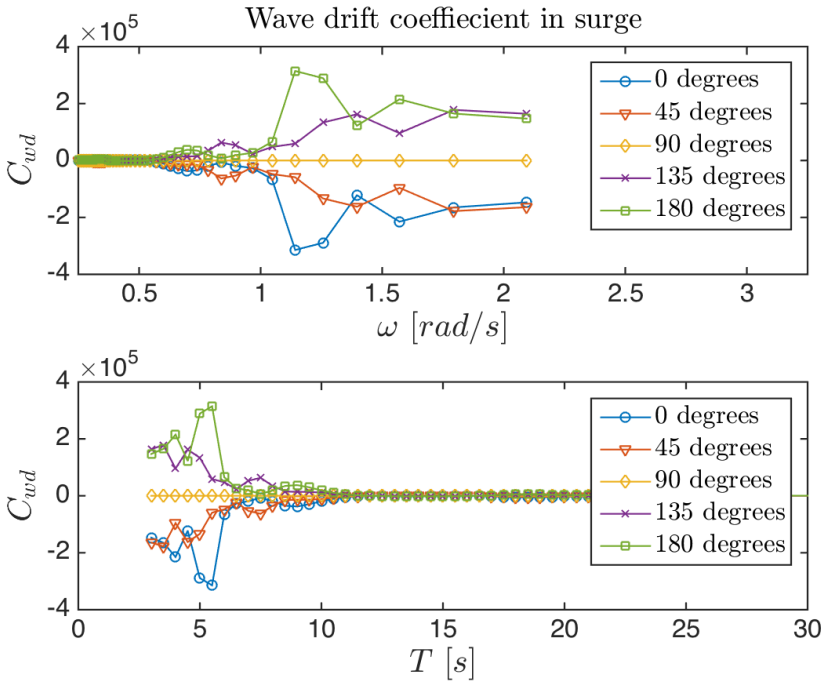

Wave drift coefficient in surge plotted against frequency and period, respectively

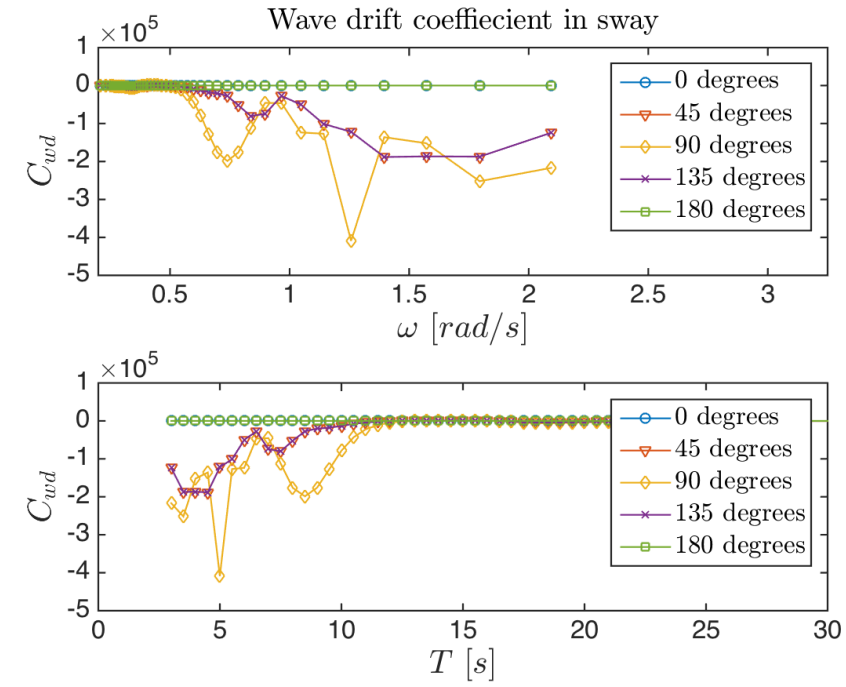

Wave drift coefficient in sway plotted against frequency and period, respectively

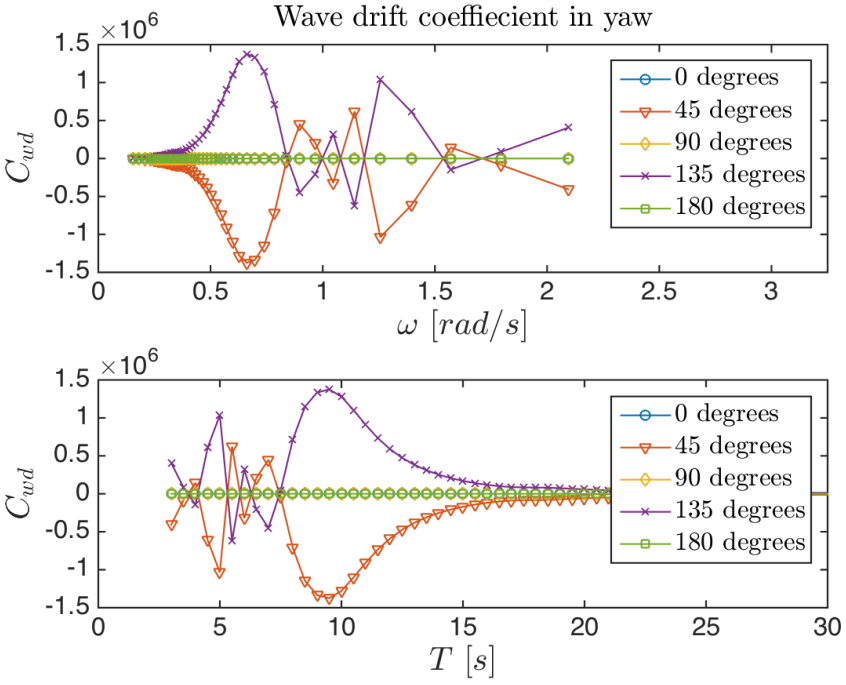

Wave drift coefficient in yaw plotted against frequency and period, respectively

A.3 Current and Wind Force Coefficients

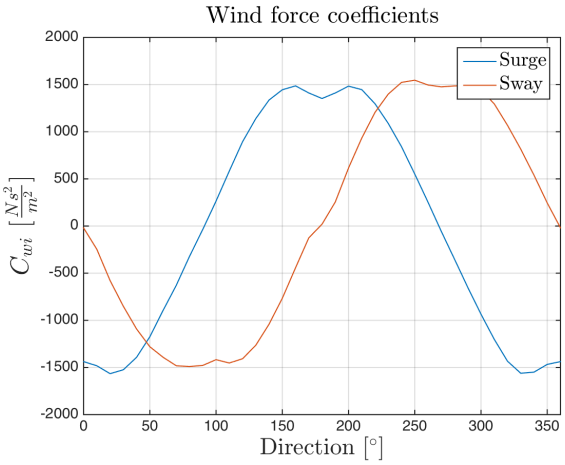

1.1.a Surge and sway

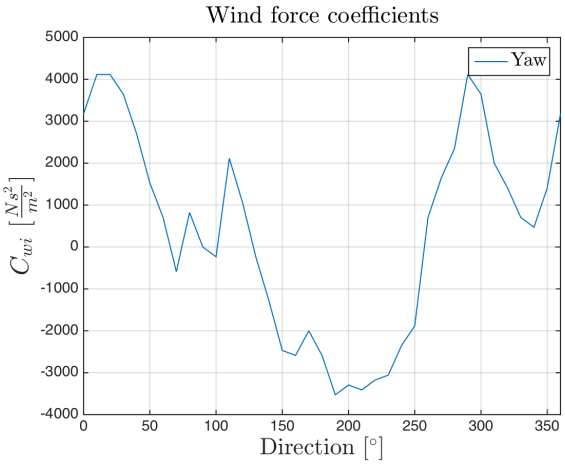

1.1.b Yaw

Wind force coefficients plotted against weather direction

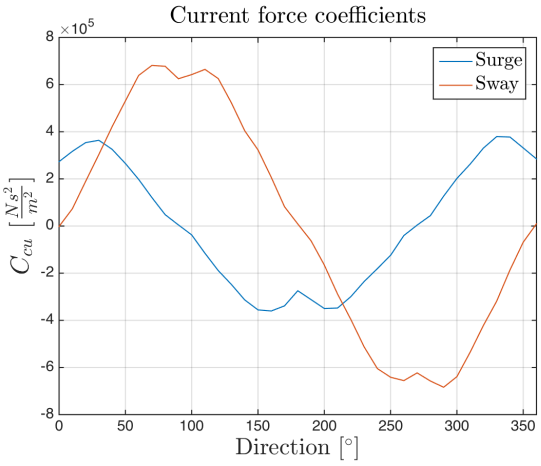

1.1.c Surge and sway

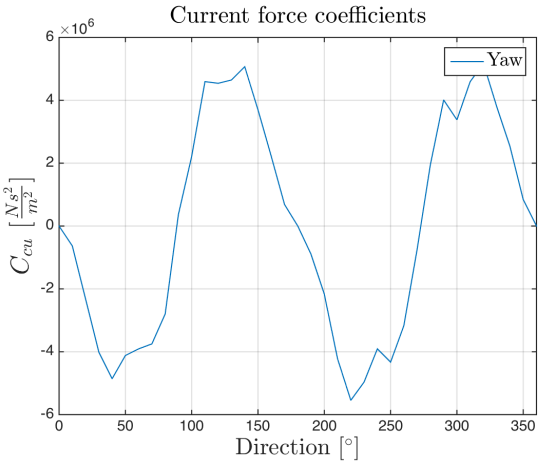

1.1.d Yaw

Current force coefficients plotted against weather direction

Appendix B

Case Study 1: SIMO Analysis of Safe Scandinavia

B.1 Decay Tests

A decay test in each DOF was executed to study the damping level present in the model, without linear damping included in the vessel properties. Plots of each decay test is given accordingly.

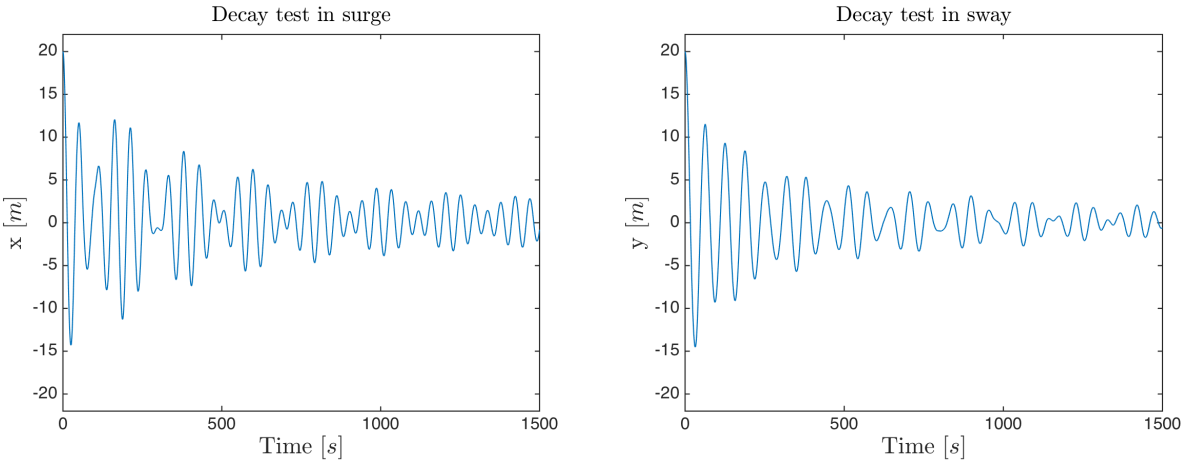

Decay test in surge (left) and sway (right)

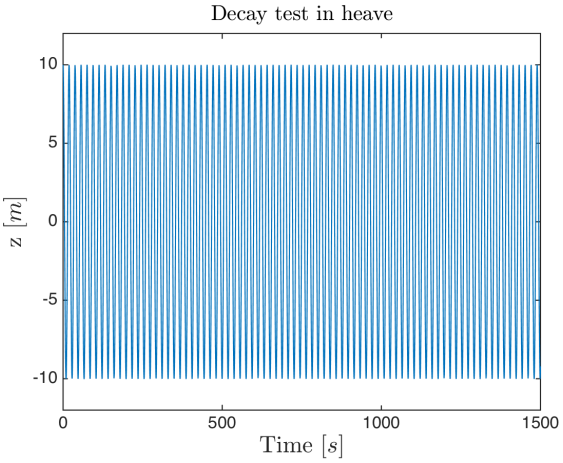

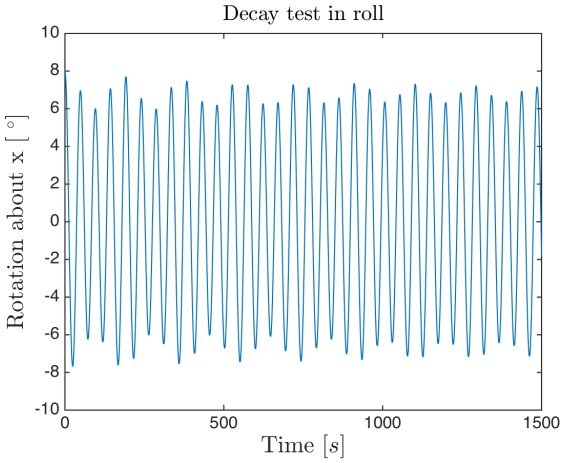

Decay test in heave (left) and roll (right)

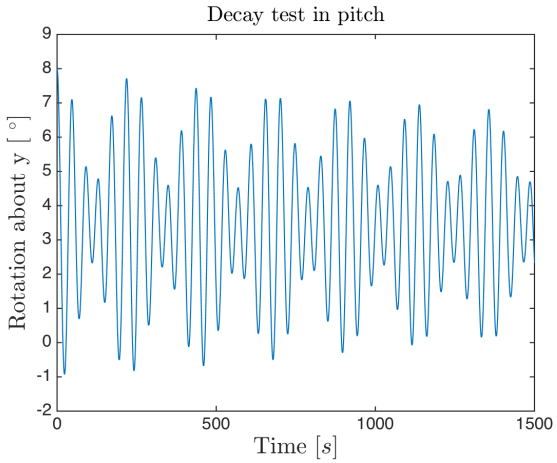

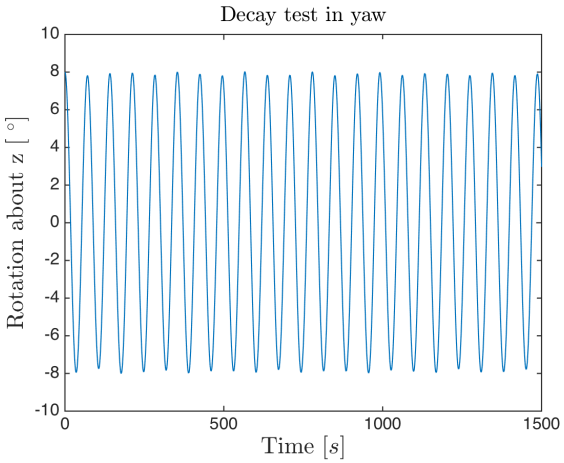

Decay test in pitch (left) and yaw (right)

B.2 Restoring Curves

Restoring curves from MIMOSA and SIMO for a weather direction of 45° and 225° following the global coordinate system in MIMOSA.

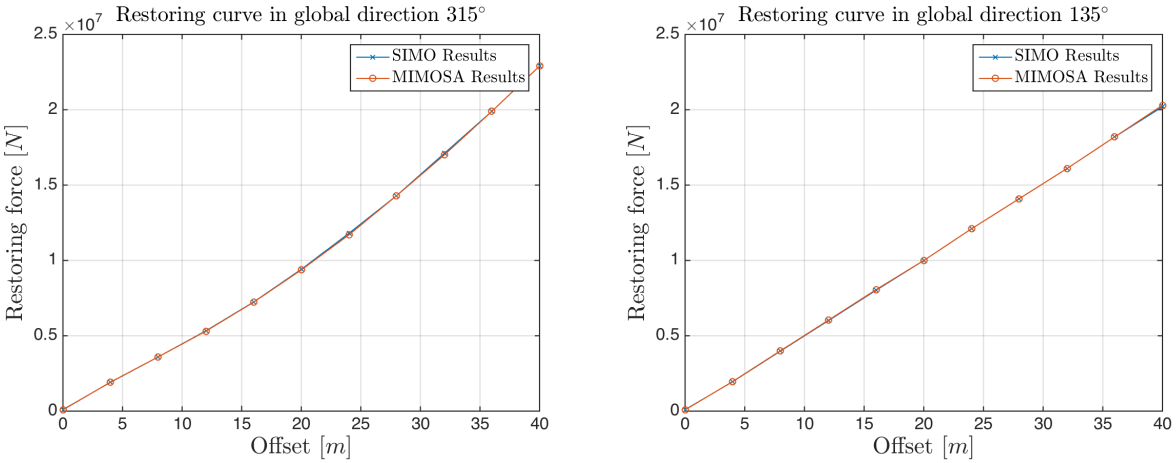

Restoring curves for offset in global direction 45° (left) and 225° (right)

B.3 Comparison of Results

Results from analyses performed in MIMOSA and SIMO with weather acting towards global 45° and 225° according to the global coordinate system defined for MIMOSA are given in this section. The proceeding tables present the WF, LF and total response in each DOF, in conjunction with LF, WF and total response in global direction 45° and 225° denoted r. Lastly, the resulting line tension for a windward and a leeward line, for each weather direction, is given.

	Surge $[m]$		**Sway** $[m]$		**Heave** $[m]$		**Roll** $[^\circ]$		**Pitch** $[^\circ]$		**Yaw** $[^\circ]$	
	max	σ	max	σ	max	σ	max	σ	max	σ	max	σ
SIMO	7.86	2.13	8.01	2.13	12.49	3.36	5.24	1.35	4.36	1.17	1.11	0.29
MIMOSA	7.84	2.08	7.78	2.07	12.13	3.24	5.08	1.32	4.41	1.16	1.13	0.29

WF vessel response with weather towards 45°

	Surge $[m]$		**Sway** $[m]$		**Heave** $[m]$		**Roll** $[^\circ]$		**Pitch** $[^\circ]$		**Yaw** $[^\circ]$	
	max	σ	max	σ	max	σ	max	σ	max	σ	max	σ
SIMO	7.85	2.12	7.99	2.14	12.49	3.36	5.26	1.35	4.35	1.16	1.11	0.29
MIMOSA	7.79	2.07	7.82	2.08	12.13	3.24	5.10	1.33	4.38	1.15	1.13	0.29

WF vessel response with weather towards 225°

		Surge $[m]$		**Sway** $[m]$		**Yaw** $[^\circ]$	
		max	σ	max	σ	max	σ
45°	SIMO	3.27	0.79	03.01	0.79	8.92	1.96
	MIMOSA	3.36	0.86	3.45	0.86	8.83	2.15
225°	SIMO	3.04	0.79	3.13	0.78	9.29	2.11
	MIMOSA	2.89	0.72	3.27	0.81	8.28	2.00

LF vessel response with weather towards 45° and 225°

		Surge $[m]$		**Sway** $[m]$		**Yaw** $[^\circ]$	
		max	σ	max	σ	max	σ
45°	SIMO	13.11	2.42	12.93	2.31	9.23	1.98
	MIMOSA	13.72	-	14.07	-	9.42	-
225°	SIMO	13.01	2.62	12.91	2.31	9.72	2.13
	MIMOSA	13.03	-	13.72	-	8.87	-

Total vessel response with weather towards 45° and 225°

Response direction		r_{stat}	r^{WF} $[m]$		r^{LF} $[m]$		r^{tot} $[m]$	
			max	σ	max	σ	max	σ
45°	SIMO	6.25	11.05	3.01	4.38	1.14	18.36	3.33
	MIMOSA	6.17	11.14	2.95	3.63	1.2	19.62	-
225°	SIMO	5.73	11.15	3.01	4.28	1.09	18.30	3.47
	MIMOSA	5.73	11.03	2.93	3.19	1.06	18.88	-

Vessel response with weather towards 45° and 225°

		Line 1		**Line 7**	
		T_{stat} $[kN]$	T_{max} $[kN]$	T_{stat} $[kN]$	T_{max} $[kN]$
45°	SIMO	452.0	1510.0	1370.0	3520.0
	MIMOSA	399.0	1690.0	1490.0	5390.0
225°	SIMO	1580.0	3760.0	638.0	1350.0
	MIMOSA	1590.0	3980.0	629.0	2470.0

Line tension in windward and leeward line with weather towards 45° and 225°

Appendix C

Case Study 2: Optimization in SIMA

C.1 Optimization Plots for Steel and Polyester system

In the following subsections plots of variation in cost, pretension, maximum offset, safety factor, segment lengths and segment diameters are presented. As the plots for Case 1 for both steel and polyester system is included in the main part of the thesis, results from Case 2, 3 and 4 is presented here. These cases are presented in the following three pages, respectively, for the polyester system, with proceeding three pages including plots given for Case 2, 3 and 4 for the steel system.

Case 2 - Polyester System

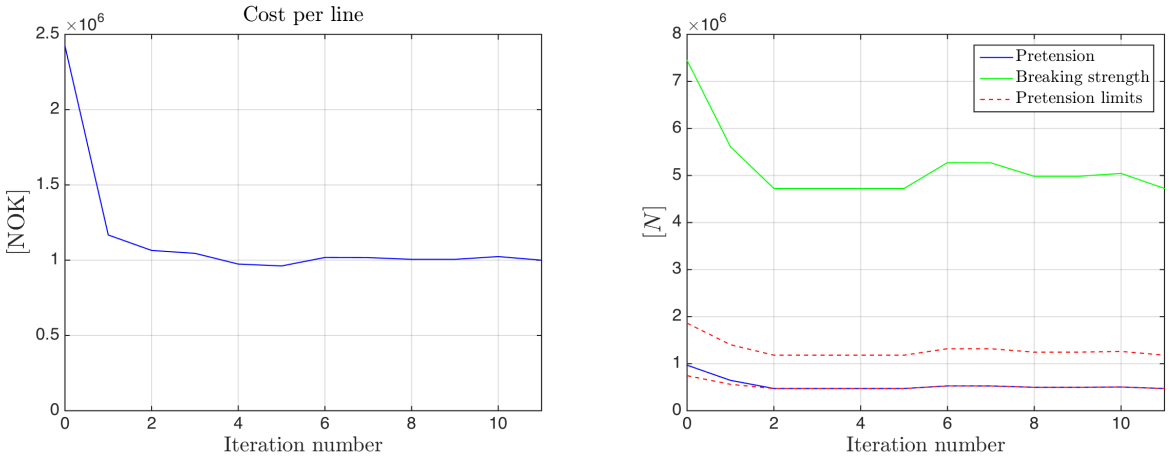

Variation in cost (left) and pretension (right)

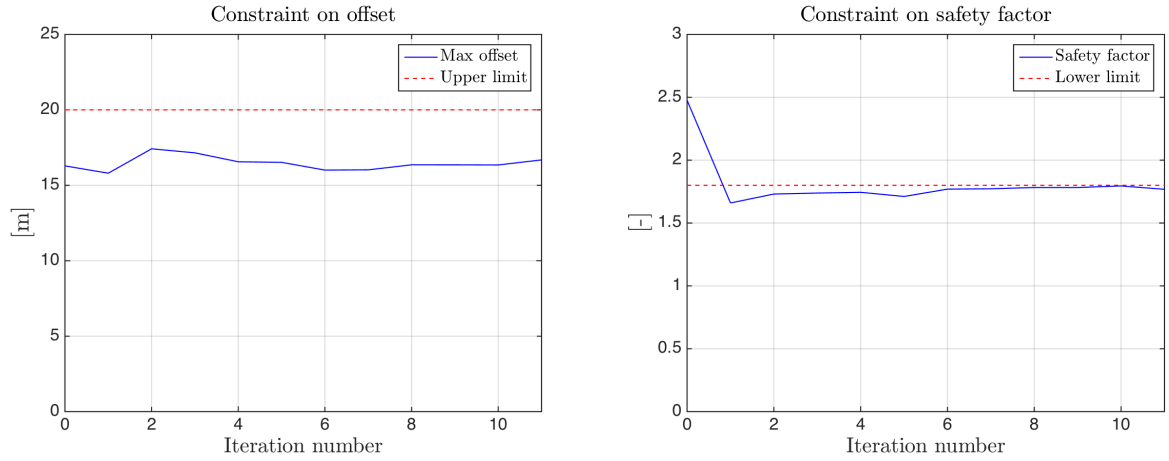

Variation in maximum offset (left) and safety factor (right) with constraint levels

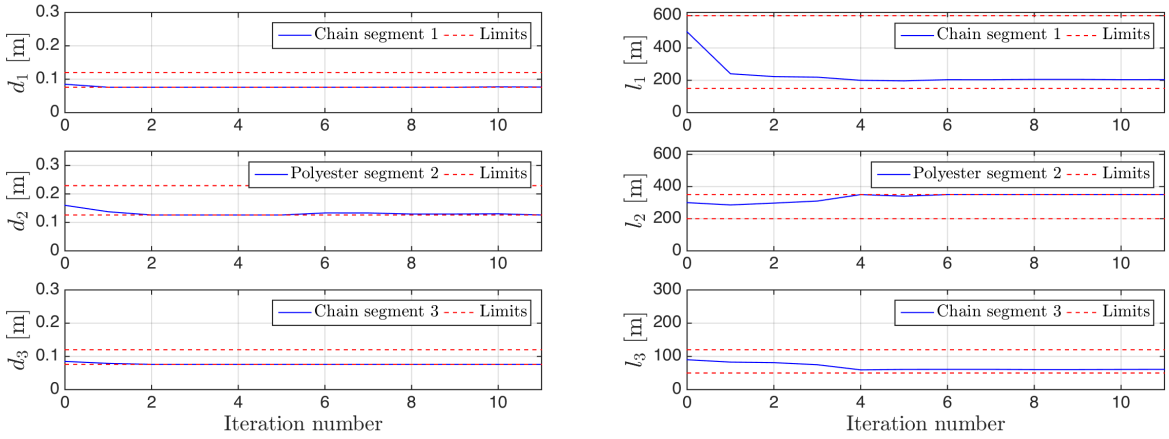

Variation in segment diameter (left) and length (rigth) with upper and lower bounds

Case 3 - Polyester System

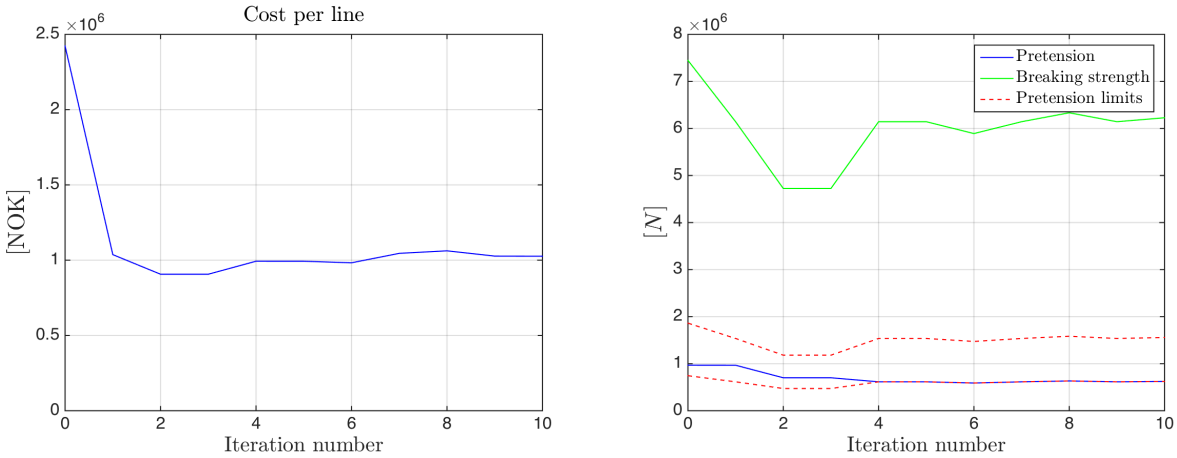

Variation in cost (left) and pretension (right)

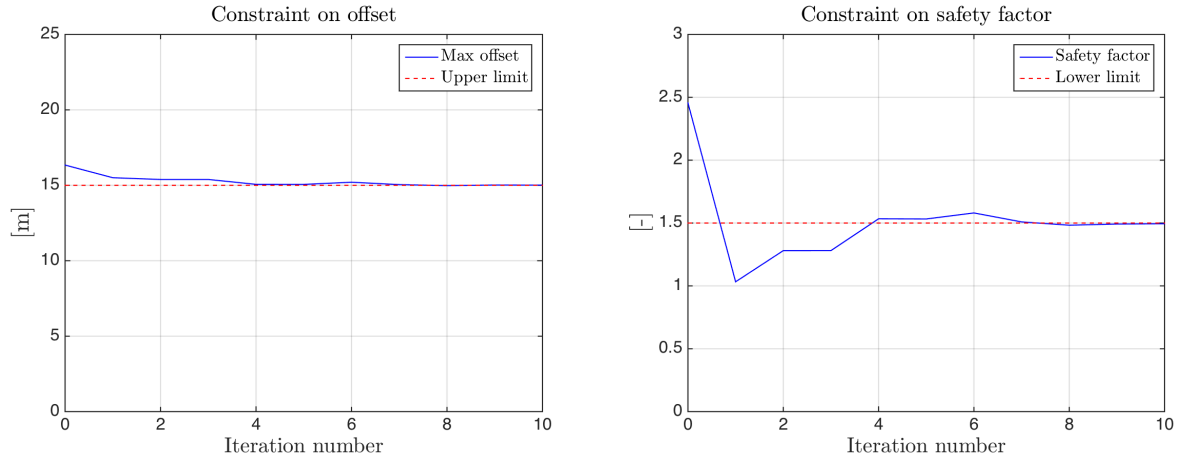

Variation in maximum offset (left) and safety factor (right) with constraint levels

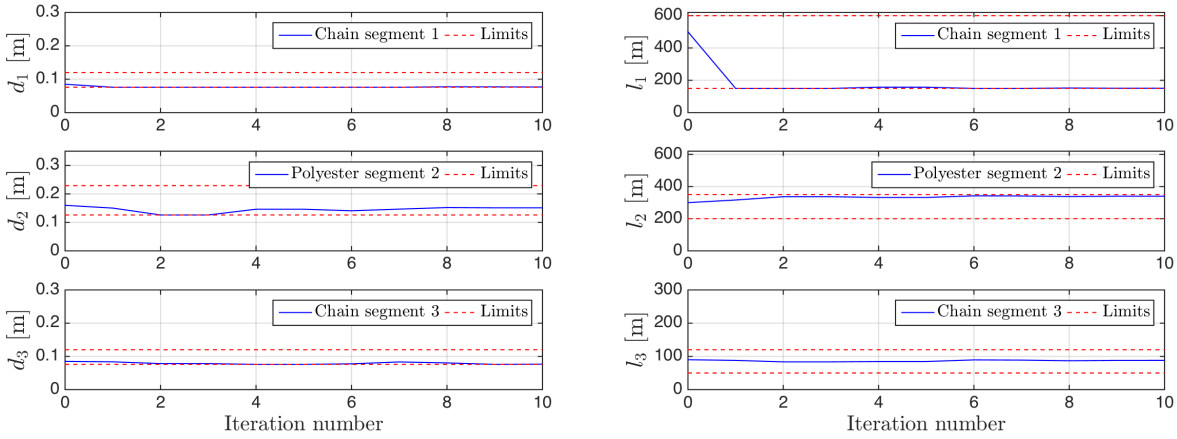

Variation in segment diameter (left) and length (rigth) with upper and lower bounds

Case 4 - Polyester System

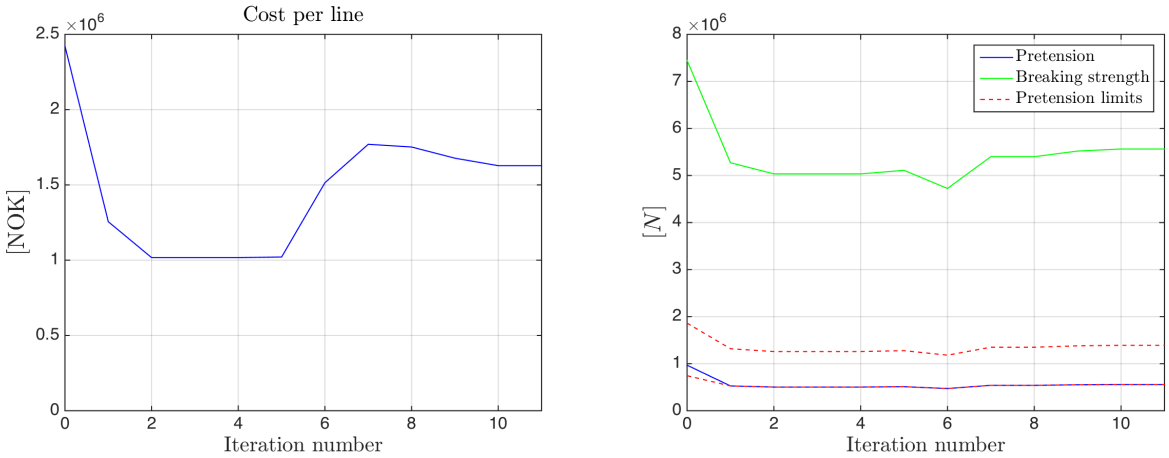

Variation in cost (left) and pretension (right)

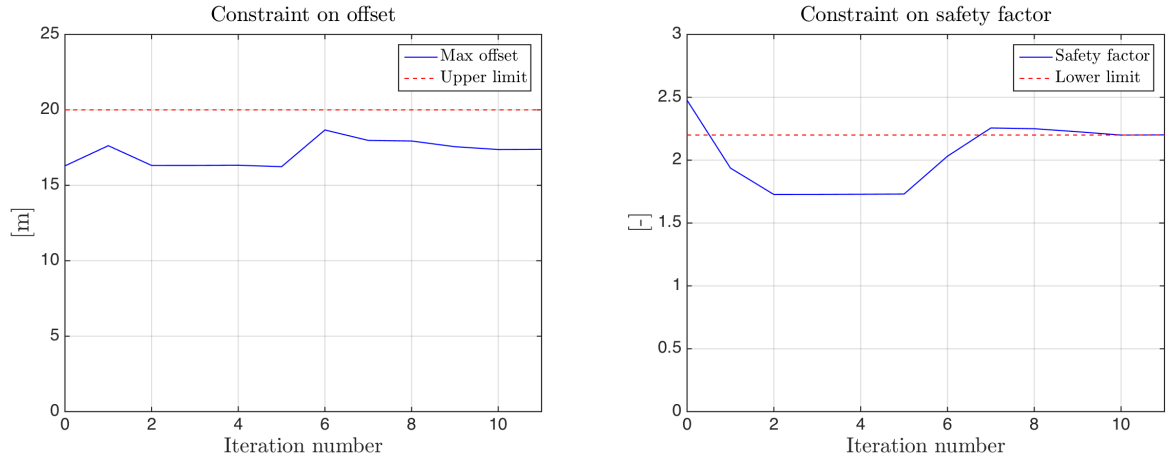

Variation in maximum offset (left) and safety factor (right) with constraint levels

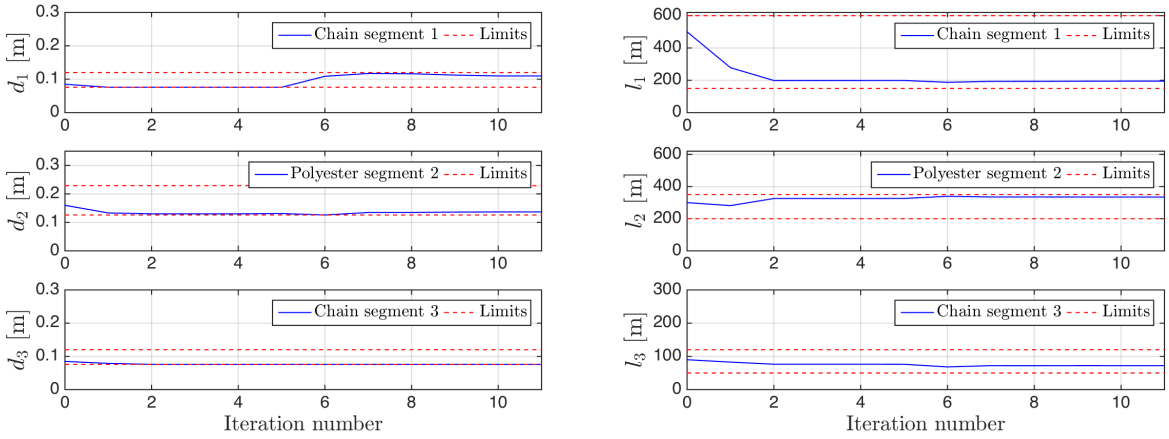

Variation in segment diameter (left) and length (rigth) with upper and lower bounds

Case 2 - Steel System

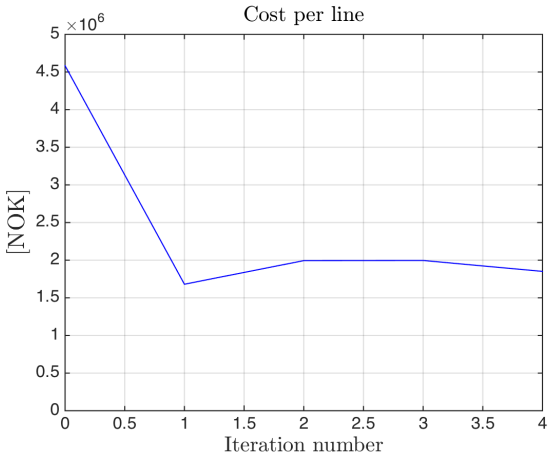

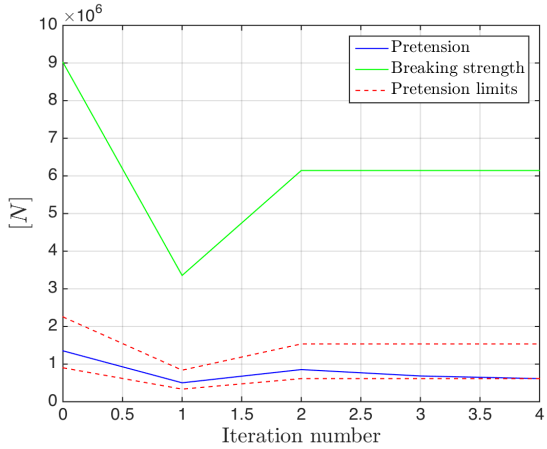

Variation in cost (left) and pretension (right)

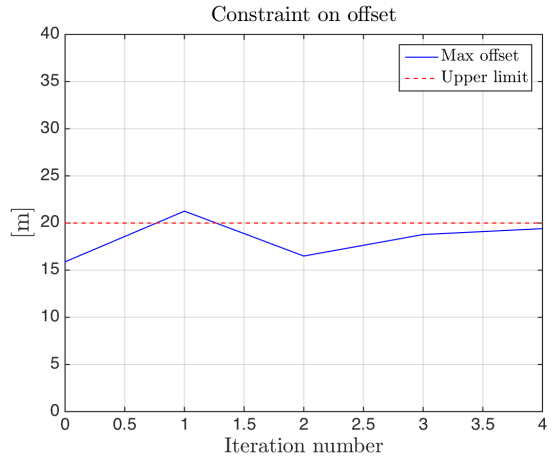

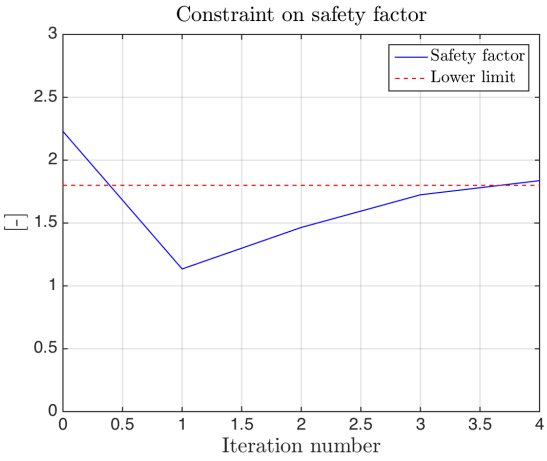

Variation in maximum offset (left) and safety factor (right) with constraint levels

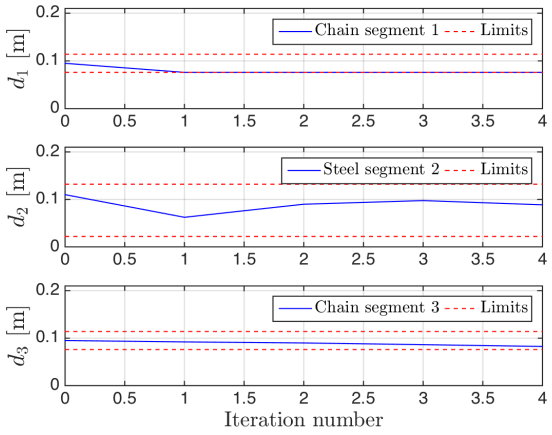

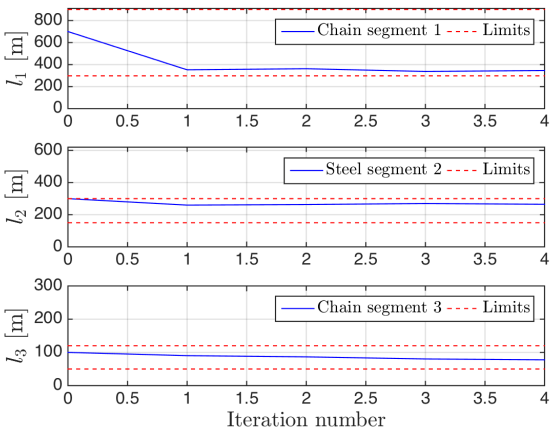

Variation in segment diameter (left) and length (rigth) with upper and lower bounds

Case 3 - Steel System

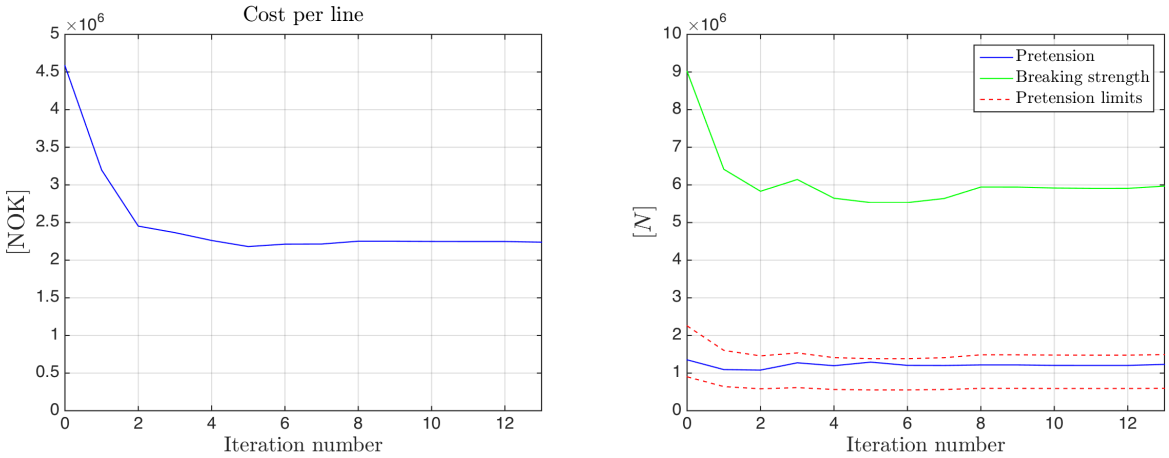

Variation in cost (left) and pretension (right)

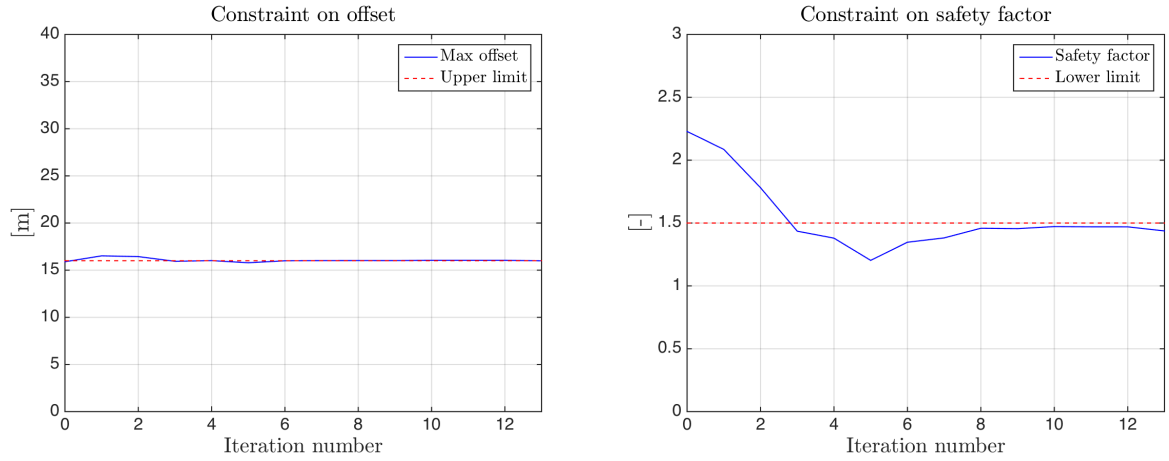

Variation in maximum offset (left) and safety factor (right) with constraint levels

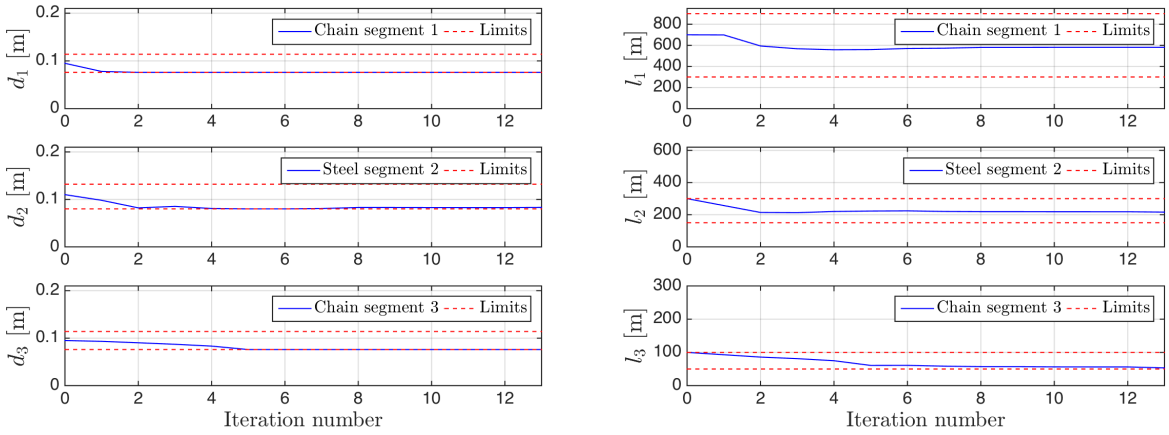

Variation in segment diameter (left) and length (rigth) with upper and lower bounds

Case 4 - Steel System

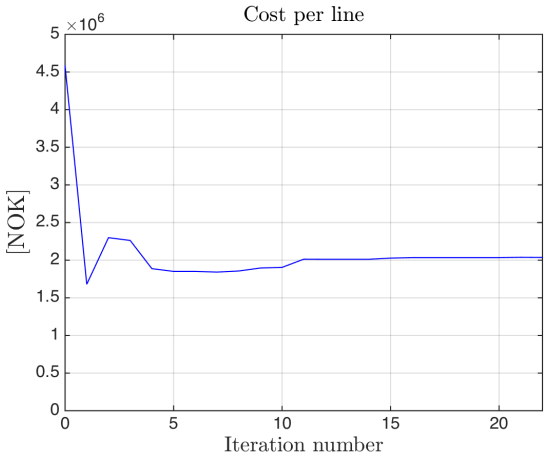

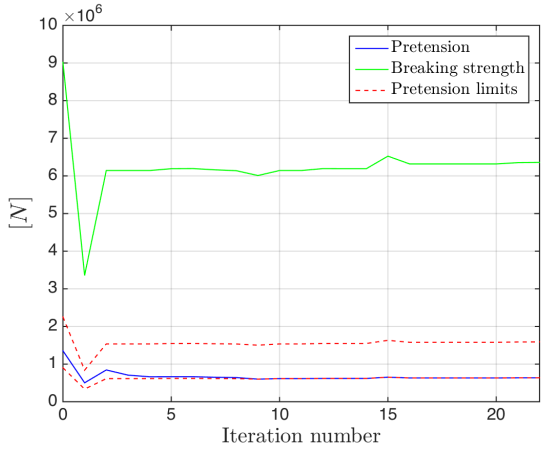

Variation in cost (left) and pretension (right)

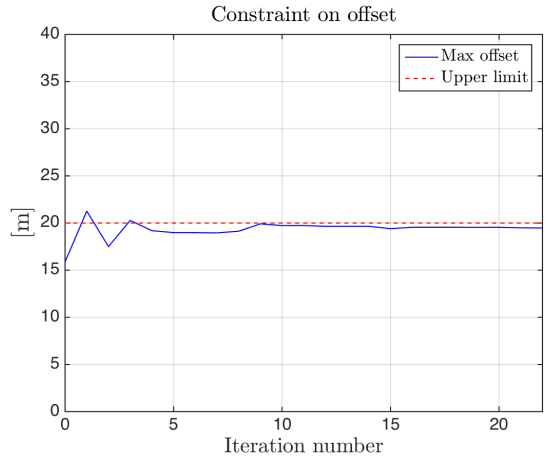

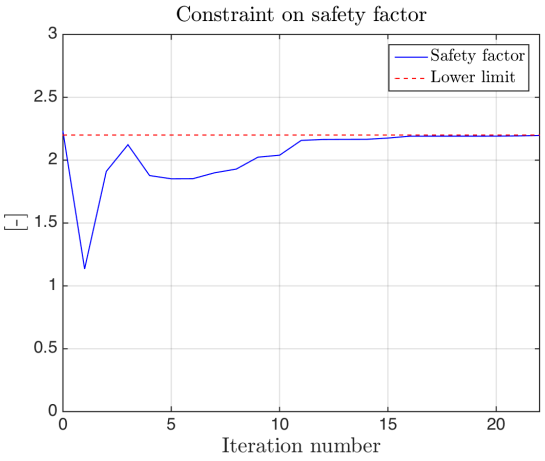

Variation in maximum offset (left) and safety factor (right) with constraint levels

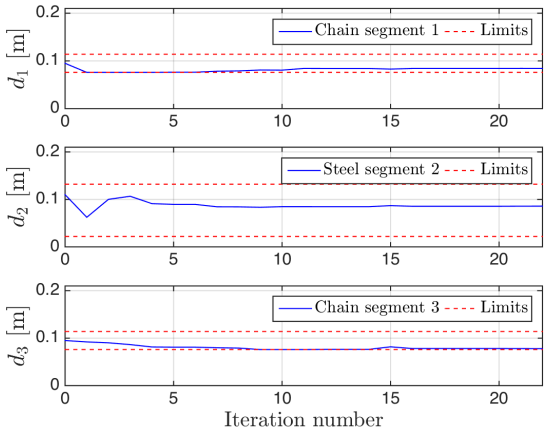

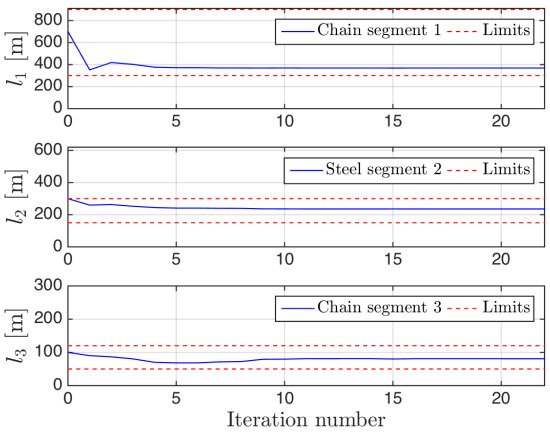

Variation in segment diameter (left) and length (rigth) with upper and lower bounds

C.2 Sensitivity Study

The following pages present optimization plots for Sensitivity 1, 2 and 3 for steel and polyester system. The optimization required different number of iterations in each case, and the dashed lines in the plots are extrapolations of the final value for the respective parameter plotted.

Sensitivity 1 - Plots for the Polyester System

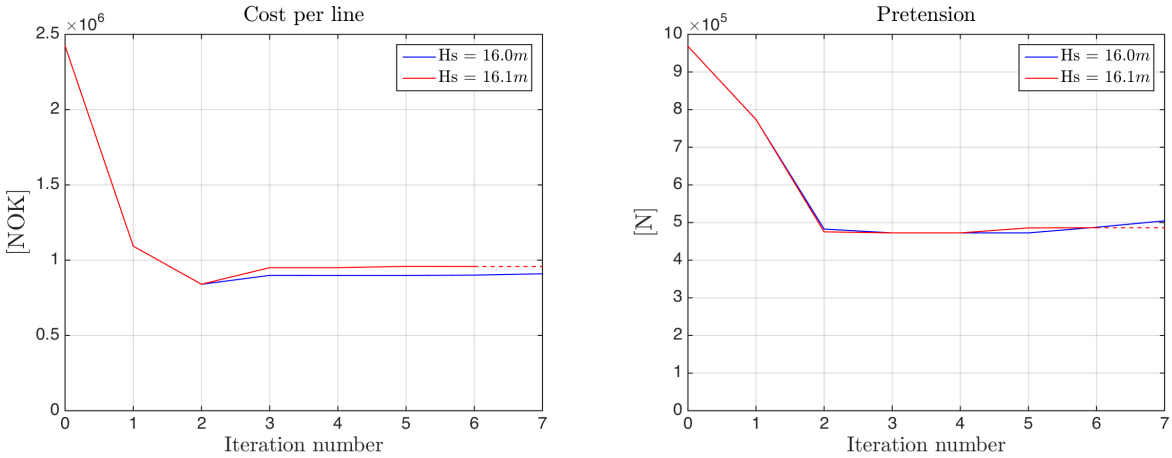

Variation in cost (left) and pretension (right) for $H_S = 16.0m$ and $H_S = 16.1m$

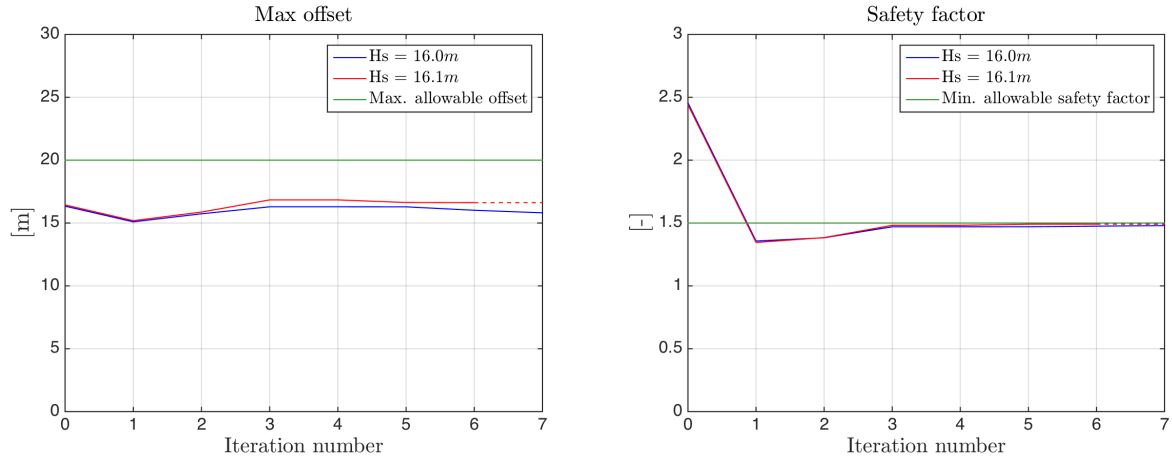

Variation in maximum offset (left) and safety factor (right) for $H_S = 16.0m$ and $H_S = 16.1m$

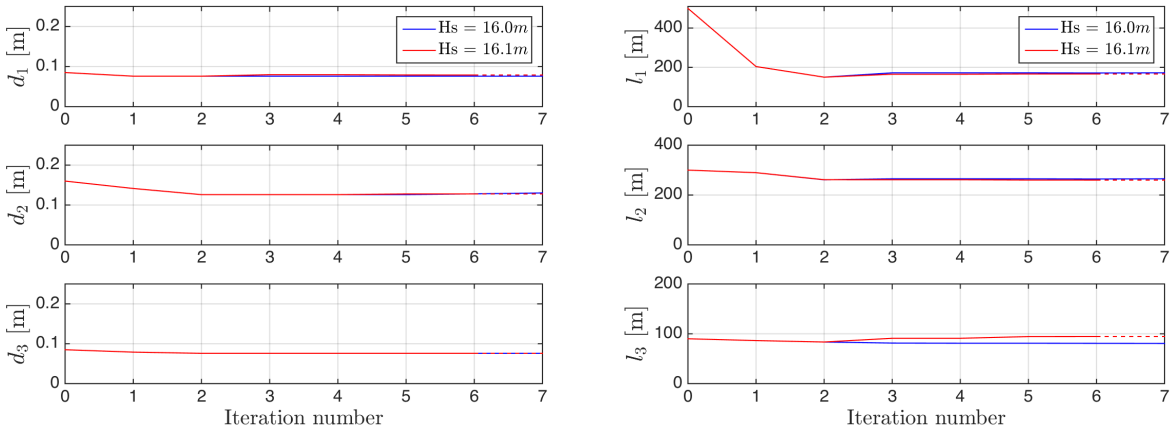

Variation in segment diameter (left) and length (rigth) for $H_S = 16.0m$ and $H_S = 16.1m$

Sensitivity 1 - Plots for the Steel System

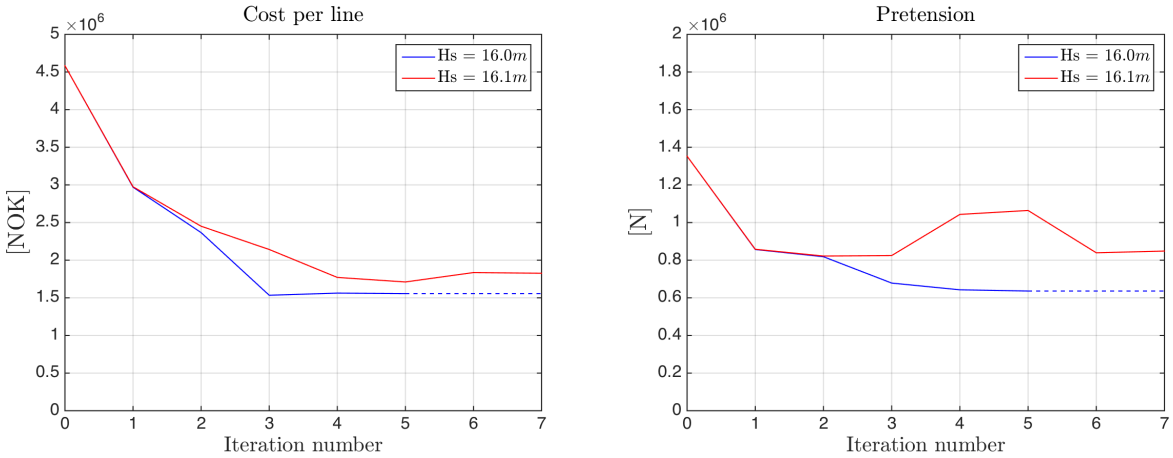

Variation in cost (left) and pretension (right) for $H_S = 16.0m$ and $H_S = 16.1m$

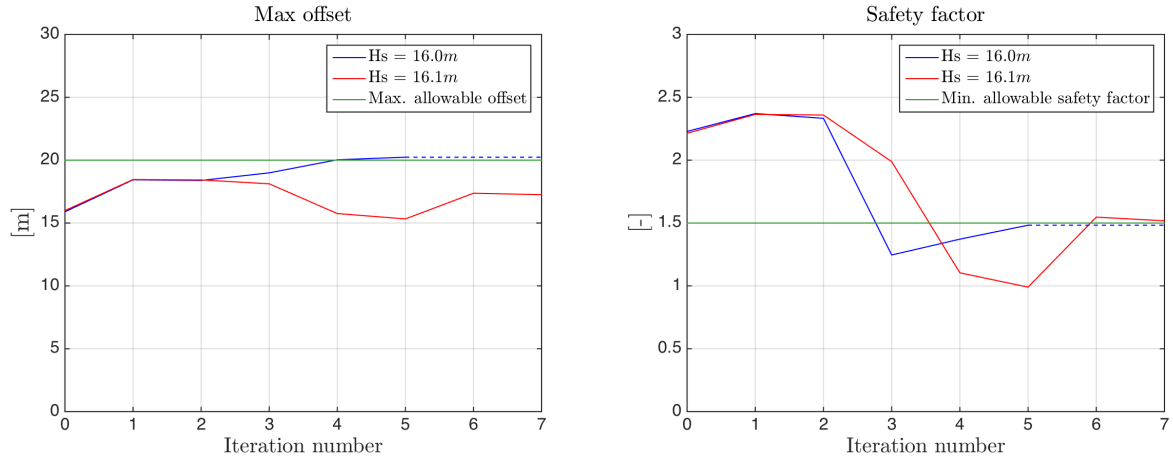

Variation in maximum offset (left) and safety factor (right) for $H_S = 16.0m$ and $H_S = 16.1m$

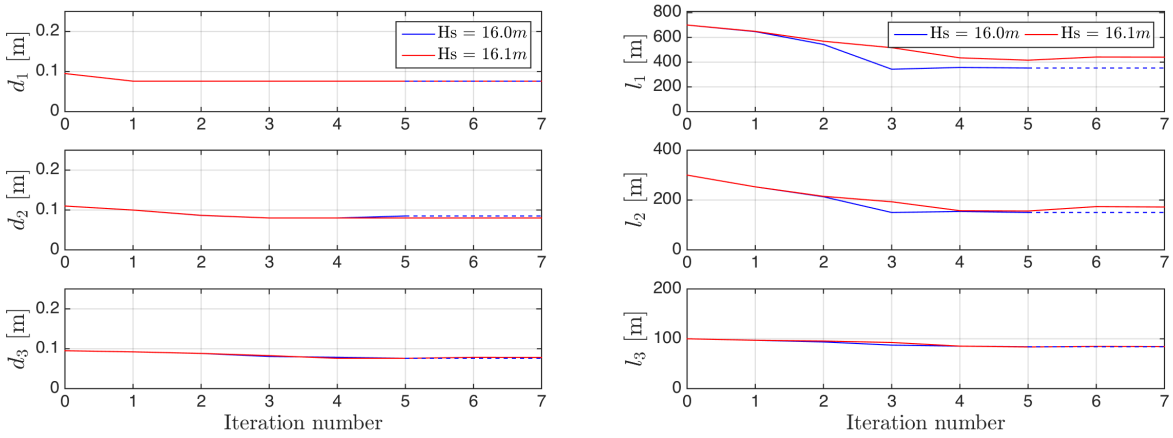

Variation in segment diameter (left) and length (rigth) for $H_S = 16.0m$ and $H_S = 16.1m$

Sensitivity 2 - Plots for the Polyester System

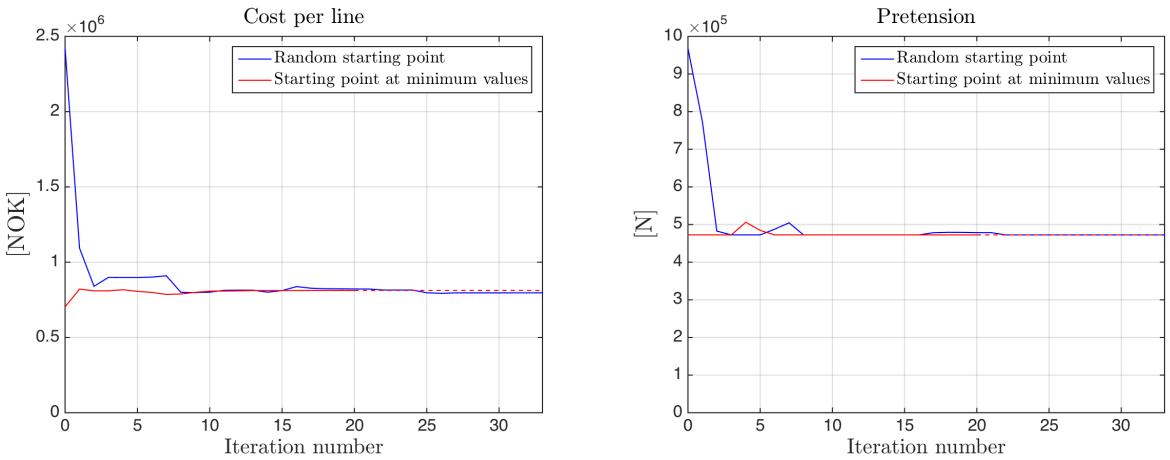

Variation in cost (left) and pretension (right) for global minimum convergence

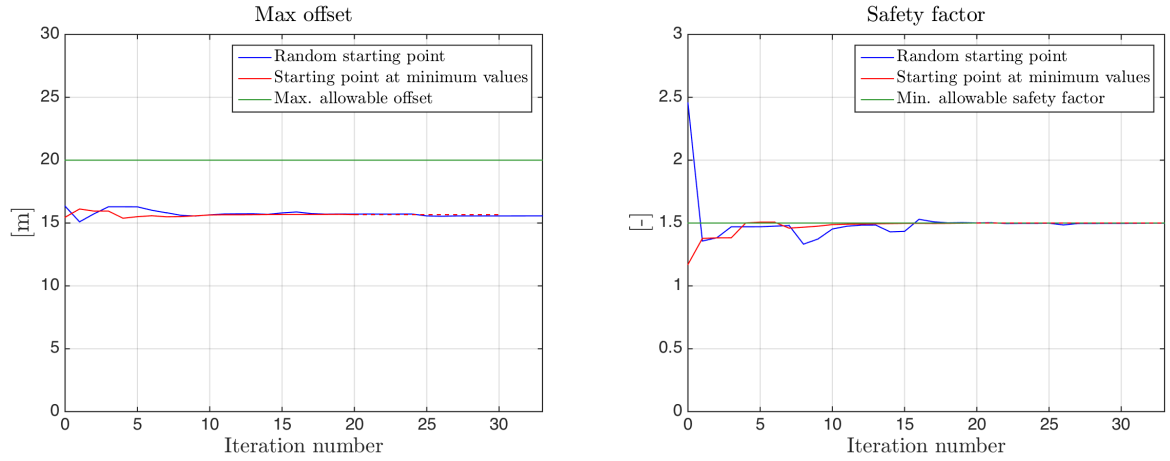

Variation in maximum offset (left) and safety factor (right) for global minimum convergence

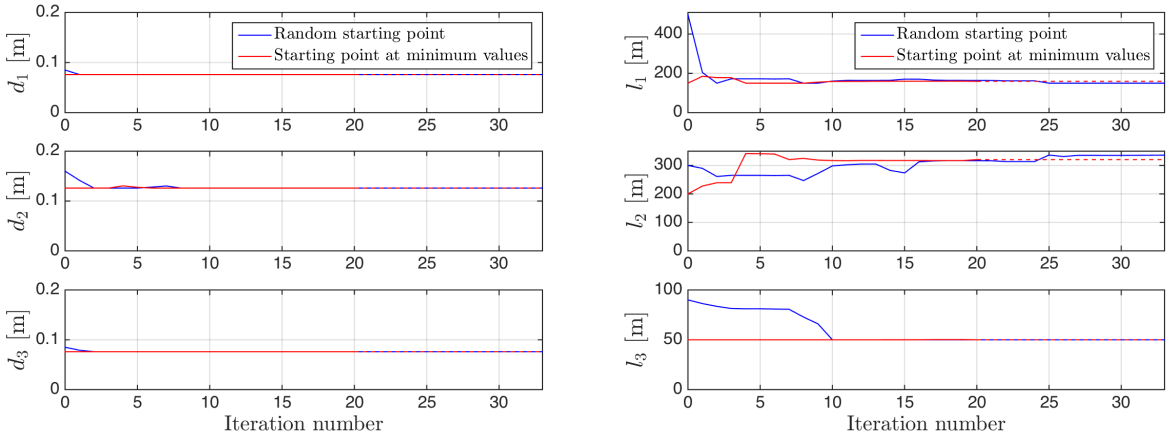

Variation in segment diameter (left) and length (rigth) for global minimum convergence

Sensitivity 2 - Plots for the Steel System

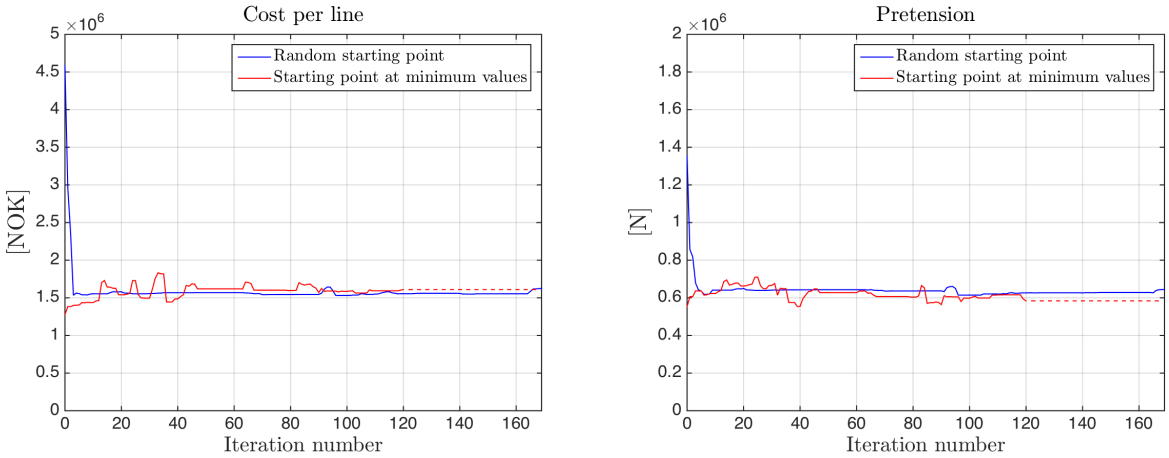

Variation in cost (left) and pretension (right) for global minimum convergence

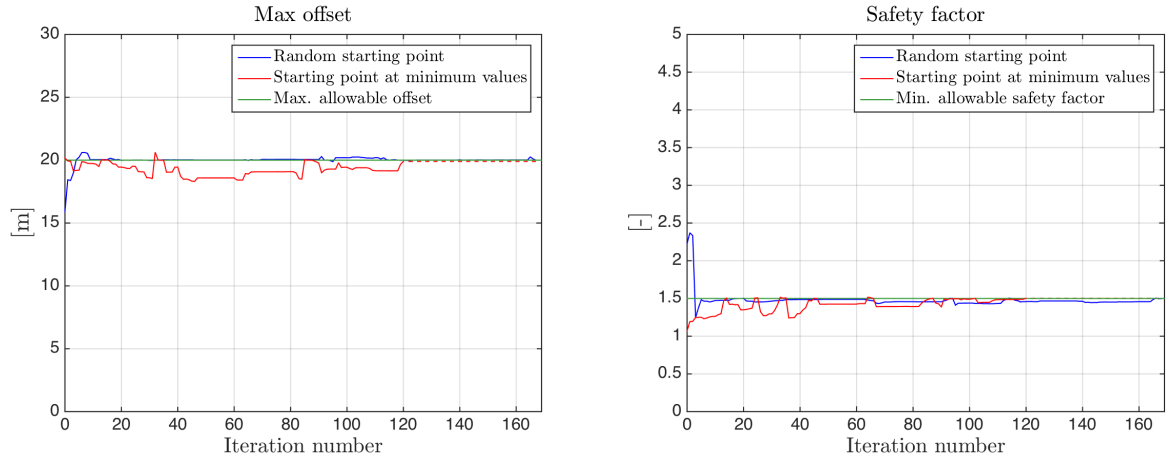

Variation in maximum offset (left) and safety factor (right) for global minimum convergence

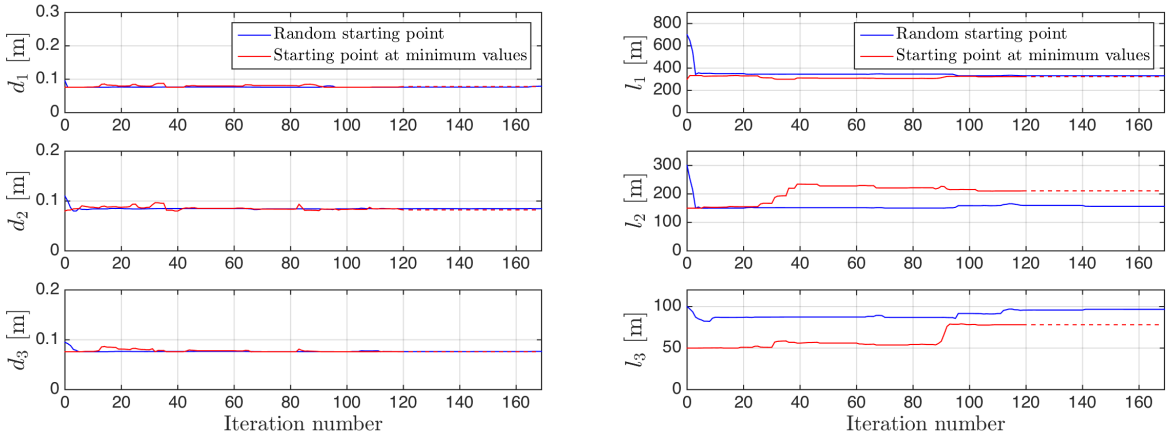

Variation in segment diameter (left) and length (rigth) for global minimum convergence

Sensitivity 3 - Plots for the Polyester System

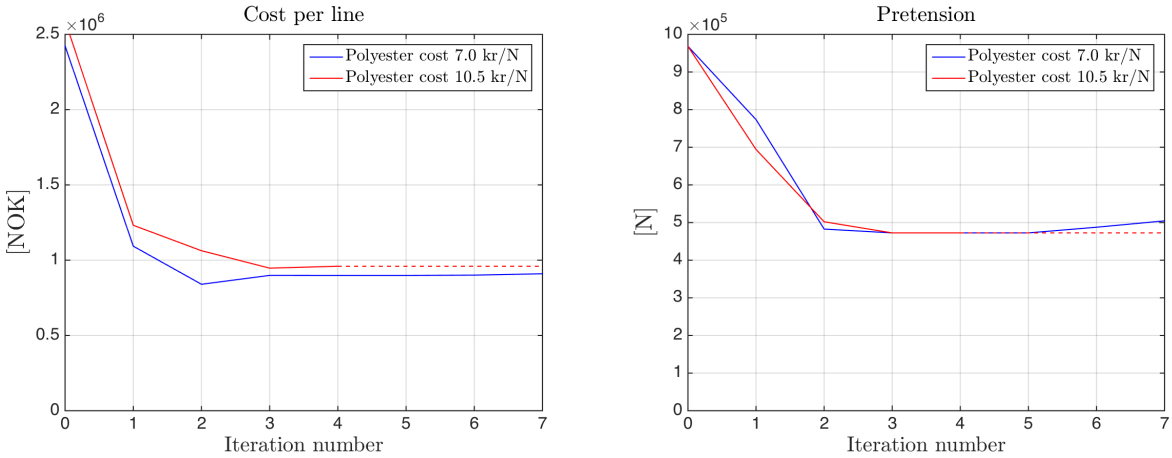

Variation in cost (left) and pretension (right) for $C_{poly} = 7.0kr$ and $C_{poly} = 10.5kr$

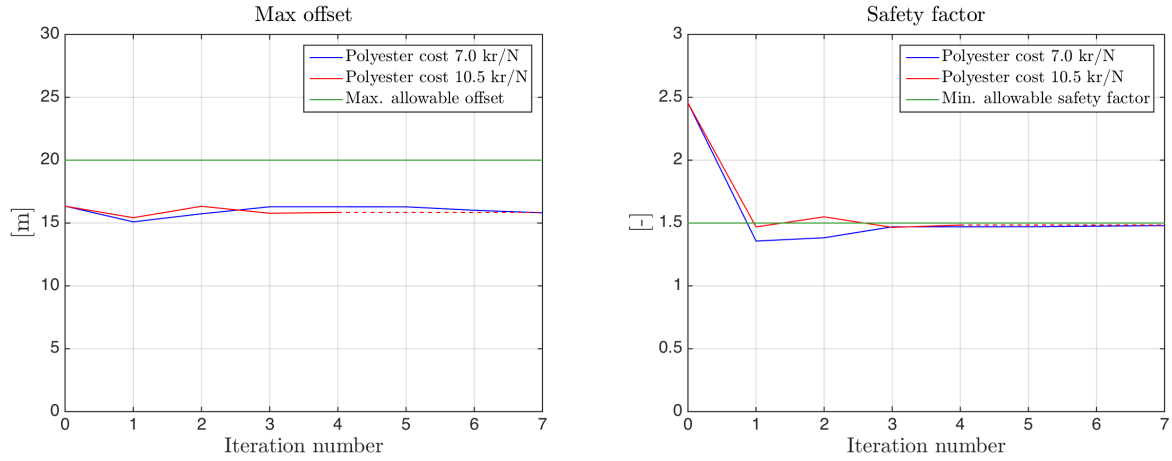

Variation in maximum offset (left) and safety factor (right) for $C_{poly} = 7.0kr$ and $C_{poly} = 10.5kr$

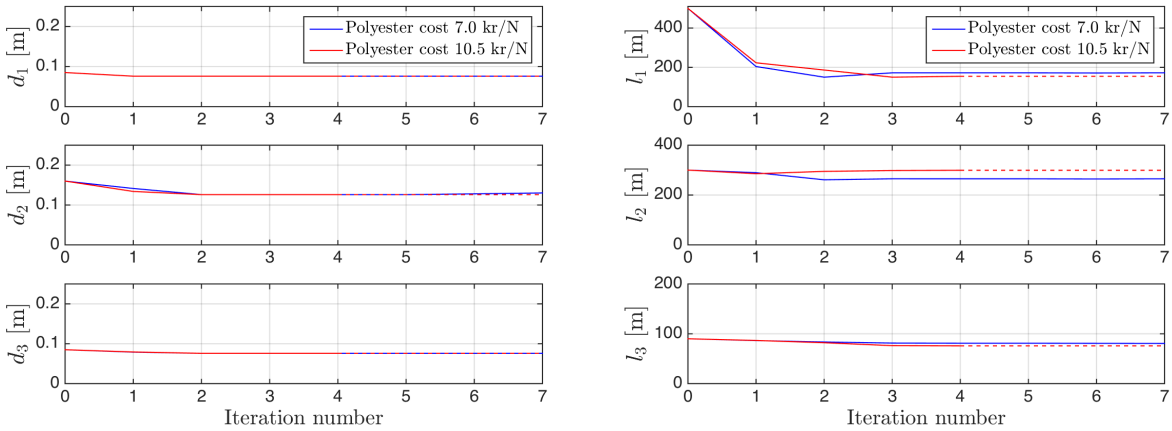

Variation in segment diameter (left) and length (rigth) for $C_{poly} = 7.0kr$ and $C_{poly} = 10.5kr$

C.3 Verification Results

Case 2

	$\bar{\boldsymbol{x}}$ $[m]$	$\boldsymbol{x^{WF}}$ $[m]$		$\boldsymbol{x^{LF}}$ $[m]$		$\boldsymbol{x^{tot}}$ $[m]$	
		max	σ	max	σ	max	σ
Steel	8.46	11.47	3.07	4.07	1.29	19.56	3.45
Polyester	6.43	11.47	3.07	3.40	1.22	17.45	3.52

Case 2 - most probable max and standard deviation in surge

	$\boldsymbol{MBL}$	$\boldsymbol{T_{stat}}$	$\boldsymbol{T_{max}}$	$\boldsymbol{sf}$
Steel	6140.0	979.0	3700.0	1.66
Polyester	4730.0	835.0	2900.0	1.63

Case 2 - Tension in heaviest loaded line, line 7

Case 3

	$\bar{\boldsymbol{x}}$ $[m]$	$\boldsymbol{x^{WF}}$ $[m]$		$\boldsymbol{x^{LF}}$ $[m]$		$\boldsymbol{x^{tot}}$ $[m]$	
		max	σ	max	σ	max	σ
Steel	4.36	11.48	3.07	3.36	0.99	16.71	3.58
Polyester	4.45	11.47	3.07	2.67	1.15	15.94	3.68

Case 3 - most probable max and standard deviation in surge

	$\boldsymbol{MBL}$	$\boldsymbol{T_{stat}}$	$\boldsymbol{T_{max}}$	$\boldsymbol{sf}$
Steel	5980.0	1550.0	4550.0	1.31
Polyester	6240.0	1070.0	4580.0	1.36

Case 3 - Tension in heaviest loaded line, line 7

Case 4

	$\bar{\boldsymbol{x}}$ $[m]$	$\boldsymbol{x^{WF}}$ $[m]$		$\boldsymbol{x^{LF}}$ $[m]$		$\boldsymbol{x^{tot}}$ $[m]$	
		max	σ	max	σ	max	σ
Steel	8.06	11.47	3.07	4.13	1.27	19.58	3.44
Polyester	6.90	11.47	3.07	3.68	1.16	18.27	3.46

Case 4 - most probable max and standard deviation in surge

	$\boldsymbol{MBL}$	$\boldsymbol{T_{stat}}$	$\boldsymbol{T_{max}}$	$\boldsymbol{sf}$
Steel	6360.0	991.0	3240.0	1.97
Polyester	5560.0	978.0	2810.0	1.98

Case 4 - Tension in heaviest loaded line, line 7

Appendix D

Overveiw of Atteched Files

poster.pdf

poster.pdf is the poster created for the master poster exhibition i May.

SIMAMasterSafeScandinavia.stask

SIMAMasterSafeScandinavia.stask includes the SIMO model of Safe Scandinavia. Additionally, it includes the mooring system utilized in Case Study 1.